CRANFIELD UNIVERSITY

EURICO GONÇALVES ASSUNÇÃO

INVESTIGATION OF CONDUCTION TO KEYHOLE MODE TRANSITION

SCHOOL OF APPLIED SCIENCES

PhD Thesis

Academic Year: 2011-2012

Supervisor: Professor S. Williams
Mr. David Yapp
July 2012

CRANFIELD UNIVERSITY

SCHOOL OF APPLIED SCIENCES

PhD

Academic Year 2011- 2012

EURICO GONÇALVES ASSUNÇÃO

INVESTIGATION OF CONDUCTION TO KEYHOLE MODE TRANSITION

Supervisor: Professor S. Williams
Mr. David Yapp

July 2012

ABSTRACT

There are two very distinct welding modes in laser welding, keyhole and conduction mode. The characteristics of keyhole laser welding; mainly high penetration, high productivity and high aspect ratio have led the industry to focus more on this mode. On the other hand, conduction mode does not have high productivity and has a low aspect ratio, but deep penetration depths can also be achieved using this mode. Despite these disadvantages conduction mode has advantages such as stability of the welding process, high quality, better control of the heat input and no spatter. These characteristics are not normally associated with laser welding, mainly due to keyhole welding being the usual operational mode. Conduction laser welding is a more complicated process than might be expected. This is because of the conflicting requirements of maximising penetration depth whilst maintaining very high quality. This means that thermal transfer needs to be maximised but vaporisation needs to be zero. The aim of this research was to fully understand conduction laser welding mode and therefore, achieve maximum penetration whilst maintaining high quality. The approach was to use power density, interaction time and beam diameter as process parameters in order to study and understand the transition between conduction and keyhole welding modes. The study included the differences between using a continuous wave laser system and a pulsed wave laser system. Most of the study was made in mild steel and was also extended to stainless steel and aluminium to include the effects of the material properties on the transition. For process optimisation the effect of system parameters, power and welding speed, on optimum beam diameter in conduction mode was also examined for aluminium and mild steel. This included a comparison between the use of a statistical empirical model and a finite element model for optimisation of the process. Finally a comparison of residual stress development in conduction and keyhole welding modes was made.

Para a minha querida Rita

e para os meus pais

ACKNOWLEDGEMENTS

It is only fair to acknowledge and thank a vast number of people that have contributed in many ways to this research.

I would like to express my immense gratitude to my supervisors Professor Stewart Williams and Mr. David Yapp for having me as a PhD student and for providing me the opportunity to conduct this research and I am grateful for the trust deposited on me. Special thanks will have to go to Professor Williams for the long discussions and for the effective guidance and constant help, and the relationship with him has inevitably evolved into a valued friendship, as it could not be otherwise.

A sincerely thanks to Dr. Paul Colegrove for his support during the duration of my PhD.

I am also particularly grateful to Brian Brooks and to Flemming Nielsen for all their assistance in the lab and for being such good friends during the duration of my PhD.

I would also like to thank Ben Hopper and Andrew Dyer for the support they gave me.

Being in a different country allowed me to meet people from different cultures that contributed to my personal and professional development. Many thanks to all of my colleagues and friends. All of them contributed for making Cranfield feel a bit like home.

Elisabete, Pedro, Nuno, Gil, Teresa, Sónia and Gonçalo helped making England feel a bit like a “little” Portugal. The long lunches and dinners, the “*chouriços e farinheiras*”, the Football matches and most important their friendship supported me during my stay at Cranfield.

Thanks to Wojciech Suder, “my lab colleague”, for the long discussions and for the exchange of ideas during my PhD.

Luis Gallar, Dio Antille and Antonio Cantarero were fine friends throughout these past four years. The early morning trips to the gym, the late lunches on Sunday and the conversations we had made this a friendship to cherish

Glenn Leighton and Matthew Rush made the number 79 of Lower Shelton Road feel like home and I am grateful for their support and friendship.

Finally, I owe a great deal to my family and relatives for the support they gave me and for making me feel that I always had a place to go back to. And most important a very special thanks to Rita for supporting me on this adventure despite the distance that separated us during this three years.

TABLE OF CONTENTS

LIST OF FIGURES

APPENDIX A

LIST OF TABLES

APPENDIX A

Abbreviations

CO_2	Carbon Dioxide
CW	continuous wave
Nd:YAG	Neodymium-doped yttrium aluminium garnet
PW	pulsed wave
TIG	Tungsten inert gas

Nomenclature

P	Power
$A_{(Beam)}$	Area of the laser beam
t_i	Interaction time
d_b	Beam diameter
V	Welding speed
f_f	Focal position
Pd_{CML}	Upper limit power density of conduction mode
T_{mp}	Temperature of the melting point
T_{vp}	Temperature of the vaporisation point
k	Thermal conductivity
ρ	Density
C_p	Specific heat capacity
L_m	Latent heat of melting
L_v	Latent heat of vaporisation
q	Power density
α	Thermal diffusivity
R	Reflectivity
$\overline{C_{ps}}$	Average specific heat for temperatures below the melting point
$\overline{C_{pl}}$	Average specific heat for temperatures between the melting and the vaporisation temperature
C_{pm}	Specific heat for temperatures between the room temperature and the melting temperature including the latent heat of melting
C_{pv}	Specific heat for temperatures between the melting temperature and the vaporisation temperature including the latent heat of vaporisation
$\overline{k_{solid}}$	Average conductivity of the material in solid state
$\overline{\alpha_{solid}}$	Average thermal diffusivity of the material in solid state
$q_{(T_{mp})}$	Power density required for melting
$\overline{k_{liquid}}$	Average conductivity of the material in liquid state
$\overline{\alpha_{liquid}}$	Average thermal diffusivity of the material in liquid state

a_0	Stress free reference
a_L	Measured lattice parameters in the longitudinal strain direction
a_T	Measured lattice parameters in the transverse strain direction
a_N	Measured lattice parameters in the normal strain direction
ν	Poisson's ratio
ε	Strain
σ	Stress
Pe	Peclet number
k_{melt}	Conductivity of molten material
ΔT	Temperature difference
μ	Viscosity
u	Average melt flow velocity

1 Introduction

In recent years, most of the research around laser welding was focused on keyhole laser welding. The constant need of increasing productivity and achieving deeper penetration has led industry to focus even more on keyhole laser welding. However, for some new applications, the requirements have been somewhat different. These new applications require not only high productivity and high penetration, but also high quality and welds with good visual appearance. Based on this, conduction laser welding is a viable alternative to keyhole laser welding and to arc welding, especially TIG welding. Conduction laser welding does not have the productivity of keyhole laser welding, however when compared to TIG welding the productivity is very similar. In terms of quality, the welds obtained in conduction mode are similar to the ones obtained in TIG welding and superior to keyhole welding.

Laser welding, depending on the processing conditions, has broadly two different operational regimes; conduction mode and keyhole mode. The beneficial characteristics of keyhole welding, especially the deep penetration depth and relatively small heat affected zone has attracted more industrial applications. On the other hand, conduction laser welding has been somewhat neglected by industry despite several advantages. Conduction welding can be a viable alternative to laser keyhole welding and to arc welding. The advantage of this welding mode is that no vaporization takes place. This means that the welds can show no porosity, no cracks and no undercut and are also free of spatter. It is also a very stable process that allows control of the heat delivered to the work piece. Due to the large beam diameters used in this mode the gap bridging ability is also enhanced. Conduction laser welding can also be achieved with significantly lower laser cost, because it does not require high beam quality or a very high power.

Because most of the recent studies carried out in laser welding are focused mainly in keyhole laser welding the knowledge on conduction laser welding mode is still limited. For example the threshold between conduction mode and keyhole mode can be traced back to the 60’s, where it was assumed that if a laser weld is done over a certain power density value it is in keyhole mode and if it is under that value it is in

conduction mode [1]. This definition is often used, completely ignoring the beam diameter, interaction time, material and type of laser, if it is continuous wave or pulsed wave, which was used in the welding process. This might lead to the incorrect use and identification of conduction laser welding.

This research presents results investigating the effect of different welding parameters, like beam diameter and interaction time, on the conduction mode threshold. Understanding the effect of these parameters on the conduction mode threshold is important when choosing to use conduction or keyhole mode. The effect of using a continuous wave or a pulsed wave laser system on the conduction mode threshold was also assessed. As also how the material properties will influence the conduction mode limits.

The main focus of this thesis was the understanding of how the limits of conduction mode are influenced by different factors, like the material, the type of laser and the welding parameters. At the same time, in order to add to the knowledge of conduction mode, a comparison between the residual stresses obtained in keyhole mode and in conduction mode was also made. Also, the identification of the optimum beam diameter for Aluminium alloy 2024, was made for a range of powers and welding speeds. These allowed a better understanding on how conduction laser welding mode should be used, and how the different welding parameters influence conduction laser welding.

The results from this work were published in relevant academic journals. A total of five papers are detailed in this thesis. In addition recommendations for further work are suggested and some examples of conduction laser welding applications that were developed during the duration of this thesis are given.

2 Thesis objectives and structure

This chapter briefly summarises the objectives of this PhD research. This project, funded by the IMRC, focused on adding to the knowledge of conduction laser welding mode. Important properties of conduction laser welding, like the importance of the beam diameter and how the interaction time and the beam diameter influence the power density at which conduction mode threshold takes place were researched. The motivation behind this PhD thesis was the possibility of evaluating and challenging already established concepts about conduction laser welding and to add to the knowledge of conduction laser welding mode.

2.1 Thesis Objectives

The primary objective of this research was to understand the effect of different laser welding parameters on the conduction to keyhole mode transition, as well as the effect of the material properties and the type of laser on this transition. This was achieved by the following separate but yet interrelated objectives:

- Understanding how the laser welding parameters of power density, interaction time and beam diameter, influence the conduction mode limits
- Compare the welds obtained in continuous wave and pulsed wave lasers, using similar parameters, allowing a better understanding on how the welding modes are influenced by the type of laser used
- Study the effect of material properties on the different laser welding modes and how these properties influence the conduction and keyhole mode limits
- Understanding how the optimum beam diameter in conduction mode is influenced by the system parameters of power and welding speed
- Characterisation of the residual stress state of the different welding modes
- Disseminate / publish results in peer reviewed scientific journals

Separated from the main objective of this work several applications of conduction laser welding were made during the duration of this PhD thesis (APPENDIX A). All

the work presented in this thesis was done at Cranfield Welding Engineering and Laser Processing Centre (WELP).

2.2 Thesis Structure

This research is structured around five journal papers published as the research progressed. The thesis format is as follows.

Chapter 3 begins by reviewing the current state of the art and literature of conduction mode laser welding. The different definitions of conduction mode, which are behind the motivation of this thesis, are shown and discussed. Some of the current knowledge of conduction laser welding mode is also reviewed in this chapter and a comparison between keyhole mode and conduction mode is also made. Finally some examples of applications where conduction mode is used are shown.

The main outcomes are shown in chapter 4 to chapter 8. All of these chapters are formatted versions of papers submitted for publication.

Chapter 4 is based on a paper that focuses on the transition from conduction to keyhole mode by increasing power density and using different beam diameters and interaction times. A continuous wave (cw) laser system was used to study the transition from conduction mode to keyhole mode. The results show that the transition between conduction and keyhole mode is not defined by a single power density value. This transition has a range of power densities that depend on the beam diameter and on the interaction time.

Chapter 5 is based on a paper looking at the transition from conduction mode to keyhole mode for different materials. Completely different materials, in terms of thermal properties, were used in this study and the effect of power density was evaluated. A comparison in terms of penetration depth in the different welding modes was made for all the materials. The experimental results show that thermal properties like conductivity, melting temperature, vaporization temperature and thermal diffusivity have an important role in the transition between the welding modes and in the penetration depths obtained.

Chapter 6 is based on a paper that focuses on a comparison between cw laser welding and pulsed wave (pw) laser welding, using interaction time, beam diameter

and power density as welding parameters. The results show that using these parameters the two lasers have very dissimilar behaviours in terms of penetration depth. Also the pulsed wave laser shows higher efficiency when compared to the continuous wave laser under the same welding conditions.

.

Chapter 7 is based on a paper that focuses on the identification of the optimum beam diameter, where the penetration depth is maximum, for aluminium 2024 for a range of power and welding speeds. The effect of the system parameters of power and welding speed on the optimum beam diameter was also assessed. The results show that these parameters influence the optimum beam diameter when in conduction mode.

Chapter 8 is a final paper that compares the residual stresses obtained in keyhole mode with the residual stresses obtained in conduction mode. The residual stress characterisation was carried at the ENGIN-X strain scanner at the ISIS, UK. It was shown that although the maximum magnitude of tensile residual stress is similar in welded specimens manufactured under different welding modes the distribution profile is quite distinguished. The conduction welding mode resulted into a larger tensile stress domain as compared to the keyhole mode.

Chapter 9 summarises and discusses the impact and contribution this work in adding to the knowledge on conduction mode laser welding.

Chapter 10 present the overall conclusions from this work and it offers recommendations for expanding this research and adding to the knowledge on conduction mode laser welding.

3 Literature review

The background and motivation that lead to this research is explained. A very succinct introduction to laser welding mainly focused on the applications is shown. The current definition of conduction laser welding mode and where does it start and finishes, based on the power density, is shown and discussed. This definition is the basis of this PhD project and most of the work done was surrounding this topic. Some studies focused on conduction laser welding are also shown and discussed, emphasizing the effect of beam diameter in this mode. A comparison between continuous wave and pulsed wave laser is given to give a better understanding of the work done in comparing this two laser types. Finally an overview of the most relevant applications of conduction laser welding mode in industry is shown. The idea is not only to emphasize how good and diverse the applications of this welding mode are, when compared to keyhole laser welding, but also to understand the flexibility of this welding process.

3.1 The use of laser welding

Since the introduction of laser in the 1960s the use of lasers in joining materials has increased considerably[2]. The variety of lasers, like the CO_2 laser, the Nd:YAG and more recently fibre laser, disk lasers and high power diode lasers come to increase the use of lasers by the industry.[2-16]. The applications of laser welding are very broad. Industries like automotive and aerospace, due to their use of light-weight structures, are the main users of laser welding [17-25].

Figure 1 - Photo of the AIRBUS A380 that has 8 welded panels in the lower fuselage (see arrows) and on the right the weld and the final panel[26]

But not only automotive and aerospace industries use laser welding. Industries like shipbuilding[27, 28], the pipeline construction[29-31], medical appliances[32-36], jewellery[37] and even in nuclear power plants[38] apply laser welding. There variety of materials where laser welding is applied is also very broad. Materials like aluminium[27, 39-46], stainless steel[47-50], titanium[51-57], copper[58-60], magnesium[61-66] and even high strength steels[67-72]. The literature about the use of laser in welding these different materials is extensive. It is clear that the range of application of laser welding is very extensive not only where it is used but also on the materials welded with this process. However the full scope for application of laser welding, partially due to quality issues, is still quite restricted.

3.2 Comparison between keyhole and conduction laser welding

There are two main operational regimes in laser welding, keyhole and conduction laser mode[1, 3]. The main difference between these two modes is the power density used in each (this will be discussed in the Chapter 3.3 - Study of the transition between conduction and keyhole mode). In this chapter the focus will be on the process differences between these two welding modes, like productivity, stability, spatter and others. The characteristics of keyhole laser welding led industry to focus on this mode. In fact all the applications mentioned in Chapter 3.1 were done using keyhole laser welding. The main characteristics of keyhole laser welding are the large penetration depth, the small heat affected zone and the high productivity of this process [3, 73, 74]. However, keyhole welding also shows several problems that may lead to high levels of porosities, instabilities, spatter (Figure 2) and other weld defects [3, 40, 75-83]. For example keyhole laser welding of aluminium shows numerous problems/difficulties. The high thermal conductivity, low boiling point elements and low viscosity are just some of the characteristics of aluminium alloys that lead to defects like loss of alloy elements, degradation of mechanical properties, excessive porosity and blow holes and to an unstable process when keyhole laser welding [81, 84-90]. Ion showed in a review paper how different aluminium series behave when keyhole laser welded. For example, when laser welding a 5000 series there is significant vaporisation of magnesium. This vaporisation creates fluctuations in the keyhole mechanism and it affects the properties of the weld. This results in coarse porosity and in an irregular weld beam. Also, the magnesium losses to the vaporisation reduces solid solution hardening and degrades the tensile strength and ductility in comparison with the base material [91]. In terms of the laser system, keyhole laser welding requires a relatively good beam quality[92].

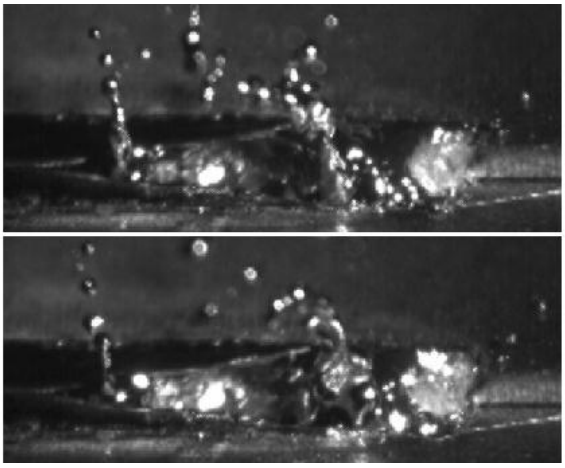

Figure 2 - High speed images of a blowout event that originates spatter in keyhole laser welding[82]

One the other hand conduction laser welding shows several advantages that have been neglected by the industry. This welding process can be a viable alternative to keyhole laser and to arc welding. The main advantage of this mode is that no vaporization takes place. Because of this the welds show no porosity, no cracks, no undercut and the welds are spatter free. It is also a stable process which allows a better control of the heat delivered to the work piece. The use of larger beams in this mode reduces fit-up problems and the laser system used does not require a high beam quality[92]. One of the disadvantages attributed to conduction mode welding was that the penetration depth of the welds was small, around 2 mm[93]. Recent work has shown that it is possible to obtain high penetration depth, see Figure 3, using conduction mode welding and that this penetration is related to the parameters chosen[92] (this will be discussed in more detail throughout this work).

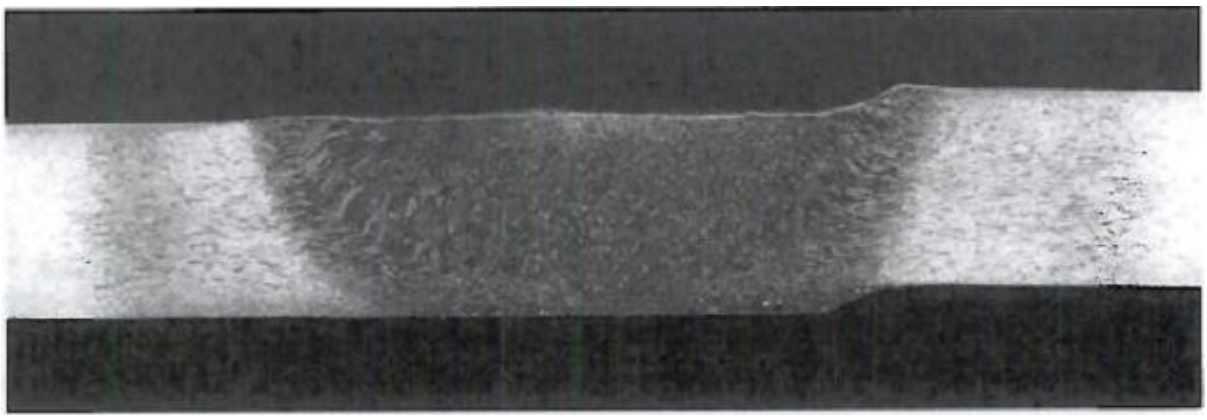

Figure 3 - Conduction laser weld with 6.35 mm of penetration[92]

One of the disadvantages of conduction mode laser welding is the coupling efficiency of this process, especially when welding high reflective materials. Coupling is basically the percentage of energy that comes from the laser that is absorbed by the material. In keyhole laser welding most of the beam is absorbed, however in conduction the amount of laser beam absorbed by the material is smaller. For example, when laser welding stainless steel the absorption of the laser beam in conduction mode is around 15 % while in keyhole mode it jumps to 65%[94]. The increase of the absorption is a good indicator of the formation of a keyhole due to the increase of the coupling. However, the values of coupling depend on several factors, like the wavelength of the laser, the surface condition, the material and the thickness of base material [89, 94, 95]. Some studies have been made in measuring the coupling for different materials. While for steel the coupling was between 20 and 90% in aluminium it varied from 10 to 80%[95-97].

Table 1 - Advantages and disadvantages of conduction and keyhole laser welding

Process	Advantages	Disadvantages
Keyhole laser welding	Low heat input which results low distortion Deep penetration welds with a high aspect ratio High productivity	Unstable process High levels of porosity High amount of spatter Loss of alloy elements Degradation of mechanical properties Less gap bridging ability/High fit up tolerance Requires a laser system with a relatively good beam quality
Conduction laser welding	No vaporisation takes place – which means no porosity, no crack and no undercut on the welds No spatter during welding Stable process with control of the heat input Good gap bridging ability due to the large beams used Does not require a laser system with a high quality beam	Low coupling efficiency Slow process/Low productivity High heat input which means higher distortion

A brief comparison between conduction and keyhole mode is shown in Table 1.It is these characteristics, completely different from the characteristics of keyhole laser welding, which make conduction mode laser welding an interesting welding process. Due to the differences on the welds obtained and on the welding process itself conduction laser welding tends to increase the applications of laser welding and not “compete” with keyhole laser welding.

3.3 Study of the transition between conduction and keyhole mode

Due to the simple nature of conduction mode not much research as gone to this process. However new research areas, like hyperbaric laser assisted welding and dissimilar materials laser welding, resulted in an increased interest in conduction mode. The major difference between conduction and keyhole welding is the power density applied to the welding area. When the power density used is insufficient to cause boiling the weld occurs in conduction mode. The alternative to this mode is keyhole mode welding, in this case the power density is enough to provide evaporation and open a hole in the melt pool. Despite different studies of these two welding modes the boundaries between them are not clear in terms of processing parameters. Often it is considered that conduction welding occurs when the power density is lower than 10^6 W/cm^2 [98-100] this value being completely independent of the welding speed and the beam diameter used. It is also sometimes considered that conduction welding occurs when the value of the laser power is low, of the order of one kilowatt; at this low value the power density at the surface of the weld material is limited. Despite these different definitions for conduction laser welding, there is one fundamental point where there seems to be agreement, which is that conduction welding occurs when the vaporisation of the material is insignificant [3, 99] or when the power density is not enough to cause boiling [98]. Another definition for conduction laser welding mode is that it shows an aspect ratio smaller than 0.5[101]. Nevertheless these definitions have one thing in common, they do not take into account other welding parameters like beam diameter and welding speed. A schematic of the current definition of conduction and keyhole laser welding is shown in Figure 4.

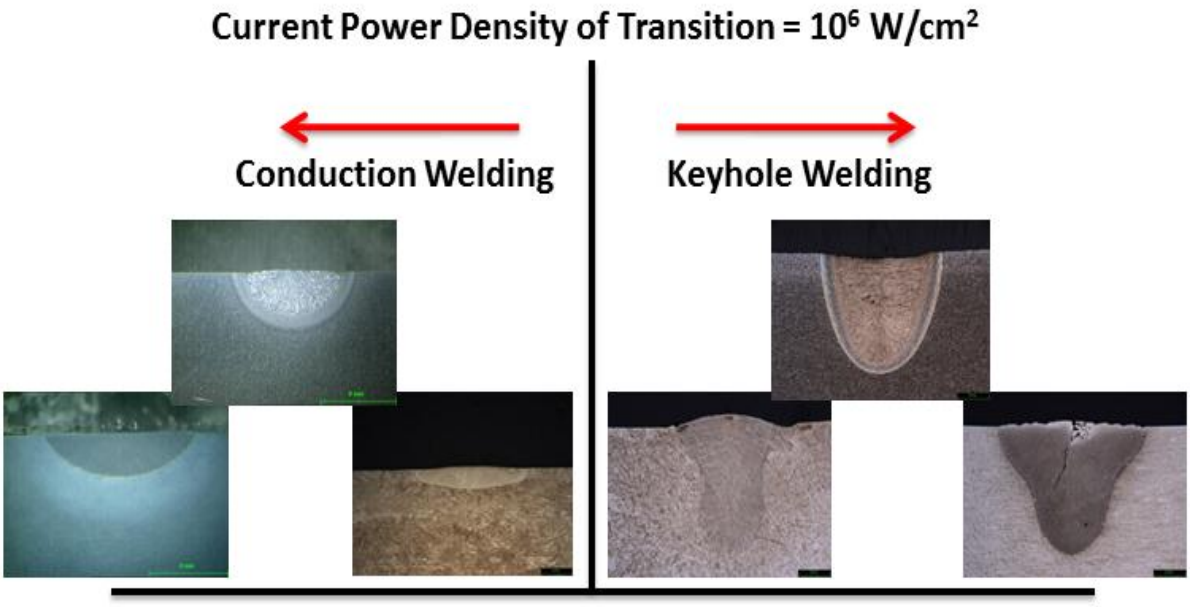

Figure 4 - Common definition of the transition between conduction and keyhole welding

There are a large number of papers, mostly based on modelling, related to the formation and the physical phenomena of keyhole laser welding [77, 102-123]. The literature in this area is extensive so a full assessment of all the work done would be exhaustive and unnecessary for this project. However, it is important to point out that none of the papers previously mentioned relate the process parameters to the formation of keyhole or evaluate the transition between conduction and keyhole mode, which is where the keyhole starts to form.

Only a few studies focused on the transition between conduction and keyhole laser welding mode were carried out. The following text shows the relevant work done in this area.

Beyer et al. studied the absorption of a laser induced plasma during laser processing for a continuous wave laser[124]. The main focus of this paper was not the study of the transition between conduction and keyhole mode. However, a relation between power density, interaction time and beam radius and the threshold power density for vaporization was established. Mainly in the region of laser welding (between 1 and 100 ms of interaction time) where the power density necessary for vaporization is dependent on the beam radius and on the material,

Figure 5. Regarding the interaction time the power density for vaporization it did not show any dependence, there was just a small effect at 1 ms interaction time for steel. However, this paper did not give any explanation for this effect. This part of the paper relied on an analytical equation that represents the temperature at the surface of the material at the centre of a Gaussian beam[125].However, no final conclusion related to the transition between conduction and keyhole laser welding was made.

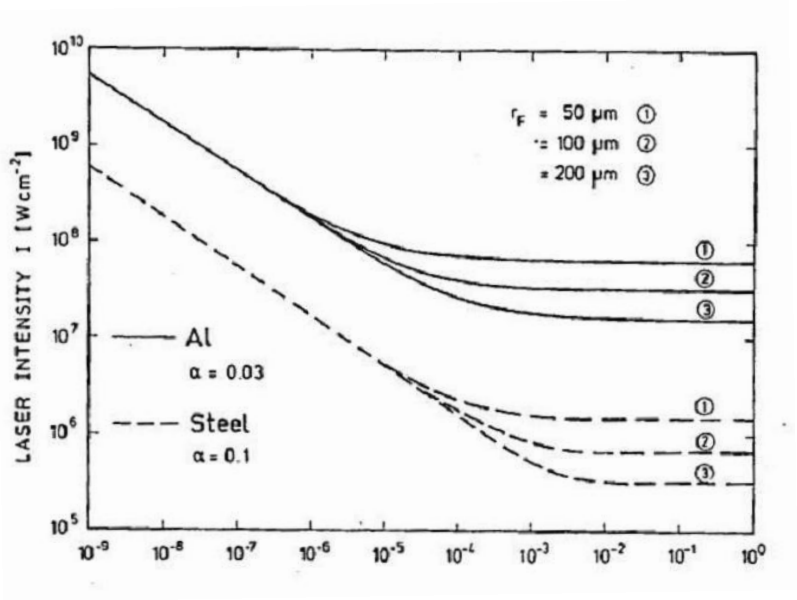

Figure 5 - Laser power density necessary to reach vaporization temperature at the centre of the beam as function of time[124]

Liu et al. [126, 127] studied the effects of process variables on pulsed laser welding, for stainless steel and aluminium, Figure 6. They concluded that the power density at which keyhole mode starts is almost independent of the pulse duration. However there was a change in the power density at which keyhole starts depending on the material. This was, in part, in agreement to what was previously considered to be true [125]. However, the threshold power density, for when keyhole starts, for Stainless Steel was 4 X 10^6 W/cm^2 and 10^6 W/cm^2 for Aluminium (which in the case of the Stainless Steel is different from the 10^6 W/cm^2 mentioned previously) and so dependent on the material [126, 127] . This study did not consider the laser beam diameter as a process variable that influences the power density, that was changed by changing the power, where keyhole starts. Also the identification of a conduction weld and a keyhole weld was done based on a single aspect ratio (depth/width), if it

was over 0.4 for stainless steel and 0.2 for aluminium than the weld was done in keyhole mode. And once again this value that separated conduction mode from keyhole mode was considered to be independent of the interaction time.

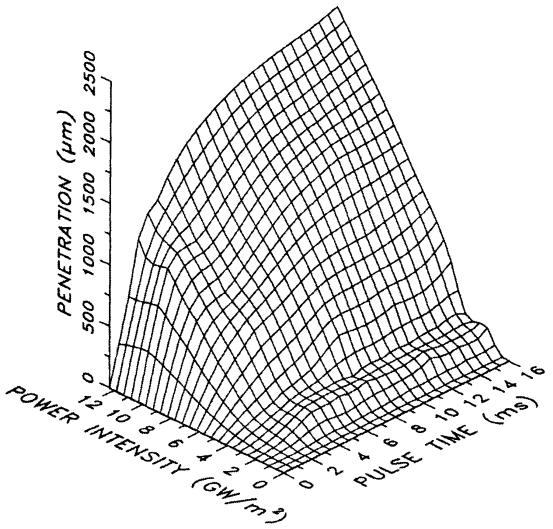

Figure 6 - Variation of penetration, for aluminium, with the power density and the pulse time[126]

Zhang et al. [128]studied the transition between the different laser welding modes using a continuous wave laser. In his work he concluded that laser power, focal position and travel speed will influence the welding mode. However the described double-U curve, Figure 7, is difficult to apply in a more broadened parameters range. By changing the beam diameter, with constant welding speed, the process parameters of power density and interaction time were also changed, making the interpretation of this curve more difficult. However he was able to evaluate that there is a transition mode between conduction and keyhole. This is opposite to what was shown previously, that there is a sharp transition between these two modes.

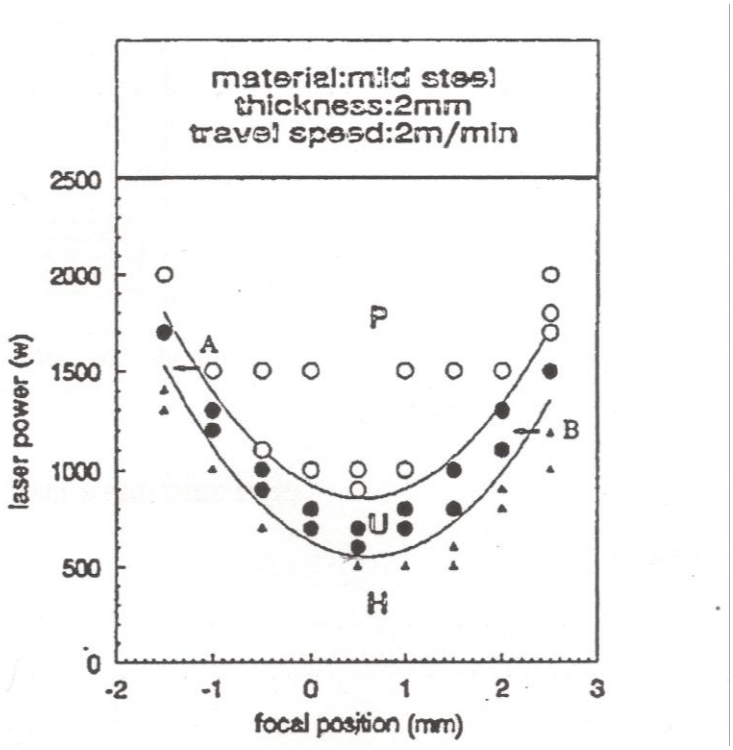

Figure 7 - Mode transition curve (double-U curve) determined by laser power and focal position. Where the empty circles represent welds done in keyhole mode, the full circles welds in the unstable mode(transition mode) and the triangles welds done in conduction mode[128]

Buvanashekaran et al. [129] using a finite-element model evaluated the welding mode based on different energy levels. They concluded that there was a range of power densities were conduction mode takes place, between 10^3 and 10^4 W/cm^2. At a welding speed of 1000 mm/min and with a beam diameter of 0.6 mm it was concluded that the transition from conduction to keyhole mode took place with 400 W of laser power. In this work despite concluding that there was a range of power densities were conduction mode took place no relation between the parameters and the welding mode was made.

Sibillano et al. [130] used real-time monitoring of the plasma, formed during the different welding regimes, to identify the welding mode. In this study a continuous wave CO_2 laser was used. The study of the plasma emission produced in laser welding was done by analysing the chemical species present in the plasma. He was able to correlate the spectroscopy data with the switching between the different

welding modes. However this study showed no relation between the welding parameters and the welding mode. It also relied on the definition that the welding mode is defined based on the power density used (>10^6 W/cm^2 for keyhole and <10^6 W/cm^2 for conduction).

Nakamura et al. [101] studied the optical and acoustic emissions from a continuous wave laser irradiated spot. By analysing the optical and acoustic emissions from the laser irradiated point he was able to evaluate the transition between keyhole and conduction mode. However the identification of the welding mode was based on the ratio between penetration and width. If the ratio was smaller than 0.5 than then weld would be in conduction mode, if it was higher it would be in keyhole mode. For a spot size between 0.23 and 0.29 mm he suggested that at 3kW the transition between conduction mode and keyhole mode would take place at a range between 6 to 8 m/min for a stainless steel (SUS 304), between 3 to 4 m/min for a mild steel (SS 400) and between 2 to 3 m/min for aluminium (A5083). However, no relation was established between the welding parameters and the welding mode. Also, the use of a single value, independent of the material, for the ratio that separates conduction mode from keyhole mode opposes what was shown by Liu et al. [126, 127].

All these works do not relate the transition from conduction to keyhole to the process parameters and how the process parameters influence the transition between conduction and keyhole. In some points the works even show different conclusions. For example, while in some cases it shows that there is a sharp transition between conduction and keyhole regime, for example in the work shown by Nakamura et al. [101]. In other works a regime between conduction and keyhole regime was identified, like it was shown it the work by Zhang et al. [128]. The presence of two or three welding modes in laser welding is also a common difference in some works. The following text shows some examples of those differences.

Zhang et al. [128] identified three kinds of laser welding process, stable Heat Conduction Welding, stable Deep Penetration Welding and Unstable Mode Welding. The existence of this Unstable Mode Welding or Transition mode was attributed to thermal focusing or to an unsuitable selection of the welding parameters. The existence of this unstable mode, which was attributed to welding mode fluctuation, was previously identified by Chen[131] and Zhang[132].

The existence of just conduction mode regime and keyhole mode regime in pw laser welds was investigated by the use of a model. The model showed by *Semak*, which is an integration of Von Allmen's model and Anisimov's model [133-135], relates metal displacement to the vaporisation recoil pressure [134]. In this model the melt displacement happens when the vaporisation recoil pressure accelerated the melt created in the fusion zone allowing this molten material to reach the edge of the molten pool. In this model it was possible to identify three different thresholds. One for when melting starts to take place, another for when displacement starts to happen and another for drilling. In this model *Semak* observed that at energies levels lower than the drilling threshold and higher than the displacement threshold was where the keyhole mode regime took place. On the other hand he assumed that the regime between the displacement threshold and the melting threshold was when the conduction mode regime took place[134], Figure 9. In this work no regime was identified between conduction and keyhole regime.

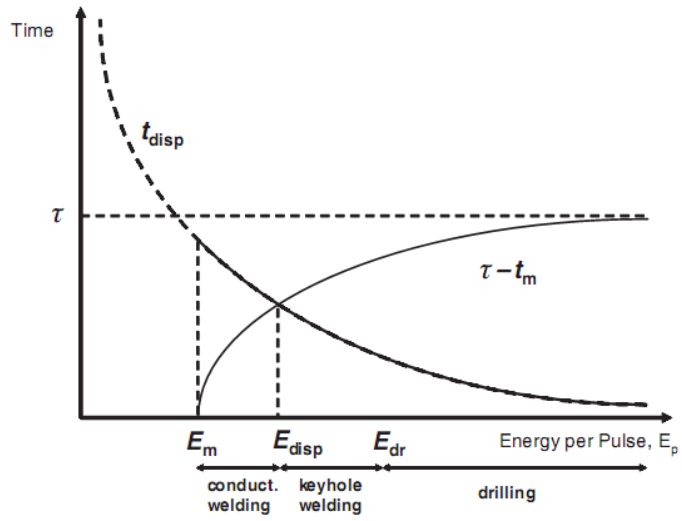

Figure 8 - Identification of the different welding regimes, conduction and keyhole, in pulsed laser welding by Semak[134]

Colegrove et al. [136] work, based on the Von Allmen drilling model, identified three different regimes in pulsed laser welding. They were conduction mode, mixed mode and keyhole mode regime, Figure 10. In the conduction mode the evaporation is limited, and the melt pool is responsible for the weld shape. In the mixed regime evaporation starts to become relevant, however the summation of the hole (caused by the evaporation of material) and of the molten material depth does not suffer a

considerable increase. In the keyhole regime the molten layer is extremely thin when compared to the depth of the hole, and the depth of the weld is mainly due to the depth of the hole. The presence of these three regimes had also been shown previously by Steen[98] and Ahmed[137].

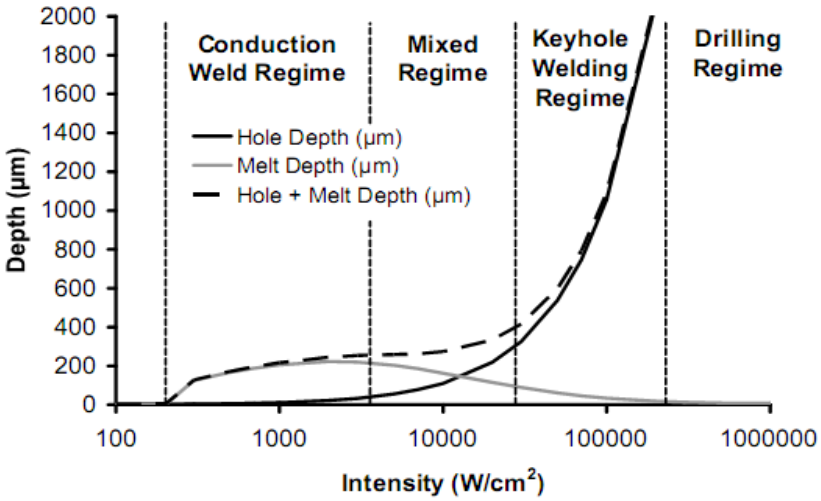

Figure 9 - Identification of three welding mode in pulsed laser welding [136]

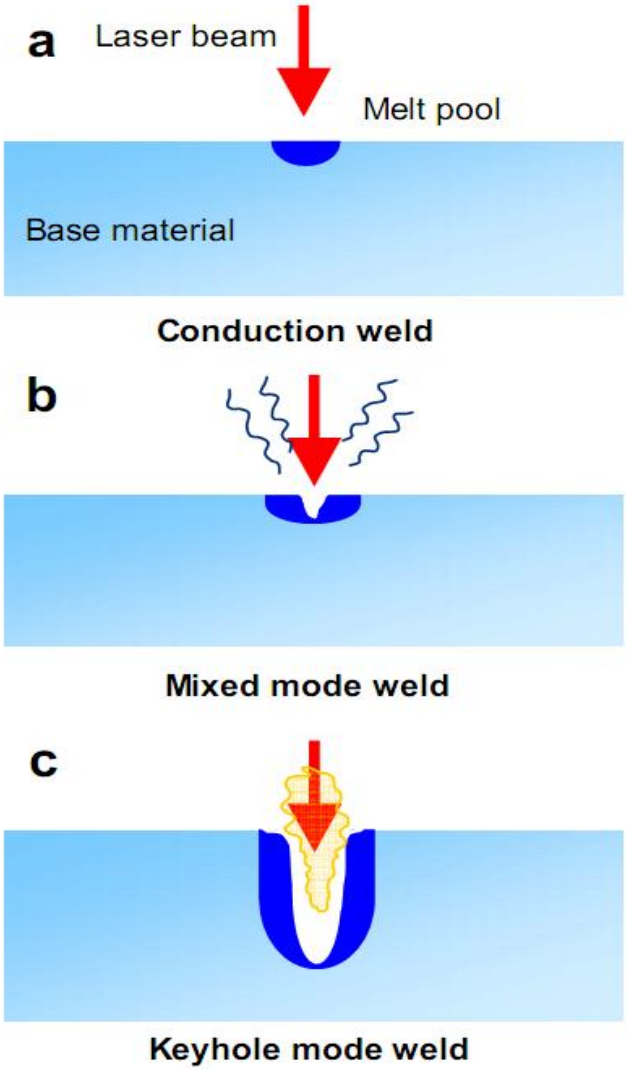

Figure 10 - The three welding regimes in pulsed laser welding[136]

Buvanashekaran et al. [129] identified three laser welding modes that are determined by the laser power and welding speed. Although, he establishes that the transition between conduction and keyhole for a 1000 mm/min welding speed would occur at 400 W beam power. If a mode between conduction and keyhole was identified these values should represent the end of conduction or the beginning of keyhole mode and not the transition between this two modes.

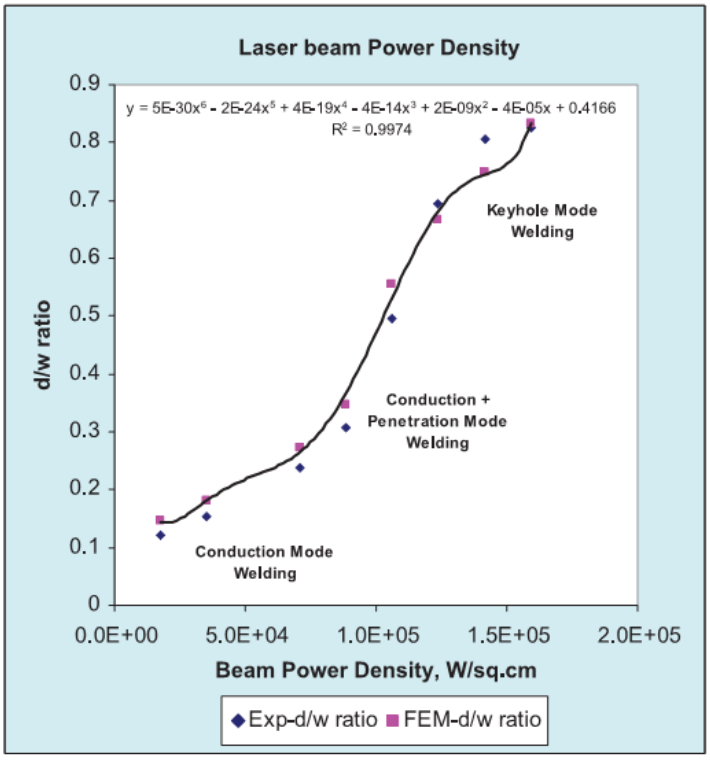

Figure 11 - Identification of the three welding modes showed by Buvanashekaran[129]

In Sibillano et al. [130] work he also identified a mixed mode in laser welding. He defined this regime as having properties of both conduction and keyhole. This was noticed when the power density was just over the threshold for keyhole mode and so it was assumed to be caused by unstable keyhole formation.

Based on the literature review the threshold of conduction laser welding mode is confusing and does not take into account the process parameters. The number of regimes and if the transition between conduction and keyhole mode is a sharp or smooth transition is also unclear and quite confusing. With several authors contradicting each other.

The following questions were identified during this literature review.

- Is the power density that limits conduction laser welding mode from keyhole mode independent of the process parameters, such as interaction time and beam diameter? If not, how will it change with the beam diameter or with the interaction time?

- Is the transition between conduction mode and keyhole mode a sharp transition or is there a regime between?
- Are these effects different in a continuous wave laser when compared to a pulsed wave laser?

3.4 Conduction laser welding background

Conduction welding mode is mainly controlled by convection and conduction. In the specific case of laser welding at high power densities a temperature gradient will be formed that itself will lead to surface-tension gradient also known as Marangoni effect. The literature about Marangoni effect is extensive, work done by Zhao[138] , Limmaneevichitr[139-141] and Chan[142, 143] are just a few examples . This effect is responsible for the geometry of the laser melt pool, like its shape and aspect ratio. The composition of the melt pool during conduction laser welding is also influenced by the Marangoni effect, mainly due to the fact that this effect is responsible for the mixing of material that happens during the laser welding process[144]. In this mode the energy is absorbed at the surface and by thermal conduction is transferred to the interior of the material [3]

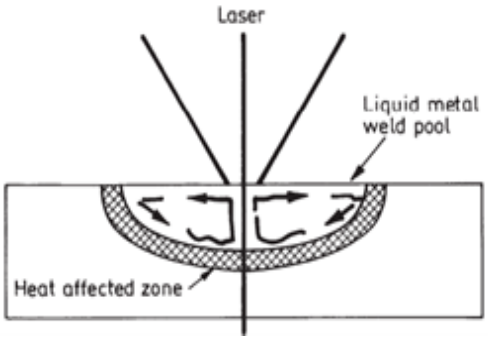

Figure 12 - Schematic of conduction laser welding[98]

Conduction welding can be a viable alternative to keyhole welding mainly due to the fact that it is a very stable process and easier to obtain high quality welds free of pores and spatter [145]. This mode takes place when the vaporisation of the material is insignificant, in other words, when the thermal power density is not high enough to cause boiling [146]. Another advantage of conduction laser welding is that it can be made with a significantly low laser cost, because it does not require a high beam quality or a very high power [99].

Some studies, based on modelling and followed by experimental validation, have shown that there is an optimum beam diameter, this means that for a certain value of power and travel speed there is a specific beam diameter in which the penetration is maximum. This phenomenon occurs when by increasing the beam diameter the temperature at the surface remains at vaporisation temperature. In other words, when welding in conduction mode a progressive increase in the spot size will result in an increase in penetration depth as long as the temperature at the surface of the work piece is maintained at boiling temperature, however when the optimum beam diameter is achieved the increase of the spot size will result in a decrease of the penetration depth because by increasing the spot size the temperature at the surface will decrease, which means it will be lower than the boiling temperature [92, 146] [145, 147].

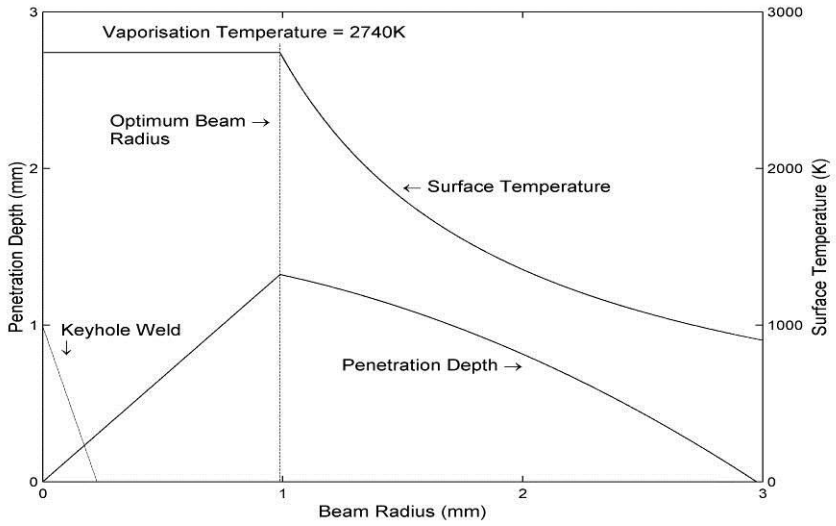

Figure 13 - Variation of the surface temperature and the penetration, with beam radius, in aluminium for a constant power and welding speed [92, 146]

Based on this principle, Figure 13, Bardin was able to control the conduction mode welding process by thermal measurements. Controlling the temperature of the welding process, keeping it just below the boiling point of the material, allowed him to obtain the maximum penetration. He also noticed that when the temperature went over the boiling temperature the presence of porosity was clear [146, 147].

One of the first works on conduction laser welding was done by Esposito et al. [148]. An evaluation of the welding parameters based on a theoretical model and experimental data was showed. One of the conclusions was that the temperature

was controlled by the beam diameter and that the raising of temperature over the boiling point would reduce the process efficiency. It was also concluded that the welding speed was related to the width desired of the weld and that the choice of the beam diameter was made by choosing a beam diameter that would provide a better coupling of the beam energy with the welding pool. He concluded that it was the beam diameter that controlled the temperature of the weld pool and that by controlling and choosing the correct beam diameter the efficiency of the welding process could be maximised[148]. However in this work the relation between welding speed, beam diameter and laser power was not fully discussed and evaluated. The principles behind this work were correct. The issue was how it related the choice of the beam diameter to the coupling and not to the control of the maximum temperature at the surface of the weld pool (as shown previously).

Paul and DebRoy [149], based on numerical solutions of Navier-Stokes equation and the equation of energy conservation, simulated the weld pool shape and the peak temperature. The results showed a good approximation to the experimental data however no evaluation of the welding parameters on the weld shape was made. They also shown that the temperature achieved in the laser-material interaction was close to the boiling point of the material. This part emphasizes that in this welding mode the no vaporization of material takes place. Zhao and DebRoy [150] also evaluated the composition change in conduction mode laser welding of aluminium. They noticed that when vaporisation takes place in conduction mode it is confined to a very small region under the laser beam. This vaporisation takes place due to a slight increase of the temperature over the boiling point of the aluminium. However based on Paul and DebRoy [149] in conduction mode the vaporisation of material should be zero.

An interesting work was done by Kell. He evaluated the use of different beam profiles in conduction laser welding, maintaining the same energy density for the different beams profiles. The used beam profiles were; Gaussian, Top-Hat, Rugby Post and Peaked edge line[151].The conclusions shown were more related to the macrostructure/weld pool dimension obtained by each beam profile and on the welded profile. However, based on Figure 14, the assumption of the paper that all the welds were made in conduction mode does not seem to be completely correct.

While the weld profile obtained using the peaked edge line is clearly in conduction mode the weld profiles obtained using the other beams might not be. The reason might be related to the irradiance distribution obtained in all the profiles, which in the case of the peaked edge line might be more suitable for conduction laser welding.

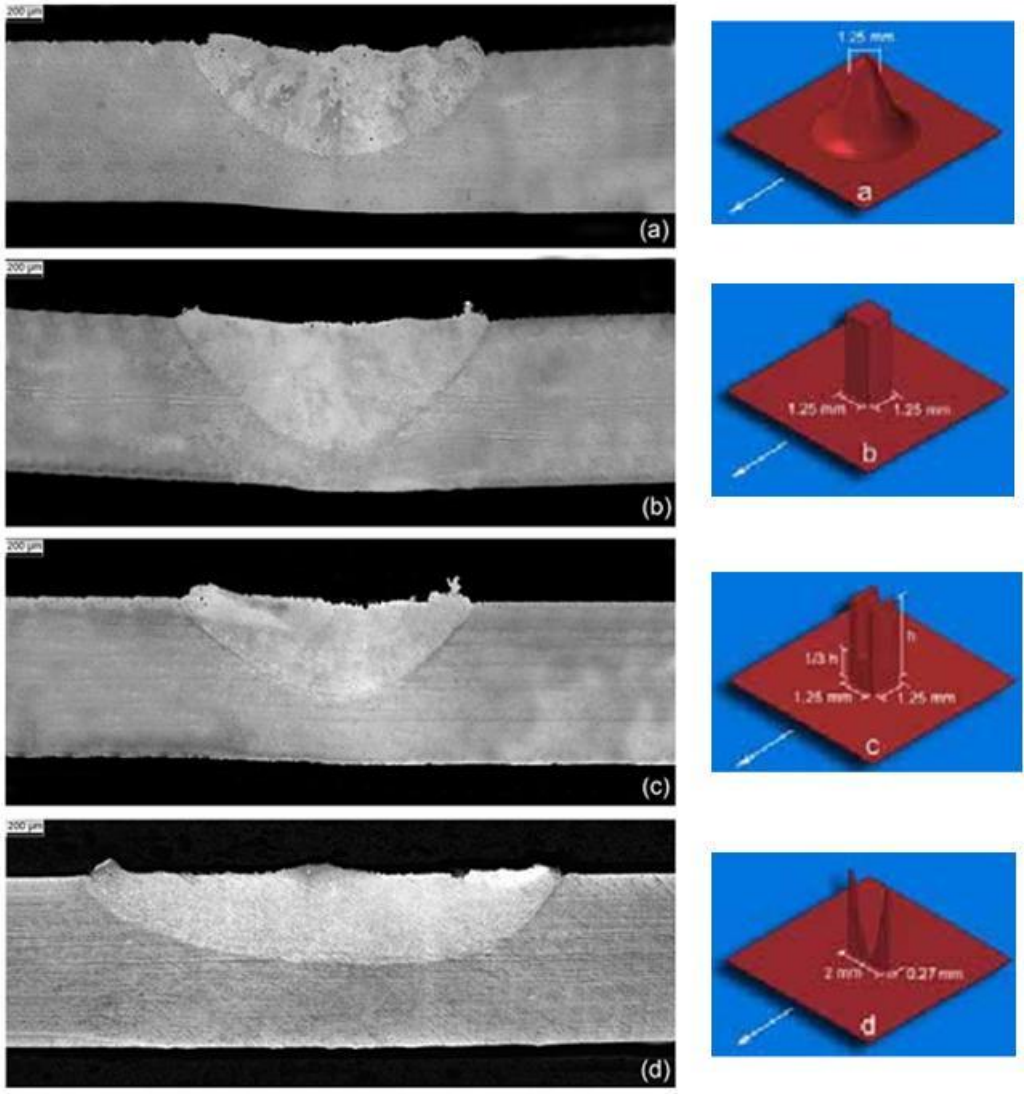

Figure 14 - Micrographs and respective beam profiles of the welds obtained a) Gaussian, b) Top-Hat, c) Rugby post and d) Peaked edged line[151]

There have been some relevant studies on conduction mode laser welding, especially the work done by Morgan[92], Bardin[146, 147] and Okon[145]. These studies will be the base for part of this thesis, especially in comparing the effect of power, welding speed and beam diameter in different materials.

3.5 Types of laser

This part of the literature review will give a very quick overview of the two main types of lasers, pulsed wave laser (pw) and continuous wave laser (cw)[3]. Focusing on the different welding parameters normally associated to each laser type. The main difference between these two lasers is the Power Output, Figure 15.

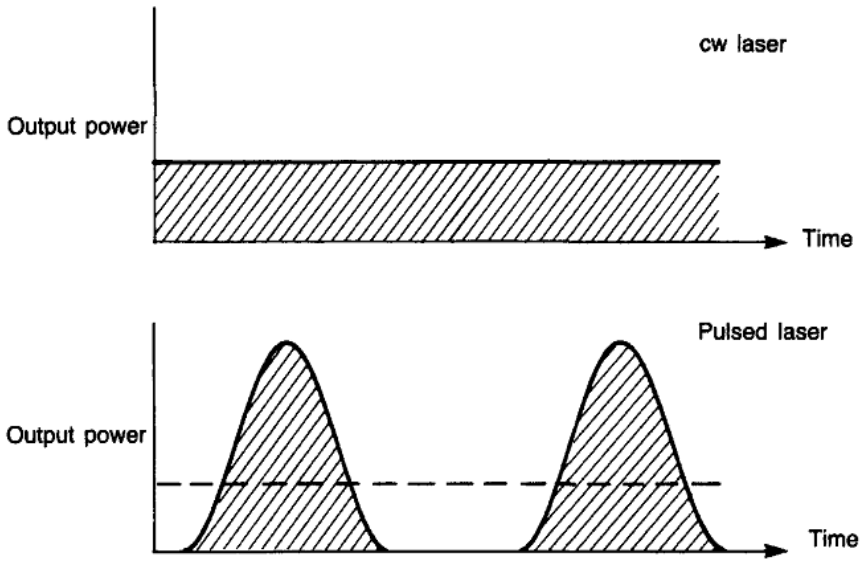

Figure 15 - Difference between the Output power of cw and pw. The energy (that is represented by the shaded area) is concentrated in pw laser[152].

More information about these two lasers can be found on text books (Ready[3] and Breck[152]). The differences between cw and pw laser are also translated in the process parameters normally used in both lasers. The normal parameters used in cw laser welding are welding speed, power and beam diameter [153, 154]. On the other hand, the parameters normally used in pw laser welding are pulse duration, pulse energy, average peak power and beam diameter [155-158]. So the difficulty in comparing these two lasers is in using the same parameters.

There have been a lot of studies on pw[138, 159-167] and cw[49, 108, 116, 117, 168-171] laser welding. However, there are fewer studies that compare cw and pw laser welding. One of the few works done in comparing these two types of lasers was done by Kuo et al. [172]. In his work he compared a pulsed and a continuous Nd:YAG laser in welding an Inconel alloy. Maintaining the same mean power, also known as average power, and the same beam diameter he evaluated the welds

obtained using different welding speeds and different peak to base power ratio. The work was not carried out with a pulsed laser but with a modulated cw laser. Also there was no “off-time” of the laser, like normally seen in pw lasers. Despite this work focused more on the porosity shown by the welds some interesting effects could be observed. It is possible to see that having a higher peak power, with the same welding speed, a higher penetration is achieved. For example, with a welding speed of 1300 mm/min full penetration was achieved with a peak power of 3090 W while it was not achieved with a peak power of 2590 W.

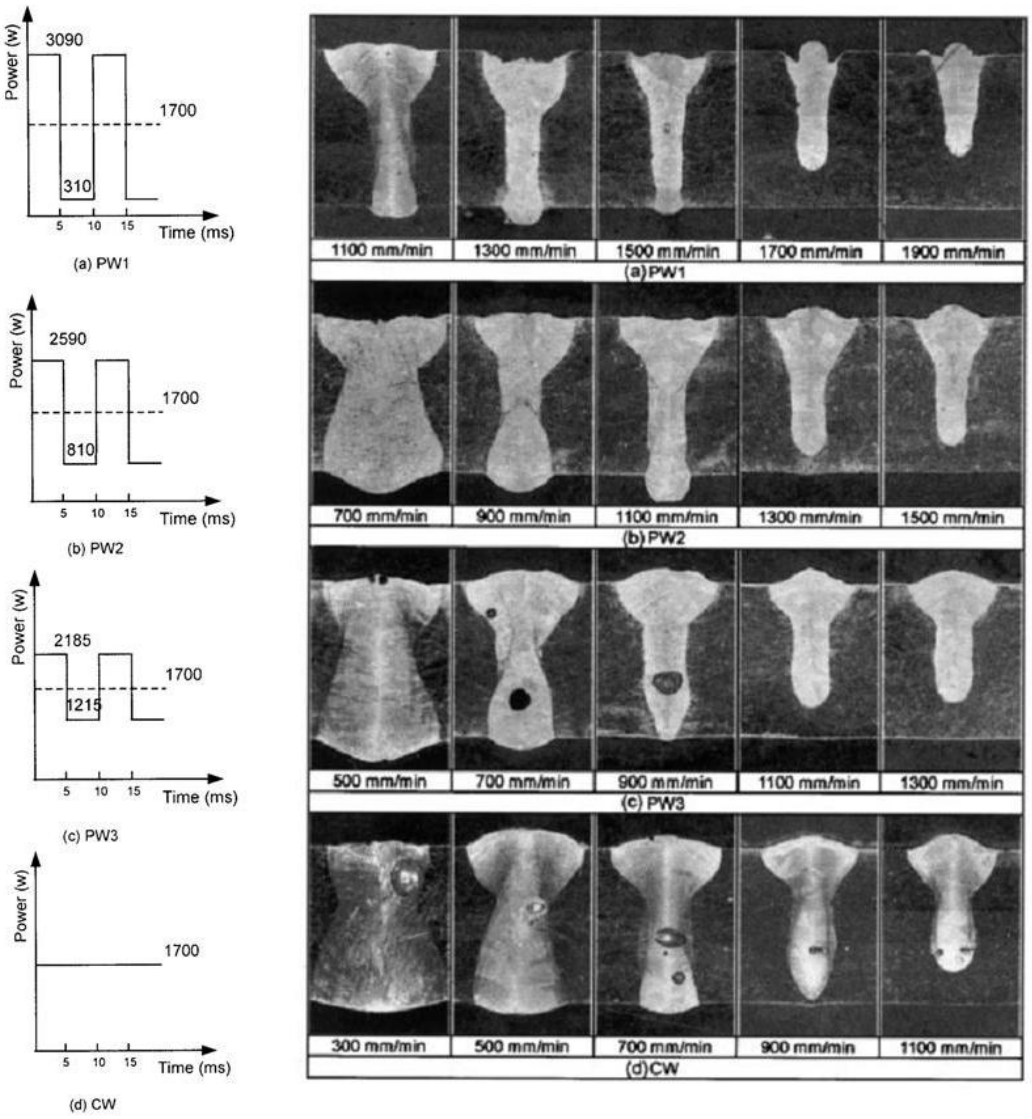

Figure 16 - Power output waveforms and respective macrographs[172]

Kuo et al. [41] used the same type of approach to evaluate the effect of pulse level in aluminium alloys. The results shown in this work were contrary to the results done on

the Inconel alloy. It was observed that in order to obtain full penetration it was required a slower welding speed for a pulse with higher peak power than it was for the continuous wave. In both works there was no justification for these two completely distinguished phenomenons.

Fuerschbach et al. [173] using power density as a common parameter for cw and pw compared these two types of lasers. He observed that using the same power density the penetration obtained in a cw CO_2 laser was higher than the penetration obtained using a pw Nd:YAG laser. However this comparison was not accurate. Mainly because there was no co-relation between the welding speed and the beam diameter of the cw CO_2 laser welds and the pulse duration and beam diameter of the pw Nd:YAG laser. This means that the comparison might have been done at completely different interaction times and beam diameters, which makes the comparison between these two laser types incorrect.

Ludovico et al. [174] evaluated the use of a CO_2 cw laser and of a Nd:YAG pw laser in welding a AA2024 aluminium alloy. In this work no comparison between the two lasers systems was made and the work focused on the possibility of welding AA2024 using either laser source. This work is an example on how, normally, a comparison between a cw and a pw laser is carried out. A comparison made between using a laser system for a specific application rather than a like for like comparison. Where the parameters chosen for the pw laser welds are similar to the parameters used in the cw laser welds.

In terms of applications pw laser welding is normally associated to micro welding, mainly due to the precision of this type of laser.

It is clear that a comparison between these two laser types, using the same process parameters, has rarely been done. Mainly because the parameters used for this two laser types are different, this makes the relation between each laser type parameters more difficult to achieve. The comparison between this two laser types is relevant for this work. This will allow an understanding if there is any difference in behaviour in conduction laser welding using a pw or a cw laser.

3.6 Applications of conduction mode

The number of applications that use conduction laser welding is very low when compared to the number of applications that use keyhole laser welding. Even the works that used conduction laser welding do not mention this welding mode. In these cases a closer look at the welding parameters proves that this mode was used. One of the first application of conduction laser welding goes back to 1970, when it was used to weld thermocouples to a sample container carried by the Apollo space shuttle[175]. Other applications like welding seals of electronic packages[176], welding non precious dental alloys[177] and welding cardiac pacemaker batteries[178] have used conduction laser welding.

One of the applications that conduction laser welding has been most used is in welding aluminium alloys. The issues of welding aluminium alloys using keyhole laser welding have been discussed in Chapter 3.2 - Comparison between keyhole and conduction laser welding. These problems in using keyhole in laser welding of aluminium alloys can be overcome by using conduction laser welding. Some examples of the application of conduction laser welding in aluminium is the work done by Morgan[92],by Okon[145] and by Sanchez-Amaya[100, 179]. The results showed that by using conduction mode laser welding it is possible to obtain welds free of pores and cracks, two defects normally associated to laser welding of aluminium. In terms of the penetration achieved Okon was able to obtain full penetration in 3 mm thick AA5083[145], Sanchez-Amaya was also able to obtain full penetration on 3 mm thick AA5083 and 2.3 mm penetration on AA6082[179], while Morgan was able to achieve full penetration on 6.35 mm thick AA2024[92].

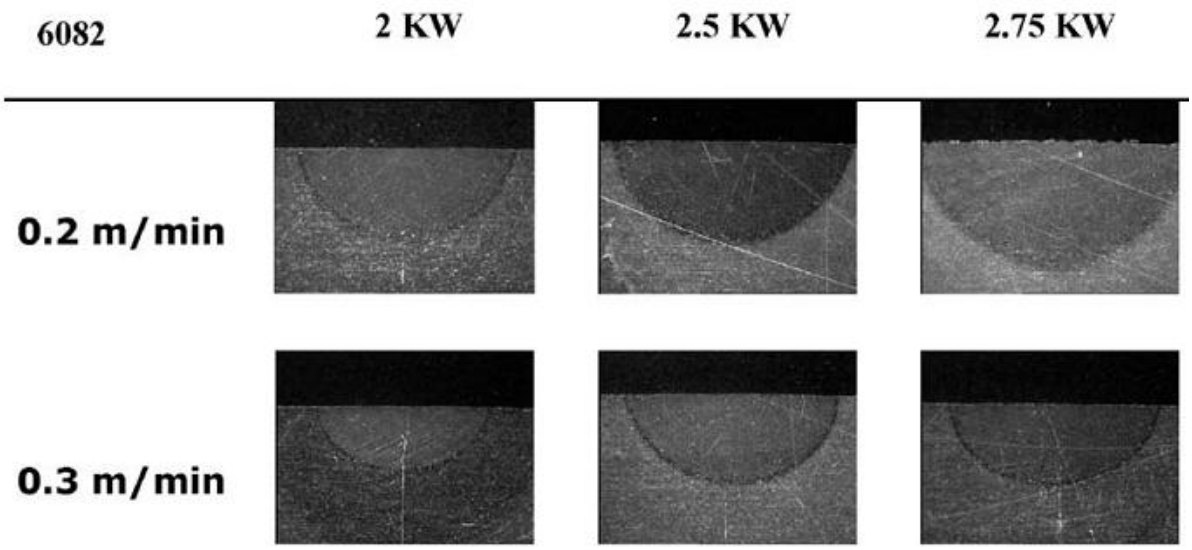

Figure 17 - Some examples of conduction laser welding in AA6083 with different power and welding speeds[179]

Another application of conduction laser welding is in joining of dissimilar materials [18, 180, 181]. One of the most used combination of materials in aluminium to steel weld. Due to the difficulty of this type of weld several studies using resistance spot welding [182, 183],arc welding [184, 185], brazing [186] and Friction Stir Welding [187, 188] have been made. However, in recent year's laser welding has been introduced as an alternative for welding steel to aluminium. Studies using keyhole welding in order to join aluminium to steel were made [189-191] but with limited success. However, studies using conduction laser welding have shown very good results [192-194]. The advantage of using conduction laser welding in this application is related to the stability of the process that allows a better control of the temperature in the interaction area between the aluminium and the steel [193].

The use of conduction mode welding on magnesium alloys has also been accessed [65, 195]. It was possible, using conduction welds, to obtain a weld with less porosity, fewer cracks and with a smaller crater. However, in these works, it is unclear if the welds were made in "pure" conduction mode. The profiles showed by the welds resemble a conduction mode. But the presence of a high vaporization in the welding process raises some issues about the use of conduction laser welding [195]. Even so the use of an "almost" conduction mode weld has shown encouraging results in laser welding of magnesium alloys.

The introduction of new high power diode lasers will increase the use of conduction laser welding[196]. Mainly because the use of this type of lasers will solve one of conduction laser welding biggest issues, the low beam absorption, due to the wavelength of these lasers. Applications like esthetical welds, brazing, cladding, soldering and polymer welding, that are normally done in conduction mode will increase[197]. Figure 18 shows some examples of conduction laser welding using a diode laser.

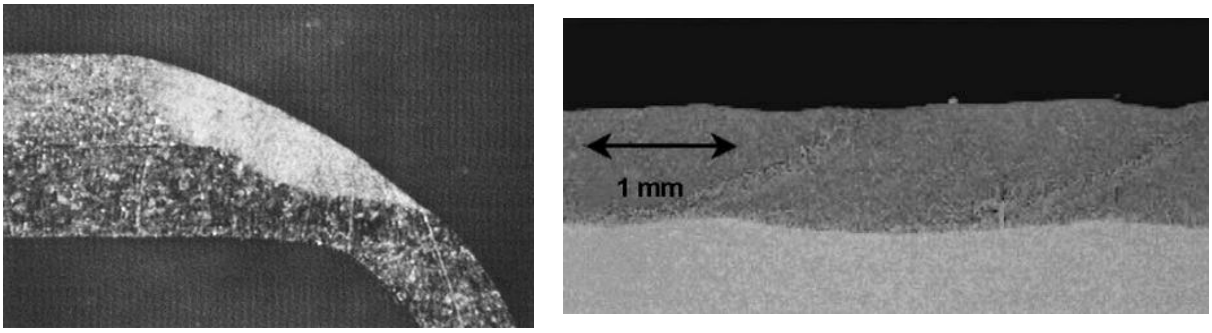

Figure 18 - Kitchen sink weld (left) and powder deposition (right)[197]

The use of high power diode laser allows the use of conduction laser welding in materials like aluminium and titanium [52, 100, 179, 196], without any concerns related to the absorption of the laser beam by the material due to the fact that the wavelength of diode lasers is better absorbed by these types of materials. Abe et al. [198, 199] showed some applications using this type of laser. However, in no part of his work he mentioned conduction laser welding mode. A closer look at the welds obtained, Figure 19, and at the characteristics of the welding process (no spatter and no plasma) it was clear that the welds were made in conduction mode. Funada and Abe also used conduction laser welding on thin film with good results [200-202].

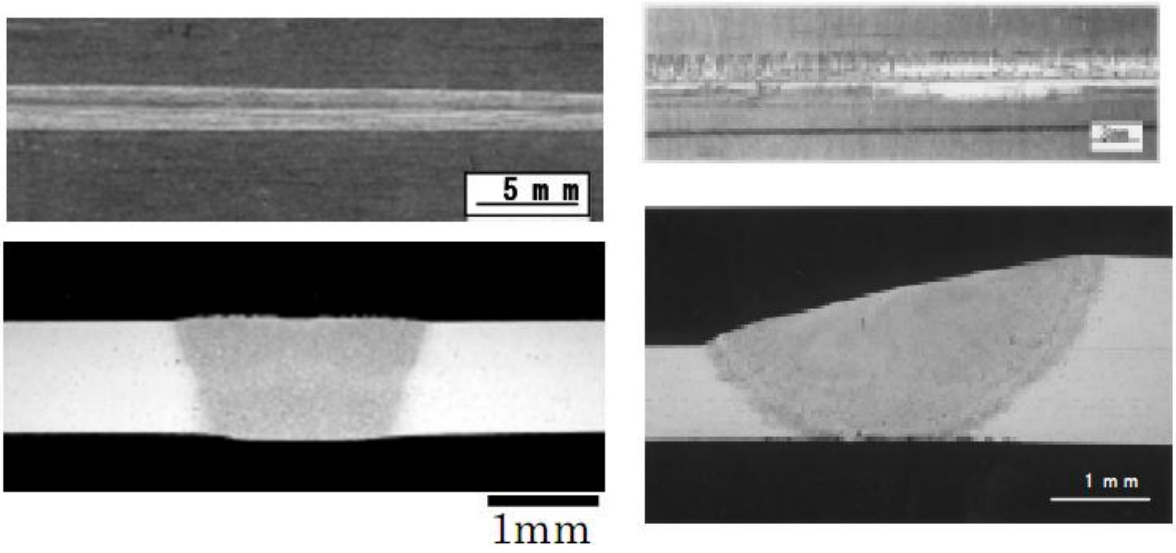

Figure 19 - Examples of conduction laser welding using a high power diode laser[198]

Bassani et a. [203] also used diode laser source to study the effect of process parameters on laser welding of an Aluminium metal matrix composite reinforced with SiC particles. In this work a comparison was made between using a CO_2 laser to create a weld in keyhole mode while a diode laser was used to produce a conduction mode weld, Figure 20. The welds obtained in conduction mode showed a good metallurgical quality and the formation of Al_4C_3 was reduced considerably when compared to the welds made under keyhole mode.

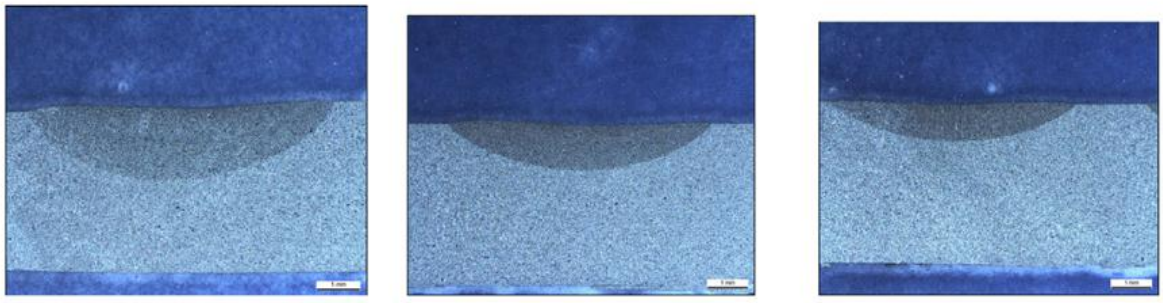

Figure 20 - Some examples of diode laser welding, in conduction mode, of A359/SiC metal matrix composite[203]

The application of a diode laser in welding titanium was also accessed by Block et al.[54]. In this work no reference to conduction laser welding was made but the

profile of the welds and the parameters used indicate that the welds were made in conduction mode, Figure 21.

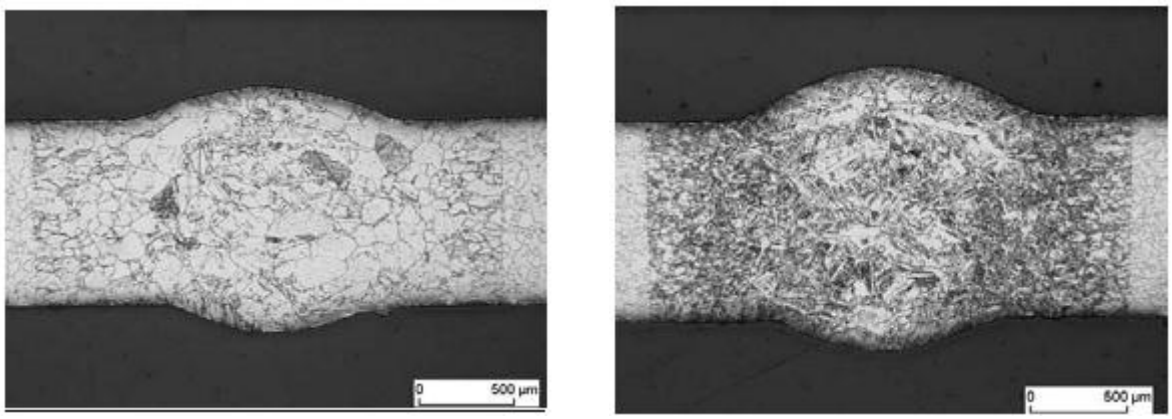

Figure 21 - Laser filler weld seams on titanium [54]

Diode lasers have also been used in laser welding magnesium alloys with good results, which include the resistance increase to corrosion and wear [204-206]. Once again there is no reference to conduction mode laser welding but the profiles shown in Figure 22, mainly the low aspect ratio, indicate that conduction was the welding mode used.

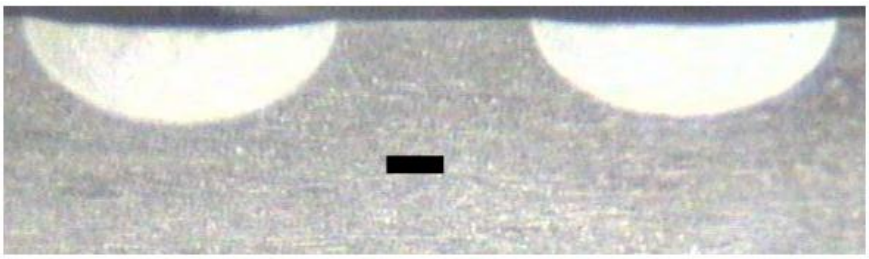

Figure 22 - Macrographs of laser welded AZ61 magnesium alloy [205]

These last applications emphasize on how the appearance of new high power diode laser will increase the use of conduction mode laser welding. With the number of applications of conduction laser welding increasing it is important to better understand the limits and the process of conduction laser welding.

However conduction mode is not only used in laser welding. Other application is laser cladding or also known as laser metal deposition [207, 208]. Despite in the

literature related to laser cladding references to conduction mode are very few. Based on the parameters used, mainly the low power densities used, the properties of the cladding process (no spatter and stable process) and the properties of the clad (free of pores) it is possible to conclude that the process is normally done in conduction mode. Some studies mention that the power densities used are below the threshold for plasma formation which means bellow the start of vaporization[208], emphasizing the fact that conduction mode is used in laser cladding. Contrary to the application of conduction mode in laser welding the number of application of laser cladding is extensive [208-217]. These types of applications is an example on how, very often, conduction mode laser welding is mistaken by keyhole laser welding. As mentioned previously the number of applications that use laser cladding is vast however it is not mentioned that laser cladding is done in conduction mode which leads to some mistakes in terms of parameterisation.

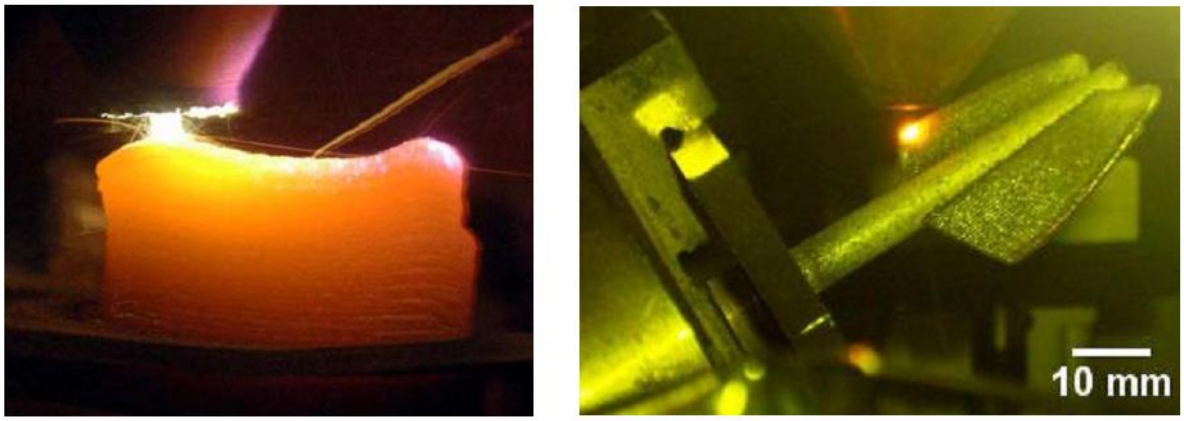

Figure 23 – Manufacturing of a 3D block of a Ti-47Al-2Cr-2Nb (left) [217] and manufacturing of a Cp-Ti tube (right) [218]

Conduction mode laser welding is also used in welding plastics. This process is sometimes referred to as laser transmission welding [219, 220]. This process requires a very controllable heat delivery to the work piece. It also requires a very stable welding process.

An innovative application of conduction mode is in underwater laser beam welding. This technique is used in the nuclear industry for repair/maintenance applications. In this application, which is a laser cladding process and not a laser welding process, the heat input to the base material needs to be extremely well controlled. The

principle behind this application is to deposit a cladding layer in order to avoid crack propagation in the base material.

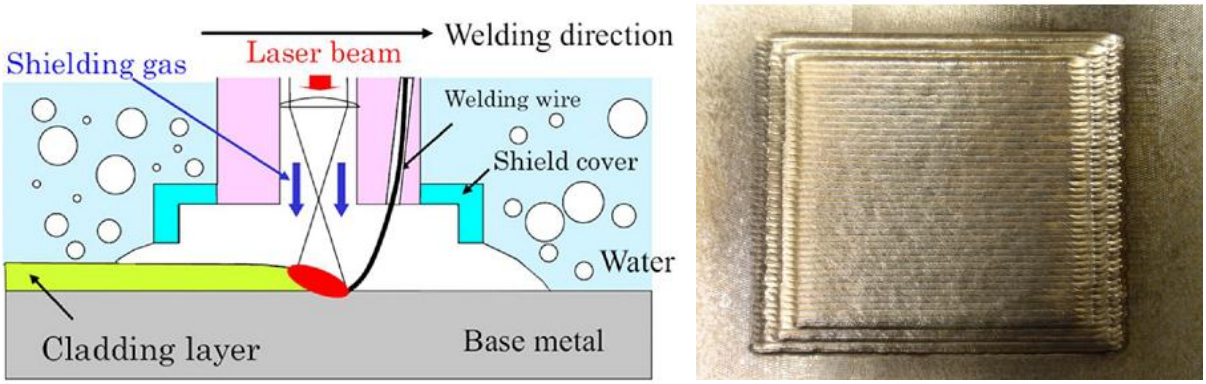

Figure 24 – Schematic of underwater laser beam welding (left) underwater laser beam welding deposit (right)[221]

These examples of applications of conduction laser welding emphasize the characteristics mentioned in Chapter 3.2. Mainly the stability of the process, the control of the heat delivered to the work piece and the quality of the welds obtained in this welding mode.

4 Interaction time and Beam Diameter effects on the Conduction Mode Threshold

This chapter presents a paper analysing the transition between conduction mode and keyhole mode. Laser welding has two distinctive modes, keyhole and conduction mode. Keyhole mode is characterized by deeper penetration and higher welding speeds, while conduction mode has better quality welds with no defects or spatter. This study focuses on the transition from conduction to keyhole mode by increasing power density and using different beam diameters and interaction times. Based upon the results it was possible to evaluate that there is a transition mode between conduction and keyhole mode. The results show that the transition between conduction and keyhole mode is not defined by a single power density value. This transition has a range of power densities that depend on the beam diameter and on the interaction time. This study allows the identification of the power density that limits conduction mode, based on parameters such as beam diameter and interaction time instead of a single power density value independent of these parameters.

E. Assunção conceived the experimental methodology in addition to all welding planning of experiments and material analysis.

S. Williams and D. Yapp provided supervision and technical advice.

E. Assunção, S. Williams, D. Yapp. "Interaction time and beam diameter effects on the conduction mode limit". Optics and Lasers in Engineering, 2012, Volume 50, Issue 6, pp. 823-828.

4.1 Introduction

There are two main modes of laser welding, conduction and keyhole[98] with many example applications of these. However the number of applications that use the keyhole mode[22, 49, 222] is considerably higher than the number of applications where conduction mode is used[100, 223]. The advantages that conduction mode presents such as no porosity, cracks and undercut in the welds along with the fact that there is no spatter during welding makes this a useful mode[92]. The main difference between conduction and keyhole mode welding is the power density applied to the welding area. In conduction mode the power density applied is insufficient to cause significant vaporisation [3, 98, 99]. While in keyhole mode the power density is high enough not only to vaporize material but to open a hole in the melt pool. Despite many studies on these two welding modes the boundaries between them are not clear in terms of processing parameters. For example sometimes the separation between conduction and keyhole welding is described as; if the power density is lower than 10^6 W/cm^2 the weld is in conduction mode, if it is higher than this it occurs in keyhole mode [3, 99, 100, 179]. Other definitions based on the power are also used, e.g. if the weld takes place with a laser power, of the order of one kilowatt; it is considered that the weld is in conduction mode [3]. These definitions only rely on the power density or laser power used during the process, completely neglecting other parameters such as the welding speed or the beam diameter used. These definitions also assume that there is a sharp transition between conduction and keyhole mode [3, 98-100, 179], meaning that there is no transition regime. The number of studies focused on the transition between conduction mode and keyhole mode is very limited. An example is the study done by Sibillano where he was able to determine the welding mode by studying the plasma/plume emission during welding based on the spectroscopy data [130]. However this study does not relate the welding parameters to the welding mode and relied on the fact that there is a single power density separating conduction mode and keyhole mode. Another study that focused on the transition between conduction and keyhole mode laser welding was carried out by Zhang et al.[128]. In his work he studied the transition between the different welding modes using laser power, focal position and travel speed as his process parameters. During this study he identified three welding modes , heat conduction welding, stable deep penetration welding and

unstable mode welding, which is the transition mode. The unstable mode welding had been previously identified by Chen et al.[131] and Zhang et al.[132] and it was attributed to thermal focusing [224, 225] , to an incorrect selection of welding parameters or to welding mode fluctuation. More studies have shown the presence of a regime between conduction mode and keyhole mode[98, 129, 136, 137, 226], while other studies just take into account two welding modes[134, 227] . The transition between conduction mode and keyhole mode is somewhat unclear, not only in terms of which and how the different process parameters will influence this transition but also related to the presence or not of a transition mode.

The depth-to-width ratio or aspect ratio is also used to distinguish between conduction and keyhole mode. It is assumed that over a certain ratio value the weld will be in keyhole mode and below it will be in conduction mode[127].

In this paper, the fundamental material interaction parameters of power density and interaction time[98, 99] are used. The specific point energy parameter is also used. The power density is calculated using the following equation,

$$\text{Power Density} = \frac{P}{A_{(Beam)}}, \qquad (1)$$

Where P is power and $A_{(Beam)}$ is the area of the laser beam. Interaction time is calculated based on the following equation;

$$t_i = \frac{d_b}{V}, \qquad (2)$$

Where d_b is the beam diameter and V is the welding speed. The interaction time can be interpreted as the heating time of the process on the centreline of the weld [99].

The specific point energy is calculated based on the following equation;

$$\text{Specific point energy} = \text{Power density} \times A_{(\text{Beam})} \times t_i, \quad (3)$$

The use of these parameters allows a like for like comparison between different beam diameters.

The objective of this paper is to investigate the current definition of conduction and keyhole mode and to see if the transition between conduction and keyhole mode is a sharp transition. An evaluation of the beam diameter and interaction time effect on the upper limit of power density for conduction mode is also made. Understanding the effect of these parameters on this limit is important when choosing to use one mode or the other.

4.2 Experimental Procedure

The welds were produced using an IPGYLR-8000 fibre laser with a maximum power of 8000 W and a wavelength of 1070 nm. The delivery system consisted of a fibre with a diameter of 300 µm. a 125 mm collimating lens and five different focal length lenses. The focusing lenses used and the respective beam diameters in focal position are shown in Table 2. By using different focusing lenses several beam diameters were obtained without defocusing and without altering the laser beam profile.

Table 2 - List of focusing lens used and respective beam diameters in the focal position

Focusing Lens	Beam Diameter in the focal position
f_f = 300 mm	0.74mm
f_f = 400 mm	0.95 mm
f_f = 500 mm	1.18 mm
f_f = 680 mm	1.61 mm
f_f = 1000 mm	2.35 mm

The focal position and the beam diameter for the different lenses used were determined using a Primes GmbH Focus monitor system. A typical beam profile is

shown in Figure 25 , indicating that the beam had an approximately ‘top-hat’ profile. The laser power was calibrated using an Ophir Laser Meter; model 20K-W.

2D profile of the Laser Beam	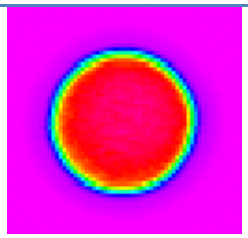
3D profile of the Laser Beam	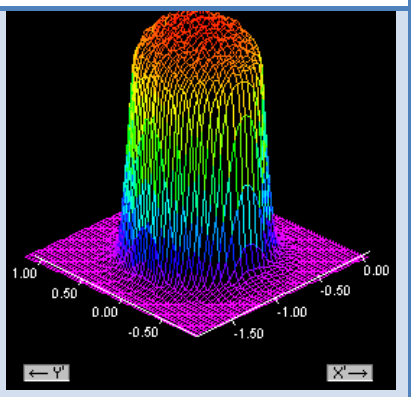

Figure 25 - 2D and 3D profile of the laser beam of the cw laser with a focussing lens of f_f = 500 mm

The experiments were carried out by increasing the laser power and maintaining a constant beam diameter. This increased the power density, equation 1, whilst maintaining a constant interaction time, equation 2. For different interaction times the beam diameter was maintained constant and the travel speed was changed in order to obtain the values required.

The material used was S355 mild steel 12 mm thick. The plates were cleaned using a wire brush and then with acetone in order to avoid organic contamination of the welds. The chemical composition of the S355 mild steel is presented in Table 15. For the metallographic preparation all the samples were mounted, polished and etched using Nital 2%.

Table 3 - Chemical composition of S355 mild steel

Element (wt%) S355 mild steel					
C	**Si**	**Mn**	**Cr**	**Ni**	**Cu**
Max 0.15	0.25/ 0.55	1.00/ 1.65	Max 0.25	Max 0.45	Max 0.3

4.3 Results

The current definition of conduction and keyhole mode based on a single power density value, independent of beam diameter or interaction time, was tested. Figure 26 shows an example of welds made at a lower power density than the 1 MW/cm^2 but do not have a conduction mode weld profile, due to the high aspect ratio of the welds and the presence of undercut [92, 101, 146].

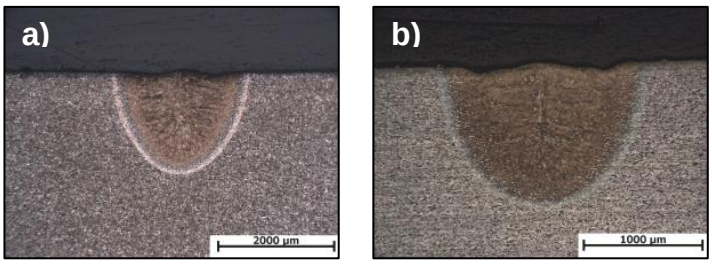

Figure 26 – a) macrographs of a weld produced with interaction time=40 ms, beam diameter=0.95 mm and power density = 0.277 MW/cm^2 b) macrograph of a weld produced with interaction time=32 ms, beam diameter= 0.95 mm and power density = 0.265 MW/cm^2

The influence of increasing the power density with a constant interaction time and beam diameter was analysed. Figure 27 shows how the penetration depth changes with the power density for a constant beam diameter of 0.95 mm and a constant interaction time of 10 ms. Figure 28 and Figure 29 show similar results for different interaction time and beam diameter respectively. For each interaction time and beam diameter it was possible to fit a fourth order polynomial, with a R^2 of 0.99, and to identify two inflection points. Combining the evaluation of the first inflection point with a visual analysis of the weld profiles it was possible to identify the power density that

separates the conduction mode regime from the transition regime. This power density represents the upper limit of conduction mode, Pd_{CML}. An evaluation of the power density influence on penetration depth for different interaction times and different beam diameters allowed for the identification of the Pd_{CML}, i.e. the maximum power density allowed to do a conduction weld for a certain interaction time and beam diameter. Based on this, three different modes can be identified: conduction mode, transition mode and keyhole mode.

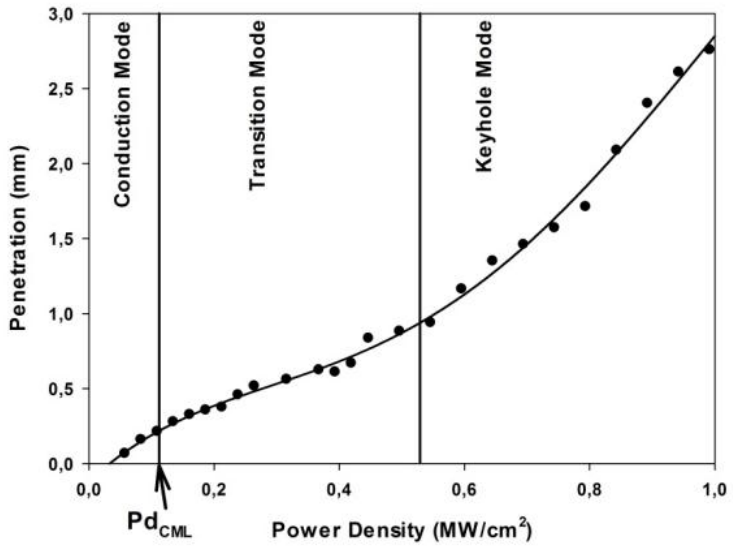

Figure 27 – Penetration depth versus power density, with increasing power, for an interaction time of 10 ms and a beam diameter of 0.95 mm

Similar behaviour was observed when using a different interaction time. Figure 28 shows the behaviour of the penetration depth with power density for an interaction time of 20 ms and a beam diameter of 0.95 mm.

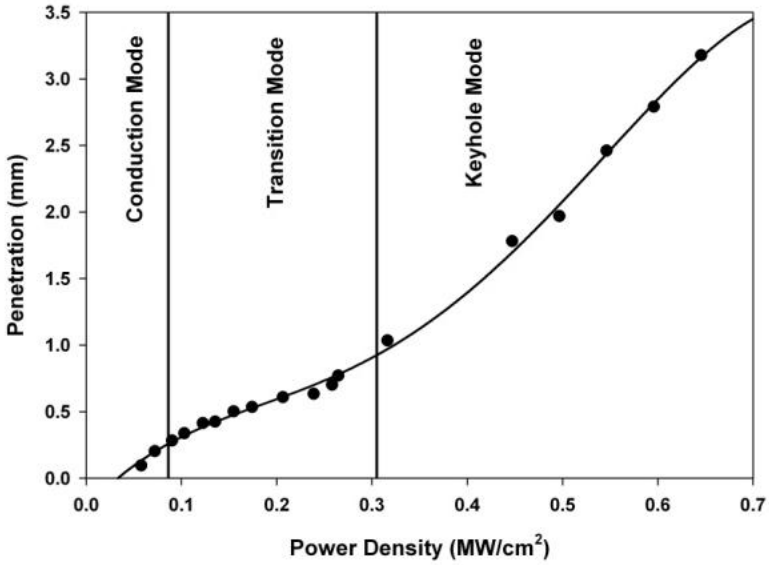

Figure 28 - Penetration depth versus power density for an interaction time of 20 ms and a beam diameter of 0.95 mm

The same three modes are present for different beam diameters. Figure 29 shows the behaviour of penetration depth with power density for an interaction time 10 ms and a beam diameter of 1.18 mm.

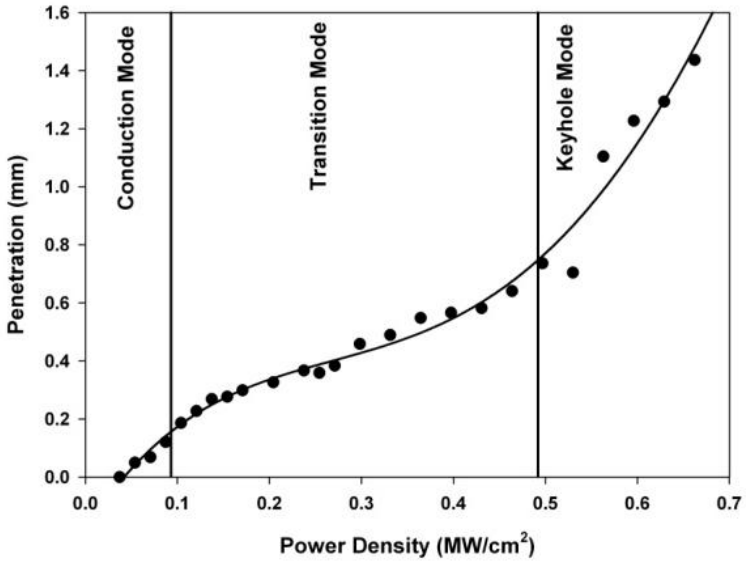

Figure 29 - Penetration depth versus power density for an interaction time of 10 ms and a beam diameter of 1.18 mm

Figure 30 shows the relationship between the Pd_{CML} and interaction time for different beam diameters. As the interaction time increases with a constant beam diameter, the Pd_{CML} decreases.

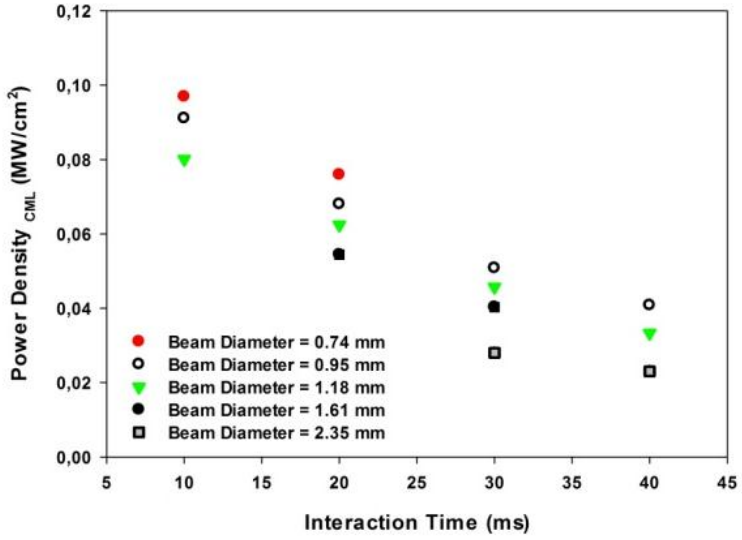

Figure 30 – Variation of the Pd_{CML} with interaction time for different beam diameters

The relation between the Pd_{CML} and the beam diameter for different interaction times is shown in Figure 31. It shows that, at a constant interaction time, the Pd_{CML} decreases with the increase in the beam diameter.

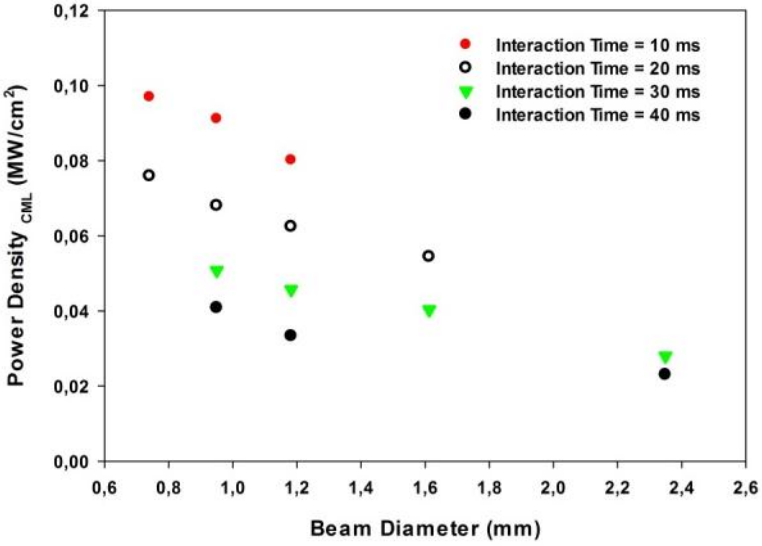

Figure 31 - Variations of the Pd_{CML} with beam diameter for different interaction times

Beam Diameter = 1.18 mm and t_i = 20 ms	Beam Diameter = 0.95 mm and t_i = 10 ms
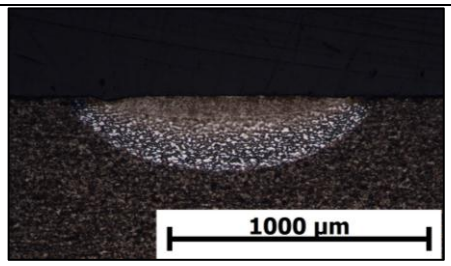	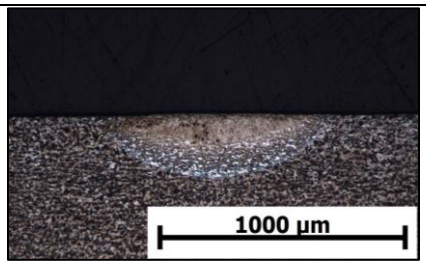
Power Density = 0.054 MW/cm^2 Conduction mode	Power Density = 0.090 MW/cm^2 Transition mode
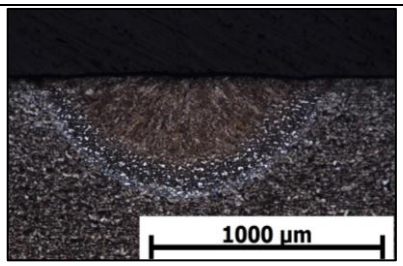	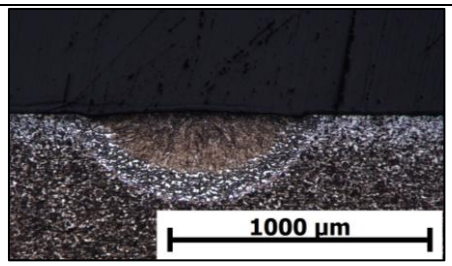
Power Density = 0.087 MW/cm^2 Transition mode	Power Density = 0.122 MW/cm^2 Transition mode
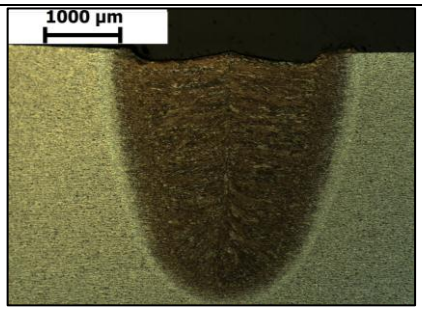	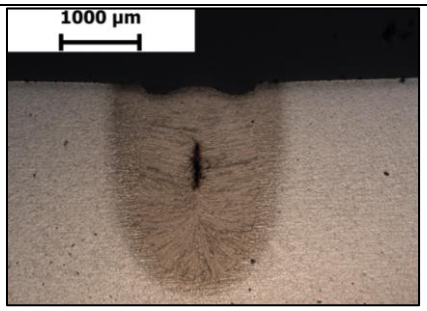
Power Density = 0.662 MW/cm^2 Keyhole mode	Power Density = 0.992 MW/cm^2 Keyhole mode

Figure 32 - Macrographs of welds done in conduction mode, transition mode and keyhole mode

Figure 32 shows how the weld profile changes from a conduction mode weld to a weld done in the transition mode. The difference of the profile before and after the Pd_{CML} can be seen. While the weld done below the limit presents a conduction

profile, shallow welds with a small aspect ratio and a very flat top profile. The weld done in the transition mode starts to show some characteristics of keyhole mode, like undercut, a not so flat top profile and a small depression at the surface. However it also has small aspect ratio which is characteristic of conduction mode.

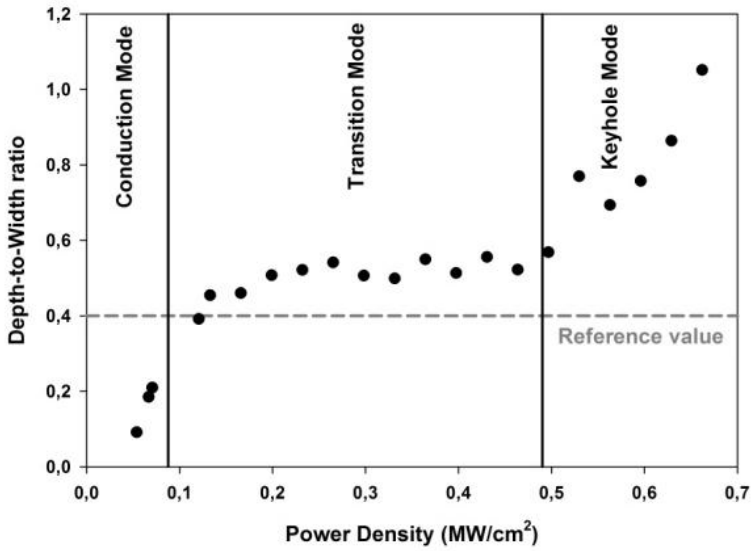

Figure 33 - Variation of the aspect ratio with the power density for beam diameter= 1.18 mm and interaction time = 20 ms

Figure 33 shows how the aspect ratio changes with the power density, for a beam diameter of 1.18mm and interaction time of 20 ms, it also shows the three distinct modes. This is also visible at different interaction time, Figure 33 and Figure 34. The dotted lines, shown in both figures, represent the aspect ratio of 0.4 which normally is used to separate conduction mode from keyhole mode[127].

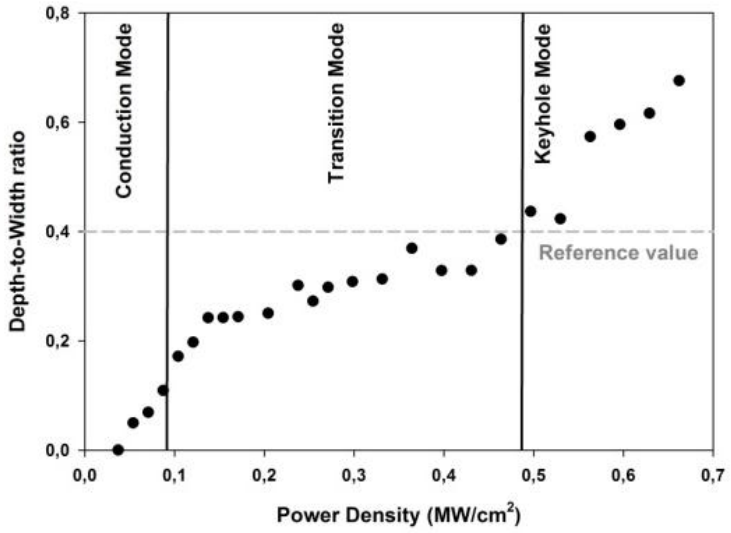

Figure 34 - Variation of the aspect ratio with the power density for beam diameter = 1.18 mm and interaction time= 10 ms

This shows that the use of the aspect ratio value to identify the welding mode is possible. During the transition mode the aspect ratio is almost constant, so this means that under this aspect ratio the weld will be in conduction mode while if the aspect ratio is higher the weld will be in keyhole mode. However the value of the ratio is not constant and it depends on the interaction time, Figure 35.

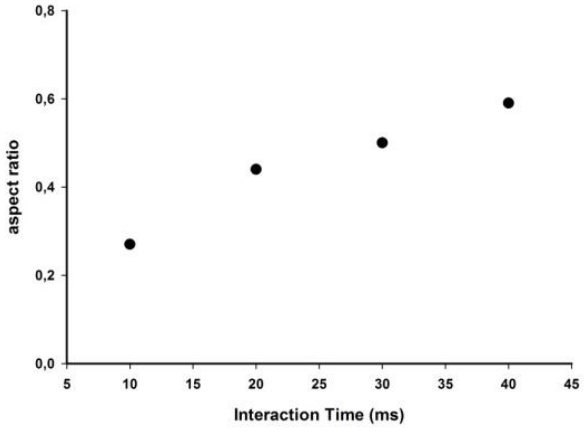

Figure 35 - Variation of the threshold aspect ratio with the interaction time for a beam diameter of 1.18 mm

4.4 Discussion

The current definition of conduction mode and keyhole mode is based on a single power density value, completely independent of other process parameters. Also the switching between conduction and keyhole mode is considered to be sharp. This work has revealed the fact that both these assumptions are incorrect. There is a transition mode between these two welding modes, as shown by Figure 27, Figure 28 and Figure 29. This transition mode is characterized by having a slower increase of the penetration depth with the increase of power density when compared to the penetration depth increase with power density in conduction and keyhole mode. The welds obtained in this mode have some similarity with the keyhole mode (mainly the presence of some undercut, a not flat top profile and a small depression at the surface). Jay Lee et al[114] also observed the existence of a transition mode between conduction and keyhole mode based on a numerical simulation that has the evaporation recoil pressure as the driving pressure for keyhole formation and the surface tension and hydrostatic pressure as the opposing pressures for keyhole formation. In Lee's work some speculation related to the power level where the transition takes place was made but no real correlation with the process parameters and the beginning of the transition mode, which is the end of the conduction mode, was made. Also no explanation as to the slow increase of the penetration with power density, in the transition mode, was given[114]. However, based on this model, the presence of this transition mode might be related to a balance between the pressures that oppose the formation of the keyhole and to the pressures that helps in the formation.

This transition mode might be caused by a region where the pressure generated by vaporization is too low to overcome the surface tension. This prevents the formation of a significant keyhole. During this mode most of the extra energy when increasing the power density, at a constant beam diameter and interaction time, is used in vaporising more material until a significant keyhole is formed. Hence there is only a small increase in penetration depth in the transition mode. A schematic of this behaviour is shown in Figure 36.

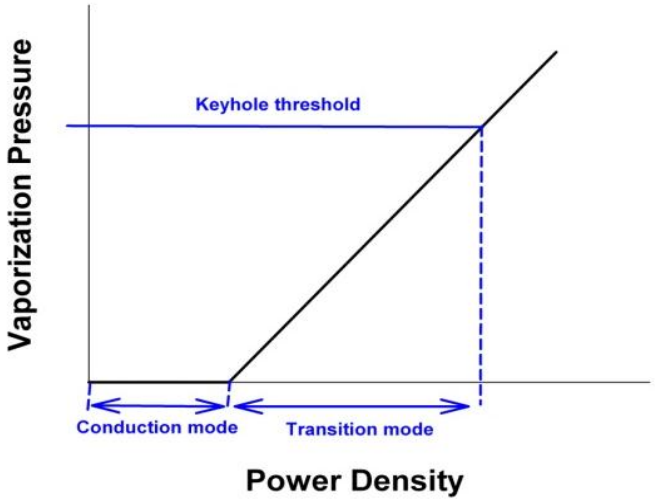

Figure 36 - Vaporization pressure versus power density

It was also observed that the beam diameter and interaction time have an effect on the Pd_{CML}, as shown in Figure 30 and Figure 31. The interaction time has a linear relationship with this power density limit. As the interaction time increases the Pd_{CML} decreases, Figure 30. This can be explained by the specific point energy. At a constant beam diameter the Pd_{CML} decreases with the increase of interaction time. This is because as the interaction time of the laser beam increases, less additional energy is necessary to change from a conduction mode to a transition mode. For a constant interaction time the Pd_{CML} decreases with an increase of beam diameter, Figure 31. This effect of the beam diameter on this limit can also be explained by the specific point energy rather than power density. At a constant interaction time the Pd_{CML} decreases with the increase of the beam diameter. This is because as the area of interaction with the laser beam is increased, more energy is necessary to change from a conduction mode to a transition mode, this means more energy is required to vaporise a larger area of material.

The evaluation of the welding regime based on the rate of change of aspect ratio is also possible. The transition mode shows a constant aspect ratio, while conduction mode and the keyhole mode show a linear increase of the ratio with power density, Figure 33 and Figure 34. Therefore if the weld has an aspect ratio lower than the one observed in the transition mode the weld is in conduction mode. However, if the aspect ratio value is higher then the weld is in keyhole mode. In transition mode the

extra energy just vaporizes more material so the aspect ratio value remains almost constant. However the aspect ratio value that separates conduction mode from keyhole mode is dependent on the interaction time, rather than being a constant single value, Figure 35.

4.5 Conclusions

In laser welding there is not a sharp transition between conduction mode and keyhole mode but a transition mode where the rate of increase of the penetration depth with power density is reduced.

The welds obtained in the transition mode show characteristics of the other two welding modes like undercut (however, less pronounced than in keyhole mode), a not flat top profile and a small depression at the surface, which are characteristic of keyhole mode, and a low aspect ratio, characteristic of conduction mode.

The Pd_{CML} is dependent on the interaction time and on beam diameter. The increase of the interaction time results in the decrease of the Pd_{CML}. While the increase of the beam diameter results in a decrease of the Pd_{CML}.

Distinguishing between conduction and keyhole mode based on a single value of the aspect ratio is not correct because this value is dependent on the interaction time.

It was also shown how the use of the fundamental material interaction parameters of interaction time and power density and also specific point energy as process parameters allows a good understanding of the results obtained.

5 Effect of Material Properties on the Conduction Mode Limit

This chapter presents a paper examining the effect of material properties on the conduction mode limit. Aluminium, mild steel and stainless steel have very dissimilar thermal properties. This study focuses on the effect of power density on the laser welding conduction mode limit in these three materials. The objective is to evaluate how these different materials will behave in conduction mode and in keyhole mode and also to understand how the thermal properties of the materials will influence the transition between the different welding modes. A comparison between the penetration depth and the melted area for the different materials under the same conditions was also made. The experimental results show that thermal properties, e.g. conductivity, melting temperature, vaporization temperature and thermal diffusivity, have an important role in the transition between the welding modes. An analytical model was developed in order to study the effect of thermal properties on the power density value necessary to achieve melting and vaporization in these materials. Also all three materials showed a transition mode between the conduction and the keyhole mode. The laser has higher penetration efficiency in aluminium in conduction mode and in the transition mode. However in the keyhole mode all three materials had very similar penetration efficiency.

E. Assunção with S. Williams and D. Yapp providing supervision conducted all the welding process development, planning of experiments, material analysis and analysis of the obtained results.

E. Assunção, D. Yapp, S. Williams. "Effect of Material Properties on the Conduction Mode Limit". Journal of Laser Applications. (Accepted, under review 11/2012)

5.1 Introduction

Laser welding has been used in a wide variety of materials. The list of examples of the application of laser welding in aluminium[22, 39], mild steel[228] and stainless steel[49] is vast. Also the number of studies on the effects of laser parameters and the number of numerical models for laser welding, that evaluate the importance of thermal properties and absorptivity, is extensive[107, 229-236] . However there are not many studies as to how these material's thermal properties will influence the welds in the conduction and keyhole welding modes. A previous study showed that in continuous wave laser welding, using mild steel, it is possible to identify three distinct welding modes, conduction mode, transition mode and keyhole mode[237] . However, how the transitions between these welding modes are influenced by the properties of the materials and how the same properties influence the characteristics of the welds in the different modes is unclear. Frequently, when evaluating if a weld is in conduction or in keyhole mode a power density value of 10^6 W/cm2 is assumed to separate these two modes. It has been shown previously that the power density limit for conduction mode is dependent on interaction time and beam diameter[237]. A study was carried out by Weckman et al and by Liu et al using a pulsed Nd:YAG laser for aluminium and stainless steel laser welding [126, 127]. The conclusion was that the transition between conduction mode and keyhole mode for aluminium took place at a power density 2.5 times greater that the power density of transition for stainless steel. In this study the definition of a conduction mode weld was based on the depth-to-width ratio, if this ratio was less than 0.4 than the weld was considered to be in conduction mode. If it was higher than the weld was considered to be in keyhole mode. However, in this study the differing coupling efficiency of each material was not taken into consideration. In addition to this the use of the ratio to identify the transition between conduction mode and keyhole mode is not completely accurate, as shown in Chapter 4[237]. The objective of this study was similar but using a continuous wave laser. However, as mentioned previously, the problem when comparing laser welding in different materials is the difference in the coupling efficiency of each material. The values of coupling efficiency depend on several factors, e.g. the wavelength of the laser, the surface condition and the material [89, 94, 95]. Some studies have been made in measuring the coupling efficiency for different materials[95-97]. For steel the coupling efficiency was between 20 and 90%

whilst in aluminium it varied from 10 to 80%. In this study, in order to overcome the coupling variation of each material, the surface was graphite coated ensuring an even coupling efficiency for all materials [100, 179].

In this paper, the fundamental material interaction parameters of power density and interaction time[98, 99] are used. The power density is calculated using the following equation,

$$\text{Power Density} = \frac{P}{A_{(Beam)}}, \qquad (4)$$

Where P is power and $A_{(Beam)}$ is the area of the laser beam. Interaction time is calculated based on the following equation;

$$t_i = \frac{d_b}{V}, \qquad (5)$$

Where d_b is the beam diameter and V is the welding speed. The interaction time can be interpreted as the heating time of the process on the centreline of the weld or how long a certain point in the spot is heated [99].

In order to compare the welds obtained in the different materials the term penetration efficiency is used. This term represents the ratio of the penetration depth of the weld bead to the spot energy from the laser beam.

The objective of this paper is to investigate how the limits of conduction mode, transition mode and keyhole mode are influenced by the material thermal properties. An evaluation of the welding modes showed by mild steel, stainless steel and aluminium is also made. Understanding the effect of the material properties on the different welding modes is important when choosing which welding mode to use.

5.2 Experimental Setup

The welds were made using an IPGYLR-8000 fibre laser with a maximum power of 8000 W and a wavelength of 1070 nm. The delivery system consisted of a fibre with a diameter of 300 µm. a 125 mm collimating lens and a 500 mm focal length lens.

The focal position and the beam diameter, for the lens used, were determined using a Primes GmbH Focus monitor system. A typical beam profile is shown in Figure 37 , and indicates that the beam has a ‘top-hat’ profile. The laser power was calibrated using an Ophir Laser Meter; model 20K-W.

2D profile of the Laser Beam	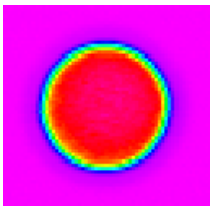
3D profile of the Laser Beam	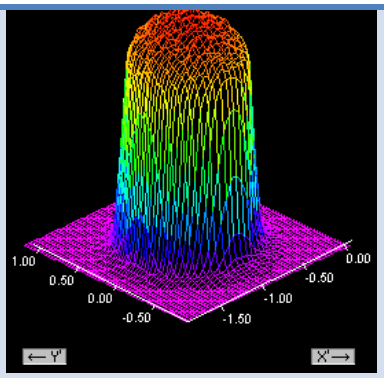

Figure 37 - 2D and 3D profile of the laser beam of the cw laser with a focussing lens of f_f = 500 mm

The experiments were carried out by increasing the laser power and maintaining a constant beam diameter, of 1.2 mm, and a constant travel speed, 3.5 m/min. This increased the power density whilst maintaining a constant interaction time of 20 ms. The laser head was kept with a 5 degrees angle in order to avoid any back reflections. Pureshield Argon was used as shielding gas in all the experiments.

The materials used were S355 mild steel, 304L stainless steel and 2024-T3 aluminium. All the plates had 12 mm of thickness and a dimension of 150 mm by 200 mm. The plates were cleaned using a wire brush and then with acetone in order to avoid contamination of the welds. After cleaning all the plates were graphite coated to ensure similar surface conditions guaranteeing similar absorption of the incident laser energy. [97, 100]. The chemical composition of S355 mild steel is shown in Table 15. For the metallographic preparation all the samples were mounted and

polished. For etching Nital 2% was used for the mild steel S355, Kalling's was used for the stainless steel 304L and Keller's was used for the aluminium 2024-T3.

Table 4 - Chemical composition of S355 mild steel

Element (wt%) S355 mild steel					
C	Si	Mn	Cr	Ni	Cu
Max 0.15	0.25/ 0.55	1.00/ 1.65	Max 0.25	Max 0.45	Max 0.3

Table 5 - Chemical composition of 304L stainless steel

Element (wt%) 304L stainless steel						
C	Si	Mn	Cr	Ni	P	N
Max 0.03	Max 0.75	Max 2.00	18.0/ 20.0	8/ 12	0.045	0.1

Table 6 - Chemical composition of 2024-T3 aluminium

Element (wt%) 2024 – T3 aluminium									
Al	Cr	Cu	Fe	Mg	Mn	Si	Ti	Zn	Others
90.7 - 94.7	Max 0.1	3.8 - 4.9	Max 0.5	1.2 - 1.8	0.3 - 0.9	Max 0.5	Max 0.15	Max 0.25	0.15

Some of the thermal properties of these materials are listed in Table 7. Where T_{mp} is the melting point, T_{vp} is the vaporization point, k is the thermal conductivity, ρ is the density, C_p is the specific heat capacity, L_m is the latent heat of melting and L_v is the latent heat of vaporization.

Table 7 - Thermal properties of S355 mild steel, 304L stainless steel and 2024-T3 aluminium at room temperature[238]

Material	Tmp (K)	Tvp (K)	k (W/m.K)	ρ (g/cm3)	Cp (J/g.K)	Lm (J/g)	Lv (J/g)
S355	1773	3363	51	7.874	0.48	247	6100
304L	1633	3100	14.8	8.020	0.47	260	6100
2024-T3	905	2743	175	2.785	0.85	366	11900

These materials differ significantly in melting temperature 905 - 1773 K, vaporization temperature 2743-3363 K and in conductivity 14.8-175 W/m.K. These differences will have an effect on the welds obtained in the different modes and on the transition between these welding modes.

5.3 Results

The influence of power density on penetration depth for stainless steel, aluminium and mild steel was evaluated for a beam diameter of 1.18 mm and an interaction time of 20 ms, and is shown in Figure 38.

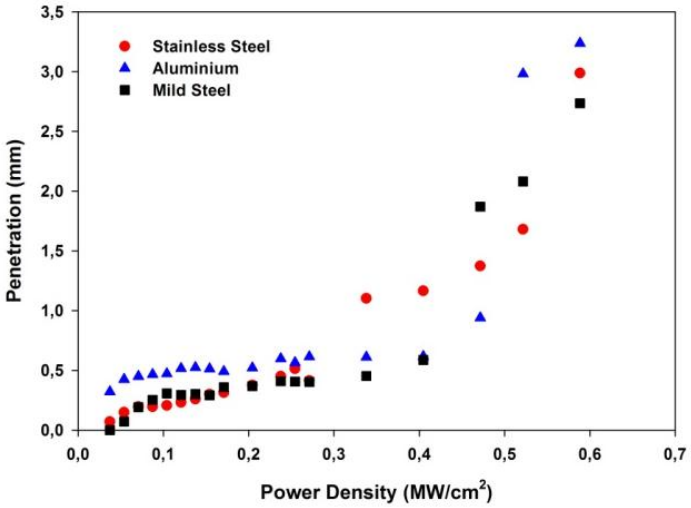

Figure 38 - Penetration depth versus power density for stainless steel, aluminium and mild steel

At the lowest power density value used, which was of 0.036 MW/cm^{2,} mild steel does not show any penetration, in contrast to stainless steel and aluminium. For power density values between 0.05 MW/cm^2 and 0.3 MW/cm^2, mild steel and stainless steel have similar penetration depths, while aluminium is higher. As the power density increases the penetration depth of mild steel and stainless steel increases quicker than that of aluminium.

The different behaviour of the materials suggests a closer look at each material individually in order to see where the welding mode changes occur.

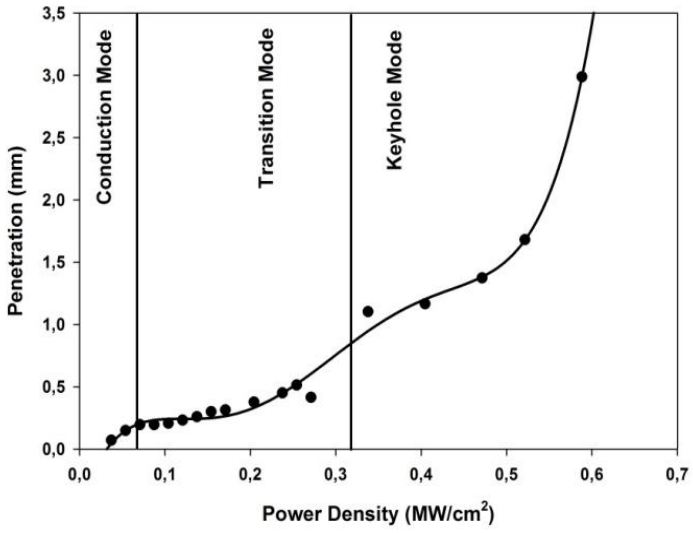

Figure 39 - Penetration depth versus power density for stainless steel

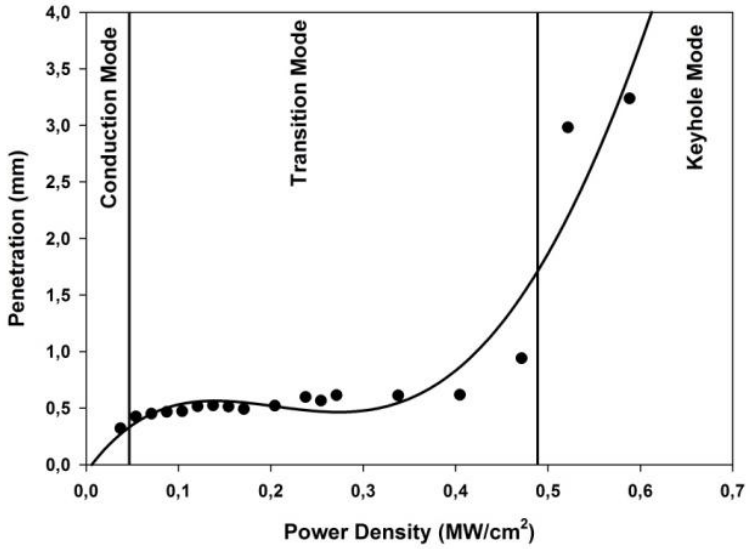

Figure 40 - Penetration depth versus power density for aluminium

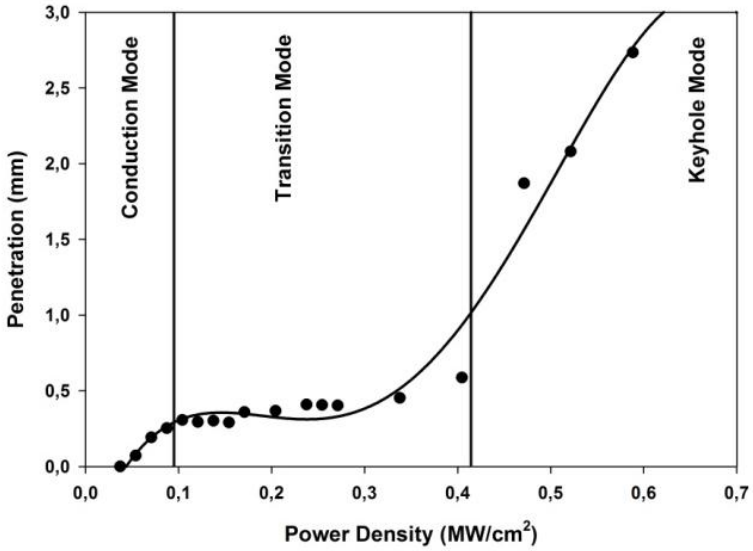

Figure 41 - Penetration depth versus power density for mild steel

Figure 39, Figure 40 and Figure 41 shows how the penetration depth changes with power density. The three welding modes (conduction, transition and keyhole) and the respective boundaries between these modes are shown. These boundaries were identified in the same manner as described previously, in chapter 4. The power density range where the transition mode takes place is much wider for aluminium than for mild and stainless steel.

Figure 42 shows how the weld profile changes with the increase of the power density for all the three materials. The changes from a conduction mode profile to a keyhole profile for stainless steel, aluminium and mild steel can be observed. Observing the macrographs, Figure 42,it is clear that the power density value at which melting for stainless steel starts is higher than the power density where aluminium starts melting because the weld done at the lowest power density value has a much higher penetration in aluminium than in stainless steel.

The difference in the weld quality from conduction mode to keyhole mode is apparent, especially in the aluminium welds. In conduction mode and in the begging of transition mode the aluminium welds present no porosity, no cracking and a flat top profile. However, at the end of the transition mode in keyhole mode cracks and porosity can be seen. This emphasizes the high quality welds obtained in conduction mode, which have no porosity, cracks and undercut[92].

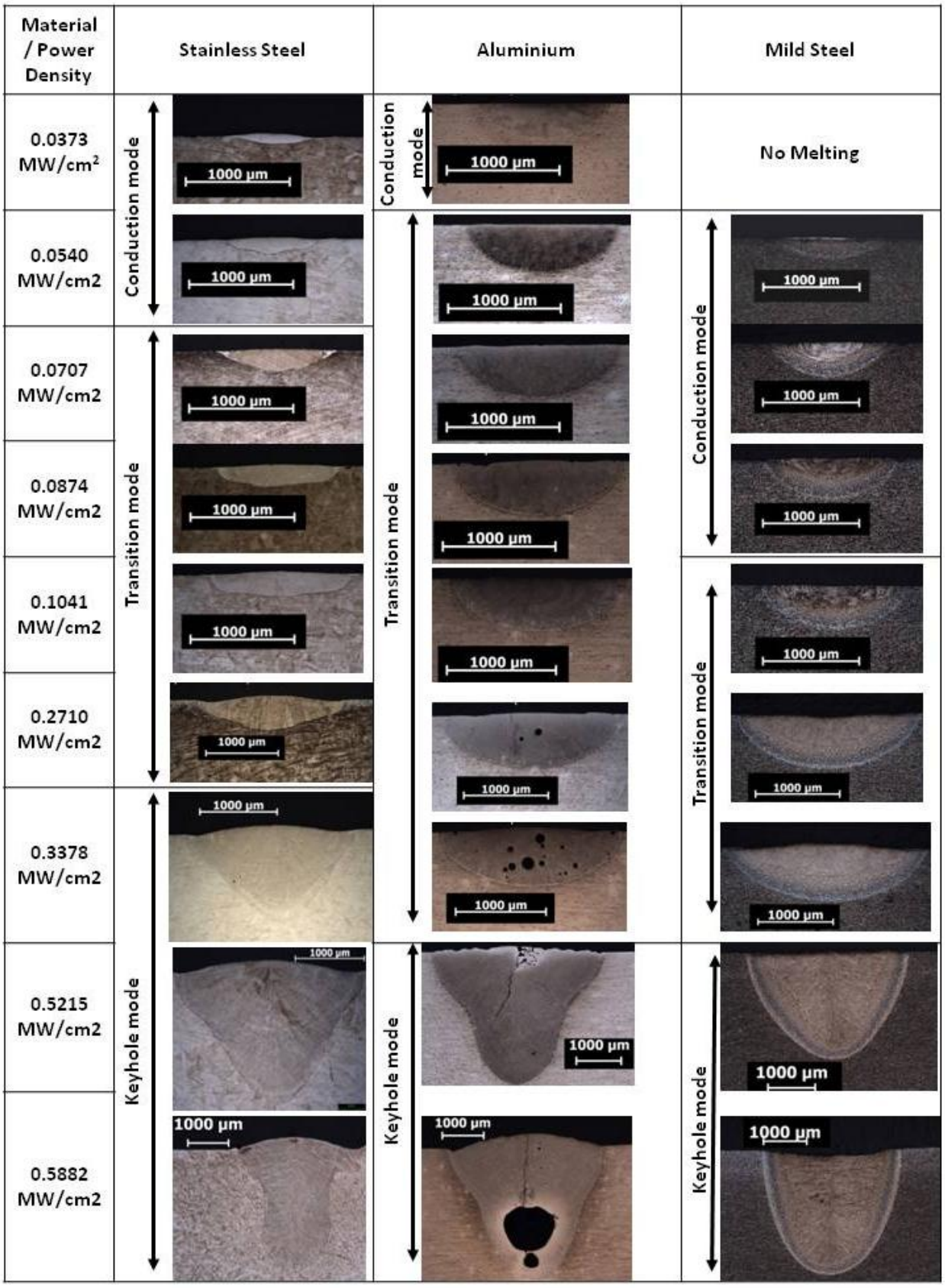

Figure 42 - Macrographs of the laser welds made in stainless steel, aluminium and mild steel

5.3.1 Analytical model

It has been observed that the thermal properties of the materials influence the transition between the modes. To gain further insight into this the following 1D analytical solution[3] has been made. An analysis was done considering that the point where the temperature is highest in a small region at the surface near the centre of the laser beam. So it is at this point where melting and vaporization will take place first[239]. The model used is a stationary point model; this model gives the same qualitative effect of material properties as a moving beam model. This model also neglects fluid flow, however considering that the point being analysed is considerably smaller than the weld pool and it is situated at the surface of that same weld pool. Also, the lateral heat flux can be neglected because the point used is considered to be at the middle and at the surface of the weld pool and so lateral heat flux can be neglected.

$$T(z,t) = \frac{2q}{k}\sqrt{\alpha t}\,\mathrm{ierfc}\left(\frac{z}{2\sqrt{\alpha t}}\right) \qquad (6)$$

Where

z is the distance from the surface of the material, at the surface z=0

q is the power density in W/m^2

α is the thermal diffusivity in m^2/s

k is thermal conductivity W/m.K

t is the interaction time

The values for the $\mathrm{ierfc}(x)$ are shown by Carslaw[125].

Considering that the hottest point will be at z=0 and that the desired value is the power density as a function of temperature we re-arrange equation 6 as follows:

$$q = \frac{T(0,t)k}{2\sqrt{\alpha t}\, ierfc(0)} \qquad (7)$$

Where ierfc(0) = 0.5642 from Carslaw[125]. Normally $q = I(1 - R)$, where I is the incident laser beam power density and R is the reflectivity. However in this study, due to the fact that all the material surfaces were graphite coated, the reflectivity is considered to be very similar between all the materials and so the reflectivity factor is not considered in this model.

In order to improve the accuracy of the analytical model the average values of temperature dependent materials properties (thermal conductivity, specific heat capacity and density) were used, instead of using the material properties at room temperature, as in previous work[127, 231, 240]. Also the analytical model has been divided in two parts, the first one that uses the thermal properties of solid material and the second one that uses the thermal properties of the liquid material. The idea in doing so is to take into account the thermal properties changes that the materials show when they change from a solid state into a liquid state. In this work the specific heat capacity, needed to calculate the thermal diffusivity, is calculated taking into account the latent heat of melting (L_m) for temperatures below the melting temperature (T_{mp}) and the latent heat of vaporization (L_v) for temperatures from the melting temperature to the vaporization temperature (T_{vp}), following [127].

$$C_{pm} = \frac{\overline{C_{ps}}(T_{mp} - 293\ K) + L_m}{(T_{mp} - 293\ K)} \qquad (8)$$

$$C_{pv} = \frac{\overline{C_{pl}}(T_{vp} - T_{mp}) + L_v}{(T_{vp} - T_{mp})} \qquad (9)$$

Where the $\overline{C_{ps}}$ is the average specific heat capacity for temperatures below the melting point and $\overline{C_{pl}}$ is the average specific heat capacity for temperatures between

the melting and the vaporization temperature. While C_{pm} is the specific heat for temperatures between the room temperature and the melting temperature including the latent heat of melting and C_{pv} is the specific heat for temperature between the melting temperature and the vaporization temperature including the latent heat of vaporization.

$$q = \begin{cases} \frac{T(0,t)\bar{k}_{solid}}{2\sqrt{\overline{\alpha_{solid}}t}\,ierfc(0)} \text{ for } 293\ K \leq T \geq T_{mp} \\ q_{(T_{mp})} + \frac{(T(0,t)-T_{mp})\bar{k}_{liquid}}{2\sqrt{\overline{\alpha_{liquid}}t}\,ierfc(0)} \text{ for } T_{mp} < T \geq T_{vp} \end{cases} \quad (10)$$

where: $\overline{k_{solid}}$ is the average conductivity and $\overline{\alpha_{solid}}$ is the average thermal diffusivity of the material in the solid state, $q_{(T_{mp})}$ is the power density required for melting calculated using the first part of Equation 10 for T(0,t) = T_{mp} while $\overline{k_{liquid}}$ and $\overline{\alpha_{liquid}}$ are the average conductivity and the average thermal diffusivity of the material in the liquid state. The values of the average thermal conductivities, the average densities and the calculated average specific heats are shown in Table 8.

Table 8 - Average values of temperature dependent material properties for solid and liquid S355, 304L and 2024-T3[238, 241]

Material	$\bar{k}$ (W/m.K)	$\bar{\rho}$ (g/cm^3)	$\overline{Cp}$ (J/g.K)	$\bar{\alpha}$ (m^2/s)
S355	35.5	7.860	0.645	5.56 x 10^{-6}
S355 Liquid	120	6.850	0.700	3.86 x 10^{-6}
304L	22.25	7.590	0.600	3.69 x 10^{-6}
304L Liquid	30.5	6.860	0.800	8.81 x 10^{-7}
2024-T3	181.5	2.729	0.975	6.82 x 10^{-5}
2024-T3 Liquid	84	2.458	1.140	3.00 x 10^{-5}

While the conductivity of mild steel S 355 and stainless steel 304L increases when it changes from solid to liquid, the opposite happens with the conductivity of aluminium 2024-T3. The other material properties, specific heat and the density, also show a change when changing from a solid to a liquid stage; however the biggest difference is noticed in the thermal conductivity. The importance of taking into account the changes in the thermal properties when the material changes from a solid state to a liquid state gains more importance in aluminium, without this change the results obtained using the analytical model would not match the results obtained experimentally.

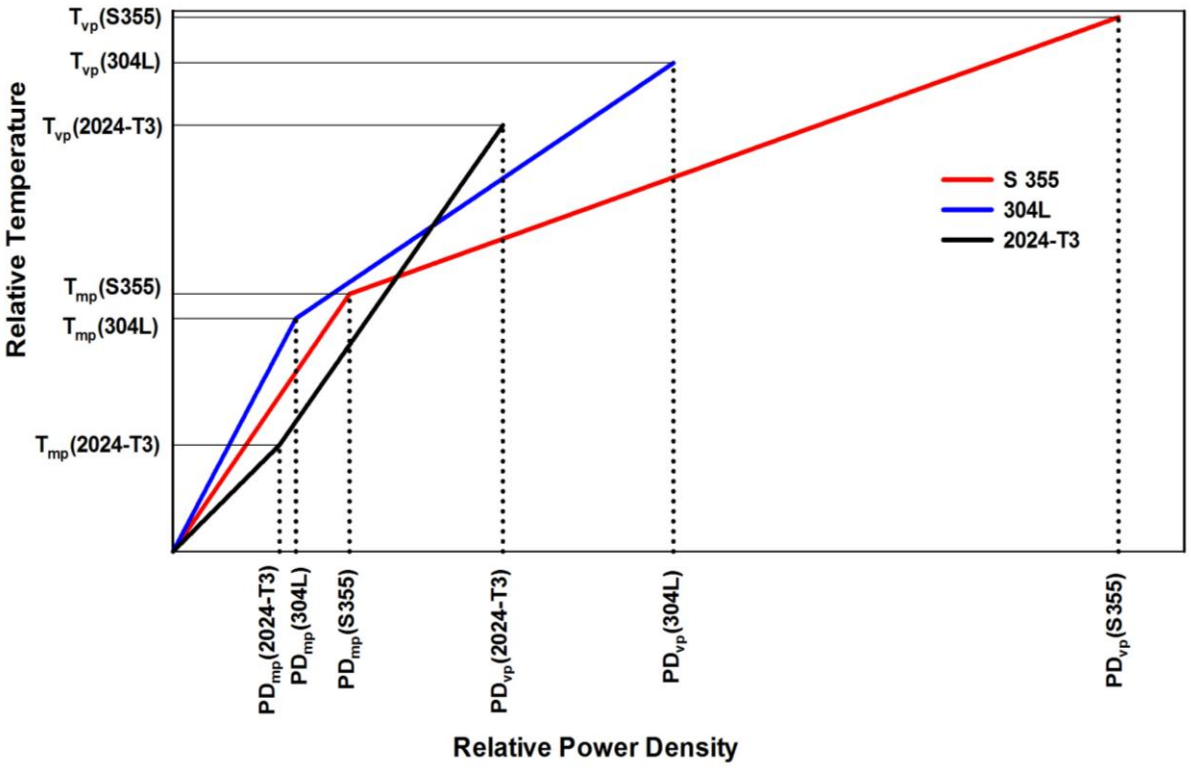

Figure 43 – Variation of the temperature with power density, based on the analytical model, for aluminium (2024-T3), mild steel (S355) and stainless steel (304L)

The analytical model results match the experimental results in that the order in which the transitions between the three welding modes occur in the different materials is similar. The trends obtained in the analytical model and in the experimental data are the same. The power density where melting starts, which is the lower limit of

conduction mode, is lower for the aluminium followed by the stainless steel and then by the mild steel. Regarding the power density where vaporisation starts, which is the upper limit of conduction mode, aluminium has the lower value followed by the stainless steel and then by the mild steel. Regarding the upper bound of the transition mode (or lower bound of keyhole mode) this analytical model does not provide any information, mainly because this model only analysis the raise of temperature up to the vaporisation temperature, that is related to the lower bound of the transition mode.

5.3.2 Comparison of the welds obtained in conduction and keyhole mode in the different materials

A direct comparison of the weld bead shape using the same power density and interaction time between all the materials in conduction mode is not possible. This is because there is not a power density value where all the materials are in conduction mode. In order to understand how each material behaves in this mode a comparison will be made using the weld profile obtained just before the conduction mode upper limit power density, i.e. where conduction mode finishes, Figure 44. At this upper limit power density aluminium has a much higher penetration efficiency, followed by mild steel and then by stainless steel.

Stainless Steel 304L	Aluminium 2024-T3	Mild Steel S355
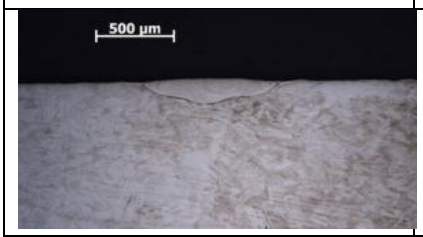	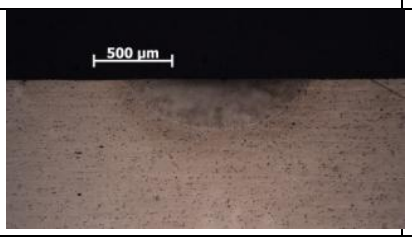	
Power Density = 0.0540 MW/cm^2 Penetration efficiency = 0.0125 mm/J	Power Density = 0.0373 MW/cm^2 Penetration efficiency = 0.0391 mm/J	Power Density = 0.0874 MW/cm^2 Penetration efficiency = 0.0131 mm/J

Figure 44 - Macrographs of the welds done in conduction mode for stainless steel, aluminium and mild steel

Stainless Steel 304L	Aluminium 2024-T3	Mild Steel S355
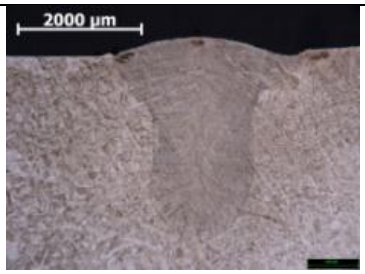	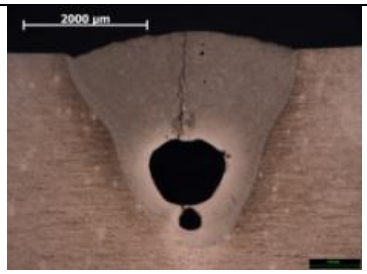	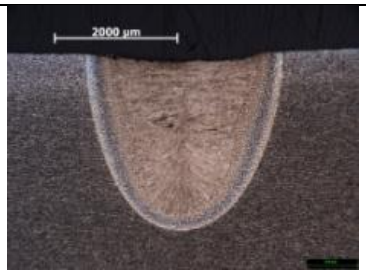
Power Density = 0.5882 MW/cm^2 Penetration efficiency = 0.0231 mm/J	Power Density = 0.5882 MW/cm^2 Penetration efficiency = 0.0251 mm/J	Power Density = 0.5882 MW/cm^2 Penetration efficiency = 0.0212 mm/J

Figure 45 - Macrographs of the welds done in keyhole mode for stainless steel, aluminium and mild steel

It is possible to do a direct comparison between the weld bead shape using the same power density and interaction time between all the materials in keyhole mode, Figure 45. In keyhole mode all the three materials have very similar penetration efficiency. However, aluminium has a higher penetration efficiency followed by stainless steel and then by mild steel.

5.4 Discussion

The transition between the different welding modes is influenced by the material thermal properties. When a material is heated up by a laser the rate of temperature rise at the centre of the laser spot will depend on the material thermal properties (assuming equal coupling efficiency). Primarily the rate of increase is controlled by thermal losses and this is confirmed in Figure 43. The rate of increase of temperature for the three materials is in inverse proportion to their thermal conductivity. Aluminium with highest conductivity has the slowest rate of temperature increase. However as aluminium has by far the lowest melting point it actually has the lowest power density requirement to initiate melting. Once in conduction mode the actual penetration depth observed depends on the thermal conductivity (ignoring fluid flow effects). In this case high thermal conductivity works in favour. This means

that aluminium shows the highest penetration efficiency, followed by mild steel and then stainless steel, as shown in Figure 44.

In the molten region the thermal properties of the materials change. It was expected that the rate of increase of temperature for the three materials would be in inverse to the material thermal conductivity. However this does not happen, as shown in Figure 43. This means that the rate of increase of the temperature is not controlled simply by the material thermal conductivity but a relation between the properties of the material (thermal conductivity, thermal diffusivity, specific heat capacity, latent heal of melting, latent heat of vaporisation and density).

The power density upper bound for conduction mode welding is determined by the onset of vaporisation. So aluminium has the lower power density requirement to initiate vaporisation, followed by stainless steel and then by mild steel, as shown in Figure 43. The threshold for keyhole mode will be determined by the point at which the vaporisation recoil pressure overcomes surface tension forces and a keyhole develops. This type of analysis cannot be done with an analytical model that just considers material thermal properties. The material that requires more power density to increase the vaporisation recoil pressure, to a value that it will overcome the surface tension forces, is aluminium. Because aluminium has the lowest power density upper bound for conduction welding and the highest threshold for keyhole welding it displays the greatest width for transition mode welding as shown in Figure 38.

The transition mode displays the weld bead characteristics of conduction mode (i.e. shallow penetration and low aspect ratio) but suffers from the poor quality of keyhole mode welding (cracks and pores) as shown in Figure 42. Often the main reason for using conduction mode welding is to achieve the very high quality that is possible in this regime. Hence it is very important to know and understand where the upper bound of conduction mode welding is, so avoid the transition regime with its quality issues. This cannot be done merely by inspecting the weld bead shape or applying some arbitrary power density value.

Once in keyhole mode all materials have very similar penetration depths for the same power density and interaction time. This indicates that the material thermal properties have very little influence in the penetration depth in this welding regime, as shown in Figure 45.

5.5 Conclusions

The lower and upper limits of conduction mode are material dependent. The material properties including melting and vaporisation temperatures, thermal conductivity, density, specific heat capacity, latent heat of melting and latent heat of vaporisation determine these limits.

All three materials studied (aluminium, mild steel and stainless steel) have a transition mode separating the conduction mode from the keyhole mode. In all the materials the transition mode is characterized by a very small increase of the penetration with an increase in power density.

Aluminium, due to its higher thermal conductivity, has a higher penetration efficiency in conduction mode, followed by mild steel and then by stainless steel.

In keyhole mode the penetration depth of all the materials is very similar. So the material thermal properties in keyhole mode have less influence on the penetration depth than in conduction mode.

6 Comparison of continuous wave and pulsed wave laser welding effects

This chapter shows a paper that focused on comparing a continuous wave and a pulsed wave laser under the same welding conditions. The welding parameters normally associated with continuous wave lasers are laser power, beam diameter and welding speed. In pulsed wave lasers the parameters used are pulse duration, energy and beam diameter. In this paper a comparison of welds obtained using the same process parameters in continuous and pulsed wave lasers is made. In order to have the same welding parameters, for both lasers, the tests were carried out using interaction time and power density as the main process parameters. The results show that using these parameters the two lasers have very dissimilar behaviour in terms of penetration depth. Also the pulsed wave laser showed higher efficiency when compared to the continuous wave laser under the same welding conditions. The effect of the spatial peak power density was also evaluated.

E. Assunção conceived the experimental methodology in addition to all welding planning of experiments and material analysis.

S. Williams and D. Yapp provided supervision and technical advice.

E. Assunção D. Yapp, S. Williams. "Comparison of continuous wave and pulsed wave laser welding effects". Optics and Lasers in Engineering. (Accepted, In review 11/2012)

6.1 Introduction

In recent years the relevance of laser welding to several industries has increased, mainly in the automotive and aerospace industry [22, 242]. There are two main types of lasers, continuous wave (CW) and pulsed wave (PW) [3]. Several studies of the effect of the different welding parameters in laser welding [243], have been made. However, most of the studies were carried out using a single type of laser, either CW [244-247] or PW [103, 166, 173, 248]. The difficulties raised in directly comparing these two types of lasers are the parameters which are utilised. The parameters normally used for characterising a pulsed laser weld are pulse energy, pulse duration and spot size. Fuershbach evaluated the effect of energy density and power density for different pulse durations [173]. The results showed that at fixed power density the penetration depth went up with longer pulse durations, which means higher energy was utilised, for a PW laser. The same paper showed a comparison between a pulsed and a continuous wave laser weld, concluding that CW lasers show higher penetration than PW lasers. However, this comparison, between PW and CW laser welds, was made without using any parameter which gives a correlation between pulse duration and the welding speed used in the CW welds. Just power density was used for comparison, neglecting the effect of interaction time of the laser beam with the material.

In this present paper, the fundamental material interaction parameters of power density and interaction time are used [98, 99], and their influence on CW and PW laser welds is investigated. The power density is calculated for both CW laser and the PW laser using the following equation,

$$\text{Average Power Density} = \frac{P}{A_{(Beam)}}, \qquad (11)$$

Where P is power and $A_{(Beam)}$ is the area of the laser beam. This power density is the average power density of the laser beam profile. In CW welds P is total power. In PW welds, P is the average pulse peak power over the duration of an individual pulse[160], equation 12.

$$\text{Average Peak Power} = \frac{Pulse\ Energy}{Pulse\ Duration}, \qquad (12)$$

A further parameter is the spatial peak power density that represents the maximum power density across the laser beam profile. This value is measured by the beam profile equipments used. For 'top-hat' profiles the spatial peak power density has the same value as the average power density.

The comparison was made between a CW weld and individual pulses (obtained with a PW laser). This allowed a comparison the physics/material science behind the interaction of a CW laser and a PW laser with the material. One of the most important fundamental material interaction parameters in this comparison is the interaction time. The interaction time can be interpreted as the time a specific point, located in the centreline of the weld, is exposed to the laser beam [99]. In CW lasers the interaction time is calculated based on the following equation;

$$t_i = \frac{d_b}{V}, \qquad (13)$$

Where d_b is the beam diameter and V is the welding speed. The interaction time is the heating time of the process on the weld centreline [99]. This equation defines the maximum interaction time, which occurs in the weld centreline, for CW laser.

In PW lasers the interaction time is the pulse duration, which represents the time that a particular point in the material is exposed to the laser beam.

Using these parameters allows a like for like comparison between CW and PW lasers.

6.2 Experimental Procedure

The two lasers used in these experiments are described below. The CW laser was an IPGYLR-8000 fibre laser with a maximum power of 8000 W and a

wavelength of 1070 nm. The delivery system consisted of a fibre with a diameter of 300 μm, a 125 mm collimating lens, and a f_f=400 mm focal length lens, this set up produced a beam diameter of 0.95 mm with a 'top-hat' profile. Also used with this set up was a f_f=250 mm focal length lens that was used in a defocused position, to produce a beam diameter of 0.95 mm with a Gaussian profile. This will allow having two different profiles with the same average power density but different spatial peak power density. The focal position and the beam diameter were determined using a Primes GmbH Focus monitor system. The laser power was calibrated using an Ophir Laser Meter; model 20K-W.

3D profile of the Laser Beam	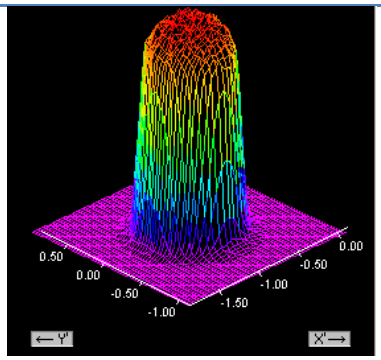 **Spatial Peak Power Density** **160.0 kW/cm^2**

Figure 46 - 3D profile of the laser beam of the cw laser with a focussing lens of f_f = 400 mm for an average power of 1000 W

3D profile of the Laser Beam	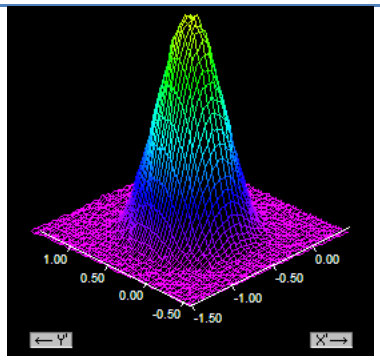 **Spatial Peak Power Density**

	222.7 kW/cm^2

Figure 47 - 3D profile of the laser beam of the cw laser using a focusing lens of f_f= 250 mm in the defocus position for an average power of 1000 W

The experiments were carried out by increasing the laser power and maintaining a constant beam diameter. This increased the power density whilst maintaining a constant interaction time. For different interaction times the beam diameter was also maintained constant and the travel speed was changed in order to obtain interaction times of 10 and 20 ms.

3D profile of the Laser Beam	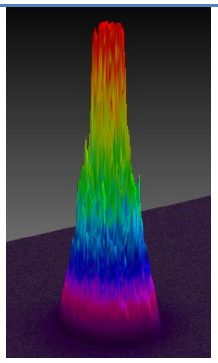 **Spatial Peak Power Density** **353.1 kW/cm^2**

Figure 48 - 3D profile of the laser beam of the pw laser with a focussing lens of f_f = 300 mm for a peak power of 1000 W

The PW welds were made using a GSI JK300 HP PW laser with a maximum average power of 300 W and a maximum peak power of 9 kW. The system consisted of a delivery fibre of 300 µm diameter and a processing tool with a collimating lens of 100 mm. The focusing lens had a focal length of f_f = 300 mm and this produced a beam diameter of 0.9 mm. The focal position and the beam diameter were determined using a Spiricon Laser Beam Analyzer; model LBA-FW-SCOR. The beam profile obtained had an approximate Gaussian distribution, Figure 48. The laser power was calibrated using a Gentec-EO power meter; model UP19K-15S-W5-DO.

The material used was S355 mild steel with 12 mm thickness. The plates were cleaned using a wire brush and then with acetone in order to avoid contamination of the welds. The chemical composition of the S355 mild steel is shown in Table 15. For the metallographic preparation all the samples were mounted, polished and etched using Nital 2%. The PW samples were mounted with an angle allowing the visualisation of weld profiles with different depths in order to identify the maximum penetration for each of the PW welds made, Figure 49.

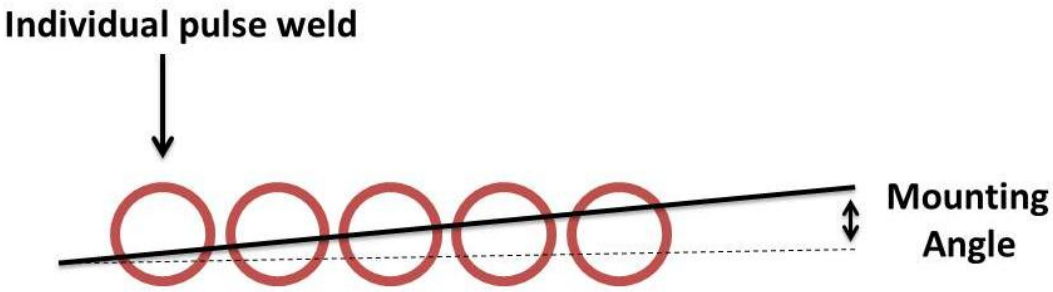

Figure 49 - Schematics on how the samples were mounted

Table 9 - Chemical composition of S355 mild steel

Element (wt%) S355 mild steel					
C	Si	Mn	Cr	Ni	Cu
Max 0.15	0.25/ 0.55	1.00/ 1.65	Max 0.25	Max 0.45	Max 0.3

6.3 Results

6.3.1 CW laser

The influence of power density on CW laser welds was analysed. The two types of beam profiles used on the CW welds, 'top-hat' and Gaussian, did not show any difference in terms of behaviour, Figure 50. This is despite the spatial peak power density of the Gaussian beam being significantly higher than that of the top hat beam, however the average power density was the same.

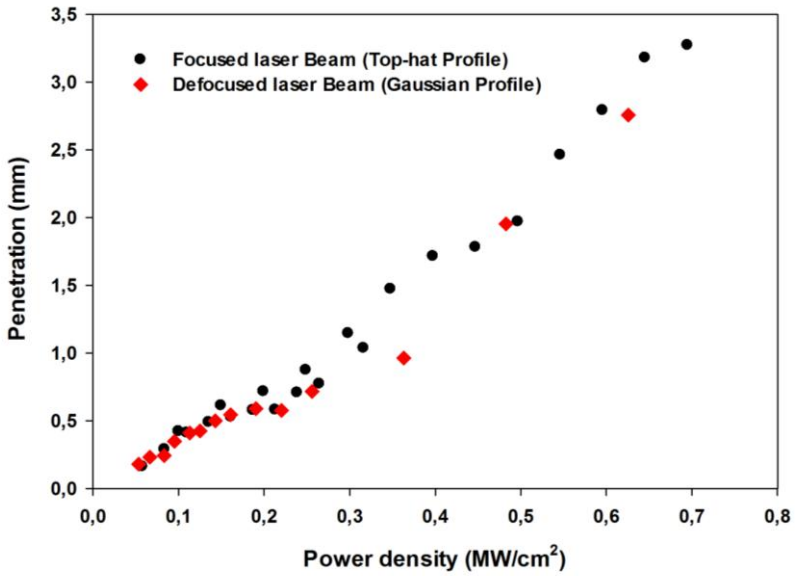

Figure 50 - Comparison of the effect of the beam profile on the behaviour of penetration with average power density, but different peak power density, for an interaction time of 20 ms

Figure 51 shows the results for an interaction time of 10 ms and beam diameter of 0.95 mm. As previously [249] three different modes can be identified: conduction mode, transition mode and keyhole mode.

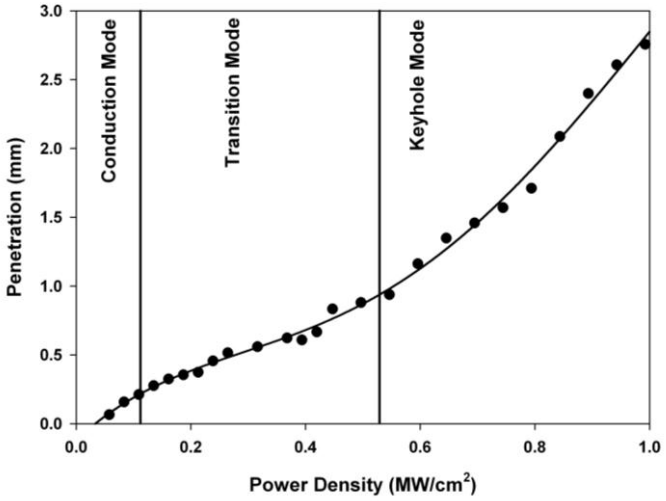

Figure 51 - Penetration versus power density for a beam diameter of 0.95 mm and an interaction time of 10 ms

6.3.2 Comparison of pulsed laser welding with continuous laser welding

Similar experiments were carried out using the pulsed laser. The objective was to evaluate if welds made under the same conditions in PW have similar behaviour and penetration.

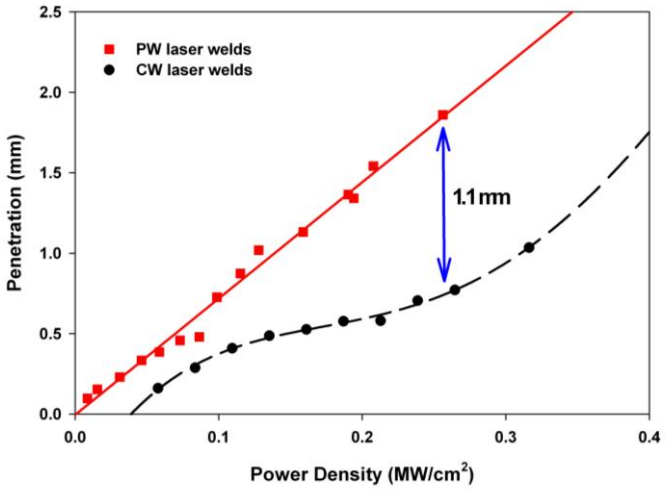

Figure 52 - Penetration depth versus power density for an interaction time of 20 ms and a beam diameter of 0.95 mm for the cw welds and a beam diameter of 0.9 mm for the pw

Figure 52 shows how the penetration depth changes with the power density for a constant beam diameter and a constant interaction time of 20 ms for PW and CW under similar conditions. In contrast to the CW process the PW process does not show the three modes identified previously [249] but an almost linear relationship between power density and penetration. However, in PW the three welding modes are still present. Considering that all the welds were done with the same interaction time it can also be seen that for the same power density the PW laser welds have deeper penetration. This difference between the penetration depth in CW and PW is more accentuated at higher average power density values in the keyhole regime.

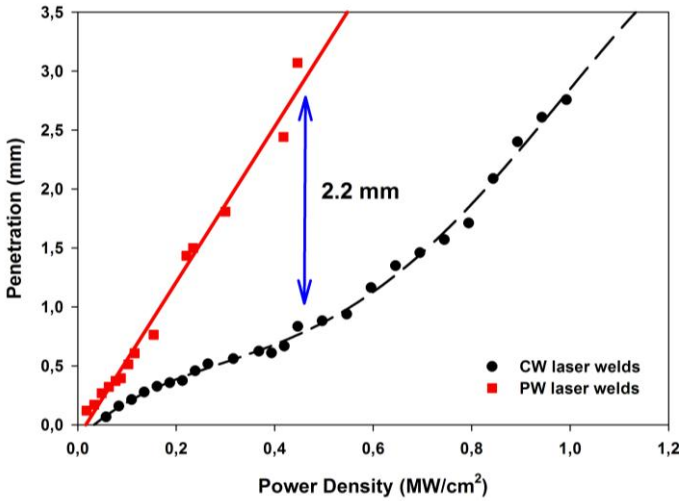

Figure 53 - Penetration depth versus power density for an interaction time 10 ms and a beam diameter of 0.95 mm for the CW welds and a beam diameter of 0.9 mm for the PW

The same behaviour was observed for an interaction time of 10 ms, Figure 53. However the difference between the penetration depth in CW and PW increased, when compared to the one obtained for an interaction time of 20 ms.

laser welds	
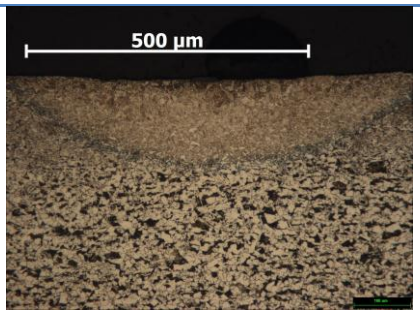	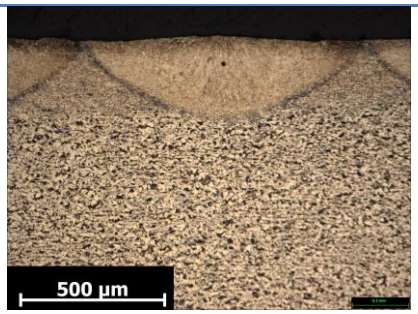
Power Density = 0.015 MW/cm^2	**Power Density = 0.031 MW/cm^2**
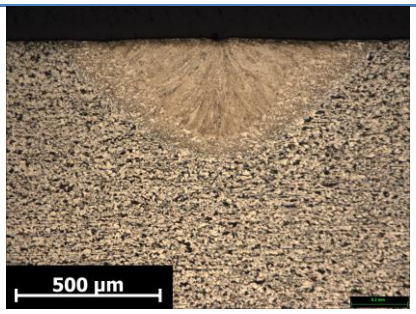	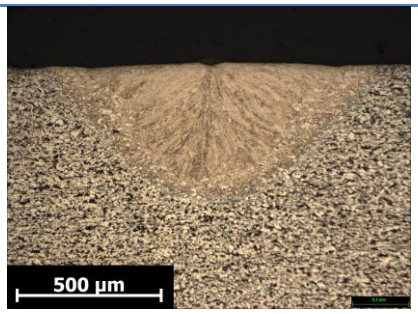
Power Density = 0.046 MW/cm^2	**Power Density = 0.059 MW/cm^2**
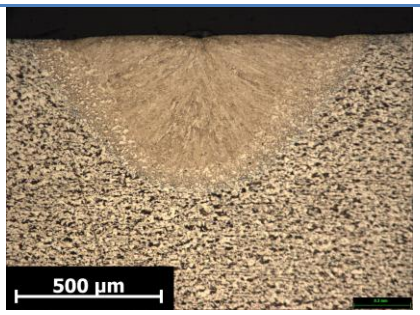	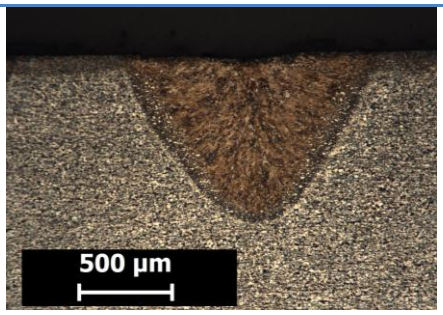
Power Density = 0.073 MW/cm^2	**Power Density = 0.115 MW/cm^2**
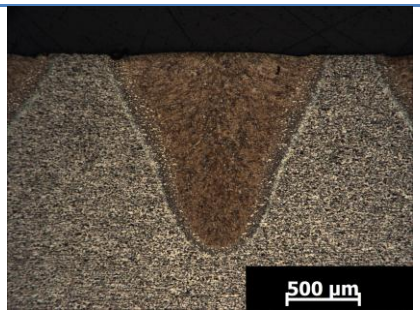	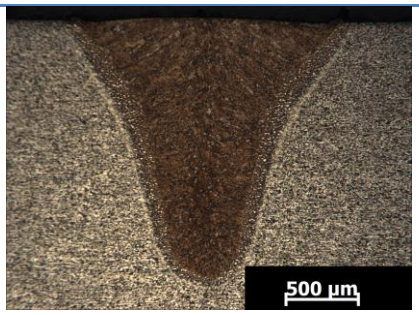
Power Density = 0.194 MW/cm^2	**Power Density = 0.256 MW/cm^2**

Figure 54 - Macrograph of PW laser welds made with beam diameter of 0.9 mm and an interaction time of 20 ms

Figure 54 shows how the weld profile changes with the increase of the power density in the PW laser welds. It can be seen that the weld profile changes from a conduction mode profile to a keyhole profile due to a considerable increase of the depth-to-width ratio of the weld profiles. The question is if there is a transition mode like the one shown for the CW laser. The small cavity noticed in some of the weld profiles (e.g. Figure 54 weld profile with power density of 0.059 MW/cm^2) is likely to be associated with melt displacement [134] in response to vapour recoil pressure. In other words, the presence of that small cavity on the top surface of some of the weld profiles is associated with the formation of a small keyhole. Welds made with average power densities below this level (the first weld that shows a cavity), can be considered to be in the conduction mode. Close inspection of Figure 52 and Figure 53 shows that there is a small range of average power densities around 0.07 MW/cm^2 where there is only a slow increase in penetration depth, This could indicate the presence of a small transition mode region in PW laser welds.

PW laser	CW laser
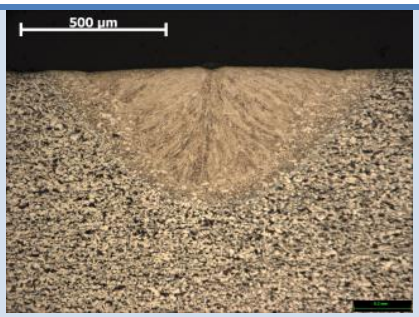	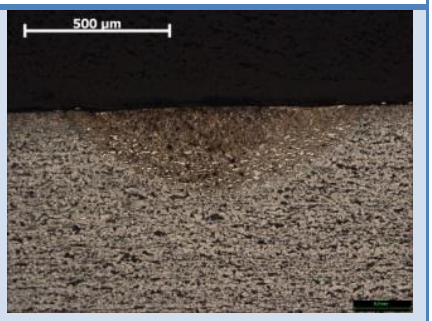
Power Density = 0.059 MW/cm2 **Penetration Efficiency = 0.05 mm/J**	**Power Density = 0.056 MW/cm2** **Penetration Efficiency = 0.02 mm/J**
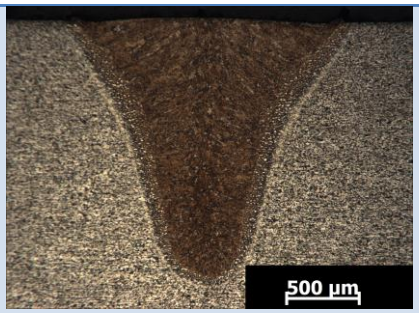	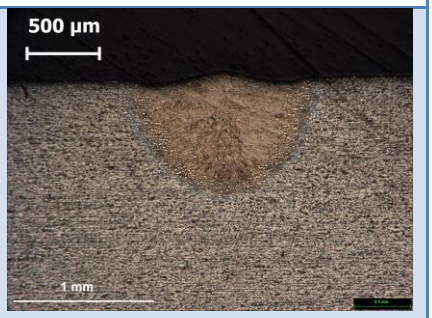
Power Density = 0.256 MW/cm2 **Penetration Efficiency = 0.06 mm/J**	**Power Density = 0.253 MW/cm2** **Penetration Efficiency = 0.02 mm/J**

Figure 55 - Macrographs of cw, on the right, (beam diameter=0.95mm) and pw, on the left,(beam diameter=0.9 mm) laser welds with an interaction time of 20ms and similar values of power density

For similar values of power density the welds made with the pw laser have a much higher penetration depth (as shown in Figure 55) and also higher penetration efficiency.

A comparison, between cw and pw laser, using interaction time, and spatial peak power density, instead of average power density, as process parameters was also made.

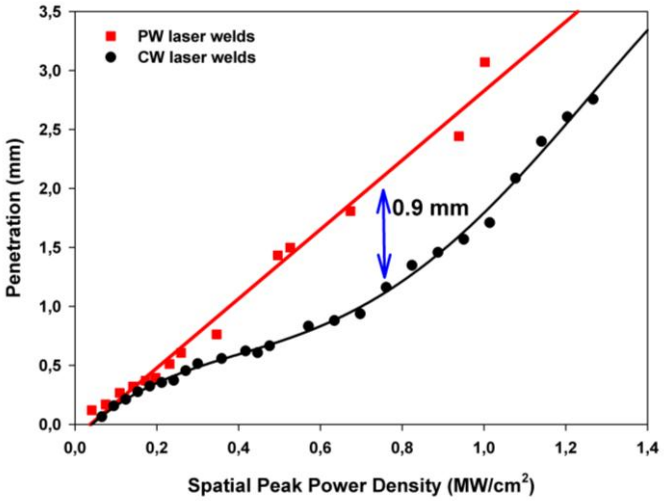

Figure 56 - Penetration versus spatial peak power density for an interaction time of 10 ms and a beam diameter of 0.95 mm for the cw welds and a beam diameter of 0.9 mm for the pw

Figure 56 shows the variation of the penetration depth with spatial peak power density for cw and pw laser welds made with an interaction time of 10 ms. Comparing with Figure 53 the difference of the penetration depth, under the same conditions, reduced from 2.2 mm to 0.9 mm. For an interaction time of 20 ms the difference in penetration depth between cw and pw when peak power density is used is negligible as shown in Figure 57.This should be compared to Figure 52, which uses average power density. ,

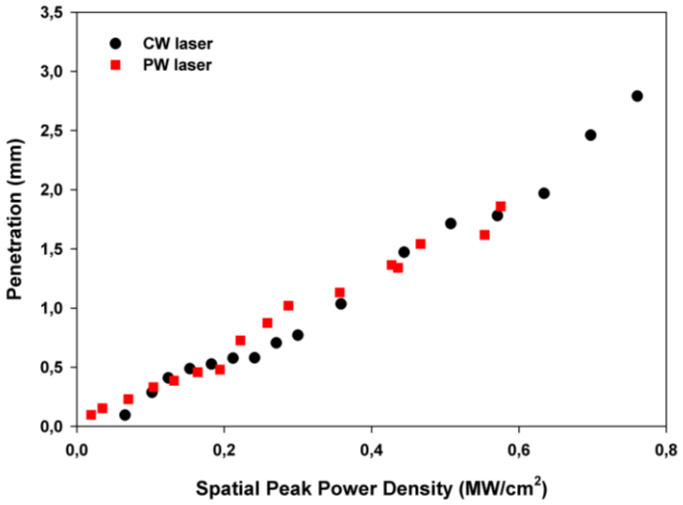

Figure 57 - Penetration versus spatial peak power density for an interaction time of 20 ms and a beam diameter of 0.95 mm for the cw welds and a beam diameter of 0.9 mm for the pw

6.4 Discussion

When comparing the results of the cw and pw laser welding samples it can be seen that the behaviour of these two systems is somewhat different.

In cw laser welds we could easily identify three different modes as outlined in Assunção et al. work [249]. On the other hand pw laser welds did not seem to have a transition mode between conduction and keyhole (Figure 52 and Figure 53). However, looking into more detail to the results it was possible to identify a small power density range where the penetration depth increased slowly, Figure 52, which might be related to the presence of a transition mode. Meaning that in PW laser three mode can also be identified, despite the fact that the transition mode is much less evident.

So why is this power density range for the transition region much smaller than the one obtained in cw laser welds, Figure 52. Also, comparing the two lasers, under the same welding conditions, the pw showed a higher penetration than the cw laser. Several studies have been made in the keyhole shape and flow

involved in pw laser welding [107, 110, 114, 163](Figure 58 shows a simplified version of a pulsed laser weld).

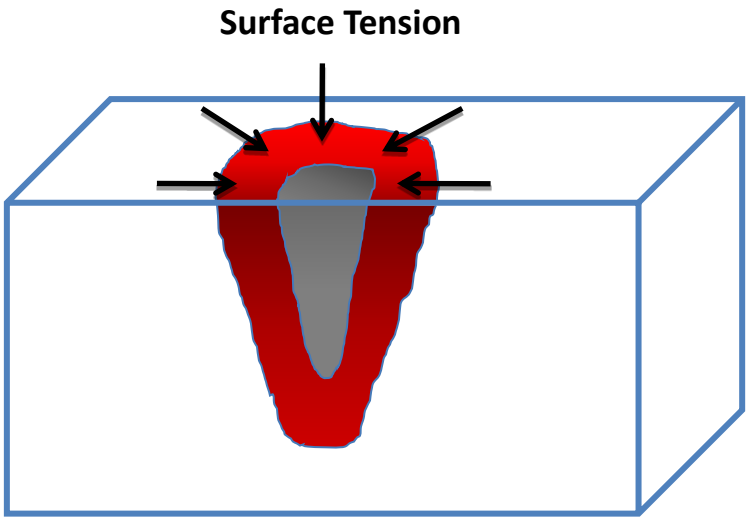

Figure 58 - Schematics of pulsed laser welding

Due to the fact that the weld pool freezes between pulses, pw laser is a stationary weld and the main force opposing the formation of a keyhole is surface tension gradient caused by the temperature gradient[107, 138, 250]. Because the temperature at the centre of the pool is higher, the surface tension gradient will drive the material inwards opposing the formation of a keyhole. This also occurs in cw laser welds, but in addition there is also an effect due to the movement of the weld pool, which also opposes the formation of the keyhole. Several studies have also been made on the keyhole shape and the effect of the welding speed on cw laser welding, supporting that in cw laser welding there is a fluid flow movement caused by the translation of the weld pool[49, 108, 170, 251]. The combination of these two effects, surface tension gradient and weld pool movement , may be responsible for the large transition mode region in cw laser welding. While in pw laser welding the only opposing force is the surface tension gradient and so the transition mode is much less evident.

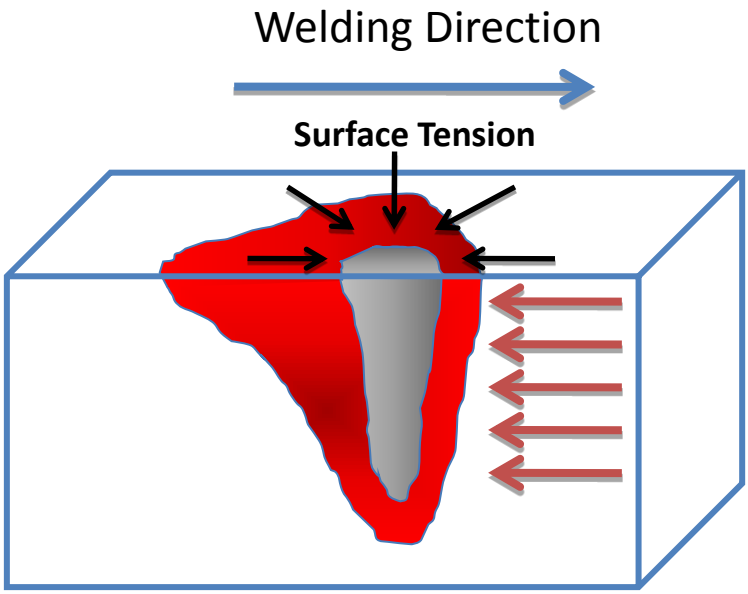

Figure 59 - Schematics of continuous wave laser welding

This difference in fluid flow in pw and cw welding may also explain the differences seen in penetration depth seen with different interaction times. The added force on the keyhole produced by the movement of the weld pool leads to delay of the onset of the keyhole mode and extended transition mode region. This delay leads to the difference in penetration depth seen between welds produced with pw or cw lasers (Figure 52 and Figure 53). The level of the opposing force will depend on the rate of translation of the weld pool – i.e. the welding velocity. The interaction time depends inversely on welding velocity. So the closure force will be higher for shorter interaction times. This means one would expect the penetration depth difference will be greater at shorter interaction times and this is confirmed by Figure 52 and Figure 53.

When using spatial peak power density instead of average power density the difference in the penetration depth, in the keyhole mode, was reduced from 2.2 mm to 0.9 mm for an interaction time of 10 ms, Figure 56. While for an interaction time of 20 ms there was no difference in the penetration, Figure 57. Comparing a Gaussian profile and a ‘top-hat’ profile, with different values of

spatial peak power density, with an interaction time of 20 ms with the cw laser there was also no difference in the penetration, Figure 50. This shows that the higher spatial peak power density of the pw laser might be one of the reasons for the higher penetration efficiency shown by this type of laser.

It should also be noted that there may be some effect due to the definition of interaction time for the cw laser. In the case of the pw laser the interaction time is defined by the pulse duration and is valid across the whole of the irradiated area. On the other hand, the interaction time calculated for the cw laser is the maximum interaction time, Equation 3, and is only valid for the centre of the beam. The closer to the edge of the beam perimeter of the laser beam the lower the interaction time, until it reaches zero at the edge of the beam. In reality an integrated value should be used. The effect of this is that the interaction time should probably be somewhat shorter which would lead to a reduced penetration depth and therefore even more of a difference between the pw and cw welds.

6.5 Conclusions

The conclusions are:

Continuous wave laser welds show a large transition mode region as it was previously observed [249] . In pw laser welds this transition mode is much less evident, narrow and difficult to identify.

When comparing the material interaction, between a CW laser and a PW laser, made under similar conditions (power density, interaction time and beam diameter) pw welds have a much higher penetration depth compared to cw welds. This highlights the much higher penetration efficiency of pw laser welding, which results in a much lower heat input requirement to achieve the same penetration depth.

These differences in behaviour are related to the combination of two effects:

- There is surface tension gradient driven fluid flow which acts in opposition to the formation of a keyhole. This fluid flow is the origin of the transition region. In cw welding there is additional fluid flow towards the keyhole due the translation of the weld pool through the material. This delays the formation of the keyhole further and leads to the wide transition region observed in cw welding. This also leads to the differing penetration depths observed for cw and pw laser welds. The size of the difference depends on the interaction time.
- The pulsed laser has a higher spatial peak power density than the continuous wave laser. This results that at 10 ms interaction time the penetration depth is higher for the pw welds. However, for 20 ms interaction time the penetration depth is the same for pw and cw welds.

7 Conduction Laser welding of Aluminium

This chapter present a study looking at conduction mode laser welding of aluminium. During the investigations, the effect of the beam diameter on the penetration depth was studied. To this aim, statistical regression and numerical simulations have been utilised. In this study, a new conduction-only thermal model of a laser weld pool has been developed which uses temperature-dependent effective thermal conductivity. In this approach, the convective part of the heat transfer process is modeled by utilising the Peclet (Pe) number calculated form fluid dynamics theory. Heat losses due to evaporation from the weld pool are considered by a heat-flux reduction method. The model has been studied for a range of welding parameters and validated against experimental data. The optimum beam diameter, where the penetration depth is maximal, was also identified. The utilised numerical simulations helped identifying the mechanisms governing the weld geometry. In this study, the effect of power and welding speed on the optimum beam diameter was also assessed as well as the influence of the beam diameter on the width of the weld.

E. Assunção planned the experiments and carried out some of the welding trials as well as the analysis of the welds. He also implemented the statistical regression to the obtained experimental data.

M. Benke developed the numerical simulation model based and analysed the results obtained with the model.

S. Williams provided supervision and technical advice.

7.1 Introduction

The need of reducing weight – especially in the automotive industry – has lead to the use of aluminium alloys[242, 252, 253]. Laser welding of aluminium alloys has been extensively researched. However, this process still presents low reliability due to the high reflectivity, high thermal conductivity, low viscosity and the presence of different alloy elements[42, 43, 89, 179, 254-256]. There are three modes of laser welding: conduction, keyhole and transition mode. The type of welding mode depends on the applied power density and interaction time[257].

When the power density is insufficient to cause significant boiling, the weld occurs in conduction mode. These welds have no pores, no cracks, no undercut and are free of spatter. In this welding mode, application of large beams reduces fit-up problems[92]. Despite these advantages, only a few studies have investigated the application of conduction mode welding[100, 179, 223]. There is also a low number of studies on the effect of the welding parameters on this laser mode. Bag and Trivedi studied the effect of power and On-time on the weld pool shape, using a finite element model with an adaptive heat source [240, 258]. Bos evaluated the weld pool size for different powers and welding speeds [259]. These and several other studies focused mainly on the effect of power and welding speed on conduction mode welds[150, 256, 260]. None of these works focused on the effect of the beam diameter in conduction laser welding.

First Morgan and Williams[92, 146] and then Okon[145] concluded that the beam diameter has a significant effect on the penetration depth. Based on their experiments, they also identified the optimum beam diameter resulting in the maximum penetration. The existence of the optimal beam diameter was explained considering evaporation temperature at the surface. It was also used to identify the physical limit of conduction mode [92, 146].

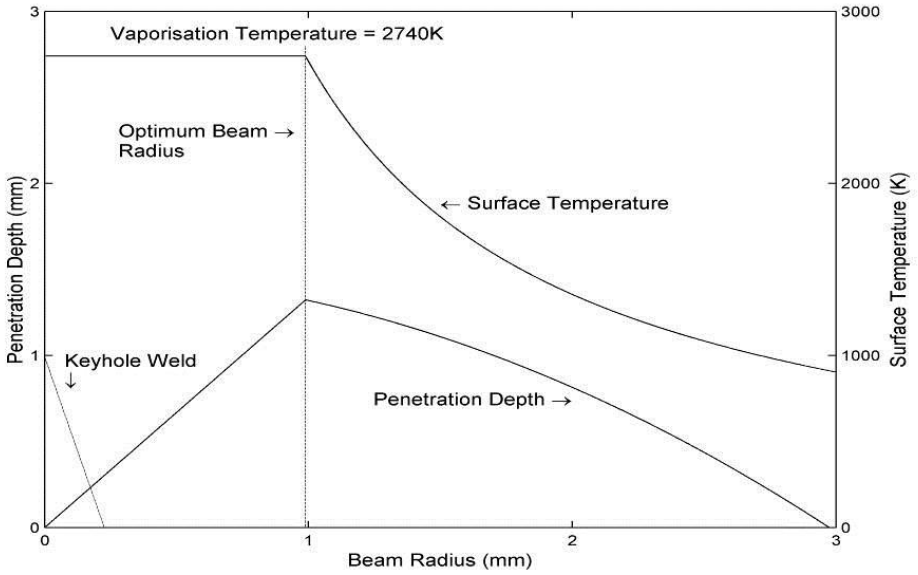

Figure 60 - Variation of the surface temperature and the penetration, with beam radius, in aluminium for a constant power and welding speed[92, 146]

Motivated by these studies, current work presents a systematic experimental, statistical and numerical investigation. In the present study, the effect of beam diameter on the penetration depth was studied for a range of welding speeds and powers using the statistical and numerical models obtained. This paper also demonstrates a new heat conduction model for weld pools. In this approach, thermal conductivity of the weld pool is considered to be temperature-dependent. Determination of the effective weld pool convection is based on the Peclet number (Pe), calculated from fluid dynamics theory. Another important feature of the model is the capability to account for evaporation heat losses. In this approach, heat losses due to evaporation are modeled utilising a local heat flux reduction algorithm. Due to its importance in practical applications, the effect of beam diameter on the weld width as also been studied.

7.2 Methodology

7.2.1 Experimental setup

Experiments were carried out on 12 mm thick, 2024 Aluminium plates (see Table 10 for chemical composition). The surface of the samples was wire brushed and cleaned with acetone. The clean surface was sprayed with graphite to increase uniform coupling of the laser beam. No shielding gas was used.

The applied IPG 8 kW continuous wave (cw) fibre laser had a 300 µm delivery fibre. The beam was collimated with a 125mm focal length lens and focused using a 250mm focal length lens. The laser head was attached to a Fanuc robot and positioned with a ten degree angle to the surface normal of the samples. Different beam diameters were obtained by changing the distance of the laser lens from the sample.

Element (wt%)	Al	Cr	Cu	Fe	Mg	Mn	Si	Ti	Zn	Others
2024–T3	90.7 - 94.7	Max 0.1	3.8 - 4.9	Max 0.5	1.2 - 1.8	0.3 - 0.9	Max 0.5	Max 0.15	Max 0.25	0.15

Table 10 - Chemical composition of aluminium alloy 2024

7.2.2 Preliminary experiments for determining process window

A set of preliminary experiments provided the necessary information for understanding the general behaviour of the process and determining the limitation of the process parameters. The experimental setup was the same as described previously. While two parameters were kept constant, the other was varied in fixed steps till an unfeasible combination was found on the basis of visual assessment of the weld. This was done to guarantee that the welds were not done in deep keyhole mode and that there was no risk of no melting.

Based on the preliminary experiments the following process window was determined:

2 kW ≤ Power ≤ 4 kW

0.1 m/min ≤ Welding Speed ≤ 2.0 m/min

3 mm ≤ Beam Diameter ≤ 12 mm

7.2.3 Development of the statistical model

Having established the process window, a D-Optimal design method [261] was chosen for the experiment. Optimal designs are computer-generated and are particularly suitable when the experimental region is irregular, the model is nonstandard (i.e. the experimenter knows beforehand some interactions will not be significant), and/or there are certain sample size requirements (i.e. reduced number of runs must be done). A design is D-Optimal if it “minimises the volume of the joint confidence region on the vector of regression coefficients” [261]. This allows the experimenter to input the necessary information, process window, constraint equations and specifies any conditions related to unnecessary model terms and sample size. The software then runs and algorithm and returns the set of experiments that have the highest D-Optimal efficiency.

For this statistical model welding speed, beam diameter and power were selected as the factors. The application of the software reduced the number of experiments and allowed the analysis and correlation of the results. The response used in the model was the penetration and the width of the obtained weld. Based on the penetration variation with the process parameters (welding speed, beam diameter and power) it was possible to determine the optimum beam diameter, which resulted on the beam diameter where the penetration was maximum for a constant power and welding speed.

The software used was the Stat-Ease Design-Expert® 7.1 which is a statistical software that creates and evaluates general factorial designs, fractional factorial

designs, optimal designs, response surfaces. The software indicated that 46 experiments were necessary to calculate the regression coefficients for the full mode.

7.2.4 Development of the Numerical Model

Numerical simulation is widely used to predict spatial distribution of the temperature during welding processes. Accuracy of the calculations strongly depends on the applied weld pool model. Therefore, appropriate description of the melt pool thermal behaviour is essential. Depending on the level of detail, two main approaches can be considered.

One is the application of fluid dynamics simulations for the molten zone [262-264]. In this approach, the fluid flow developing in the weld pool is simulated. Thus, convective heat transfer is determined explicitly. In such models, a coupled system of fluid flow and heat transfer equations is solved [263, 265]. To calculate the dimensions of the molten region, the solid-liquid interface is tracked. Although this approach is quite sophisticated, computational requirements make it less favourable for most practical applications.

An alternative option is the application of a simple conduction heat transfer model. In this case, convective heat transfer is modelled, rather than calculated explicitly. Here, melt flow convection is considered by enhanced thermal conductivity of the molten region [266]. To accurately determine the effective thermal conductivity of the weld pool, De and DebRoy [267] presented a multi-variable optimisation method.

In the present study, a thermal model of laser welds has been developed. The model parameters – absorptivity of the material and cooling rate of the backing plate – were determined from experiments.

For this, bead on plate welds were performed on 12 mm thick Al2024 T3 samples. Sample sizes were 150 mm x 200 mm and 300 mm x 300 mm, for the 0.5 m/min and the 0.1 m/min travel speed trials, respectively. The plates were coated with graphite to ensure uniform absorptivity of the samples. An

extraction fan providing 900 m^3/h volume flow rate was directed at the top surface of the sample.

The applied laser source was an IPG 8 kW continuous wave fibre laser. The beam was delivered by a 300 µm diameter fibre which was collimated with a 125 mm focal length lens and focused using a 250 mm focal length lens. At the focal point, this produced a beam profile with a top hat distribution. These experiments were carried out away from the focus in order to achieve the large beam diameters required for laser conduction welding. Consequently, the resulting beam profile had a quasi-Gaussian heat distribution. Continuous motion of the laser head was ensured by a Fanuc robot. During the experiments, thermal histories were registered by K-type thermocouples attached to the top surface of the plates.

The thermal cycle of the performed welds was described by a steady state heat transfer model. To simulate the constant travel speed of the laser spot, the workpiece was moving under the steady heat source in the model. The simulated weld geometry was determined by tracking the liquidus isotherm.

During the simulations, a surface heat source with ideal Gaussian heat flux distribution was considered. Heat loss due to evaporation was taken into account by a heat flux reduction algorithm developed and implemented by the authors. Simulations involving evaporation were performed in two steps. In the first step, the temperature distribution was calculated without considering evaporation heat losses. In the next step, surface temperature under the heat source was monitored. If an element`s surface temperature exceeded the evaporation limit, the input heat flux was reduced. Moderate reduction of the heat flux was performed when the surface temperature was higher than the evaporation limit.

Experimental trials were performed under two different cooling conditions. In the first case, the sample was tightly clamped to a copper backing bar and the extraction fan running. In the second case, the sample was unclamped, the backing bar removed and the fan turned off. During the simulations, the applied

cooling conditions were represented using different values of convection coefficients. On the free surfaces, the convection coefficient was 20 W/m^{2}K for the ventilated case and 5 W/m^{2}K considering natural convection [268]. The cooling effect of the tightly clamped copper backing bar was modelled with 150 W/m^{2}K. Cooling of the unclamped back plate was considered with 10 W/m^{2}K. Convection parameters of the back plate were determined from fitting to experimental results. Free stream temperature was 293 K for all cases.

For the 2024 alloy, a density of ρ = 2770 kg/m^3 was assumed [238]. Specific heat (cp) was considered to be temperature dependent, the values were adopted from Richard`s work [269]. Thermal conductivity of Al 2024 in solid phase was considered to be k = 190 W/mK [238]. As the material melts, conductivity changes to k_{melt} = 85 W/mK [238].

This value however does not represent the thermal behaviour of the weld pool. Due to fluid flow, heat transfer phenomenon is rather more complex than this. To address this issue, effective thermal conductivity based on melt flow convection has been determined. The flow field developing in laser welds is surface tension dominated [270]. Thus, the velocity scale is calculated as [265]:

$$u_{R,0} = \left[\frac{\left(\partial\gamma/\partial T\right)^2 \left(\Delta T\right)^2}{\rho\mu L} \right]^{1/3} \qquad (14)$$

Here, $\partial\gamma/\partial T$ is the surface tension coefficient, ΔT is the temperature difference across the weld pool and μ is viscosity. For aluminium, $\partial\gamma/\partial T$ = 3.5 x 10^{-4} N/mK and μ = 1.1 x 10^{-3} kg/ms [265]. Fluid flow simulations of aluminium weld pools by Tsai and Kou [270] and Farzadi et al [271] showed that the average melt flow velocity is several orders of magnitude smaller than the velocity scale. The average melt flow velocity, u was calculated as

$$u = 0.0015 \cdot u_{R,0}\,. \qquad (15)$$

In heat transfer theory, the ratio between convective heat transfer and heat conduction is described by a dimensionless parameter, the Peclet number [268]. By its definition,

$$\mathrm{Pe} = (\rho\, c_p\, u\, L) / k_{melt} \qquad (16)$$

with u average melt flow velocity and L weld pool width. Having the Peclet number (eq. (16)) in hand, effective thermal conductivity can be formulated as:

$$k_{eff} = k_{melt}\,(1 + \mathrm{Pe}). \qquad (17)$$

As equation (14) shows, the melt flow velocity scale – thus convection phenomenon – is influenced by the temperature. In the model, this effect was represented by temperature-dependent effective conductivity of the weld pool. During the calculations, thermal conductivity was set to keff = 85 W/mK at the liquidus temperature, Tliq = 911 K [238]. At the evaporation temperature Tevp = 2743 K [238], effective thermal conductivity was defined by equation (17). Conductivity values between these temperatures were calculated using linear interpolation. For the calculation of the Pe number, weld pool width L was determined by tracking the liquidus isotherm.

It is important to point out the dependency of the weld geometry on the temperature field, thus implicitly, on the Pe number. Due to this relation, effective conductivity values have been iteratively re-calculated until the difference between successive keff values became less than 5 W/mK.

7.3 Results and discussion

7.3.1 Statistical analysis

The purpose of the developed statistical model was to study the effect of the different welding parameters on the penetration obtained in conduction laser

welding of aluminium. To determine the relationship between the variables and the response, an analysis of variance (ANOVA) was performed.

Statistical test	Penetration model	Width model
R^2	0.9829	0.9511
Adjusted-R^2	0.9694	0.9389
Pred-R^2	0.9046	0.9091
Adeq. Precision	40.894	45.833
p-Values	<0.0001	<0.0001

Table 11 - Statistical tests performed on the final models

Table 11 shows the coefficients of determination (R^2) and adjusted-R^2 for the two responses. In both cases the R^2 coefficients are over 95%, which means that the variability in the data can be explained by the models [261]. The p-value helps the decision maker to determine the significance of the data, and its threshold is normally 0.05 [261], which in the case of the two responses this value was smaller than the threshold value. Pred-R^2 values, which predict the variability explained by the model for new data, are in reasonable agreement with the adjusted-R^2 values and in the two responses the Adeq. Precision tests, which measure the signal-to-noise ratio, are greater than 4, which is the minimum accepted value for this term.

To evaluate the model reliability further, four additional welds were done. The penetrations were then compared with those predicted by the model, Table 12. The obtained values were within the confidence interval proving the reliability of the model.

Penetration Depth (mm)	
DoE model	**Experimental Data**
2.69	2.54
0.80	0.77
3.15	3.00
4.70	4.85

Table 12 - Comparison of the penetration obtained experimentally with the penetration obtained with the DoE model

The performed experiments allowed us to study the influence of individual parameters, such as power and welding speed on the optimal beam diameter. Conduction mode laser welds have been performed utilising the parameter combinations determined by DoE. The resulting penetration depths have been used as basic points for the regression surface fitted over the investigated parameter range. Figure 61 and Figure 62 illustrates the regression surfaces for 3 kW and 4 kW laser powers, respectively.

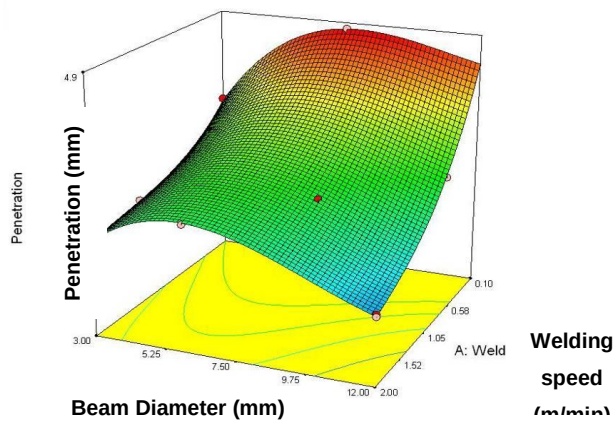

Figure 61 - Surface plot for a constant Power of 4 kW

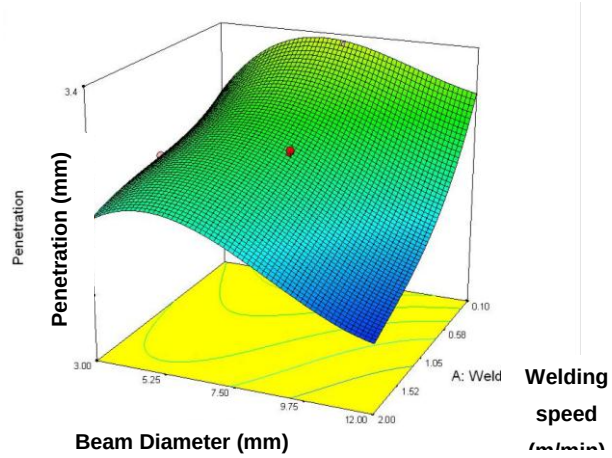

Figure 62 - Surface plot for a constant Power of 3 kW

Plotting the same data, but in two dimensions, maintaining one of the parameters constant the graphs in Figure 63, Figure 64 and Figure 65 are obtained. The lines represent data obtained with the statistical model while the points are actual data points, obtained by measuring actual welds. All of this Figures show the accuracy of the obtained statistical model.

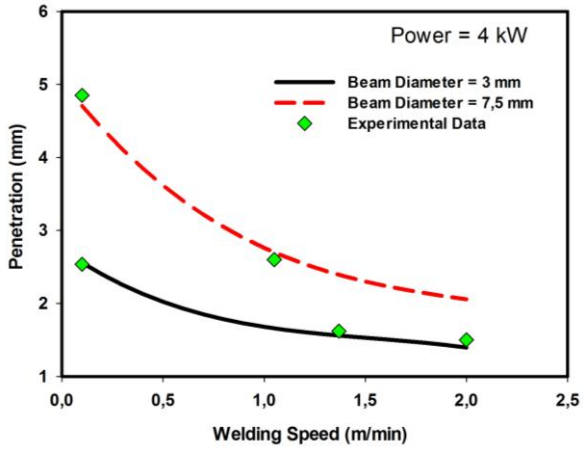

Figure 63 - Variation of the penetration with the welding speed with different beam diameters for a constant power of 4 kW.

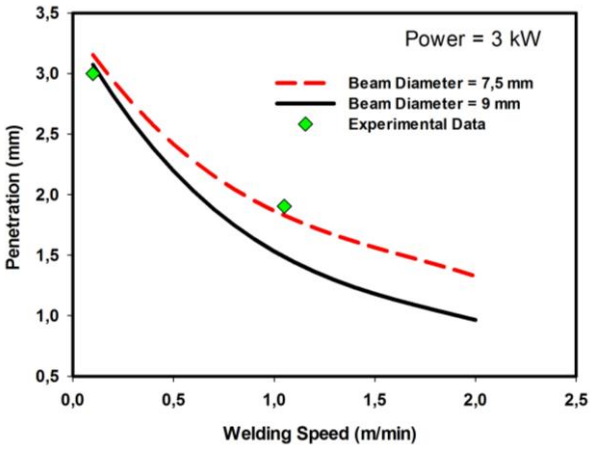

Figure 64 - Variation of the penetration with the welding speed with different beam diameters for a constant power of 3 kW.

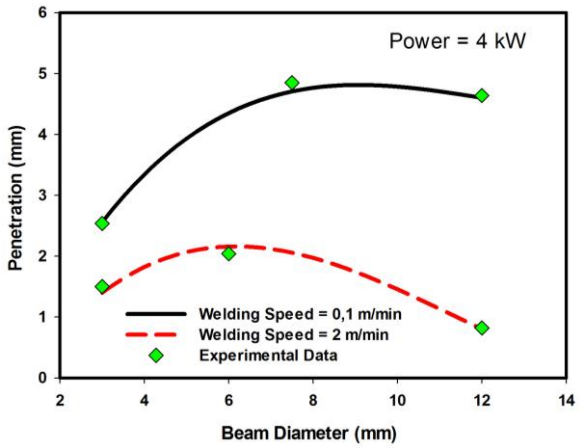

Figure 65 - Variation of the penetration with the beam diameter with different welding speeds for a constant power of 4 kW.

Figure 63 and Figure 64 clearly indicate that penetration decreases with increasing welding speed, for a constant power and beam diameter. The beam diameter however has a different effect on the penetration depth, Figure 65. This effect will be discussed further in this study.

7.3.2 Numerical model

Numerical simulation of the steady state heat transfer has been performed to determine the penetration depths for various welding parameter combinations.

Figure 66, Figure 67, Figure 68 and Figure 69 demonstrate the temperature histories calculated and measured for different combinations of the welding parameters. Measurement points are located halfway between the start and end point of the weld, 5 and 10 mm from the edge of the laser beam.

The temperature graphs show good agreement between the simulations and the experimental values. The maximum difference between the calculated and measured peak temperatures is 25K. During the simulations, absorptivity values of 90% and 65% were used for the 0.5 m/min and 0.1 m/min travel speed trials. These values were determined by fitting the calculated peak temperatures to the experimental data.

For trials using v = 0.5 m/min welding speed, the calculated heating and cooling rates agree well with the measured ones. When considering the case with v = 0.1 m/min welding speed, the calculated heating and cooling rates show interesting behaviour. The simulation predicts slower heating in the first 80 seconds and accurate heating rate close to the peak temperatures. When considering the cooling phase, the calculated cooling rates match with the measured data in the first 20 seconds. After this initial period, the calculation predicts slower cooling compared to the measurement.

It is important to remark that in the early stage of the simulated heating cycle, a significant 60 K temperature surplus can be observed. This temperature increment leads to the observed change in the heating rate. Similar early stage temperature increment can also be observed for trials with higher welding speed. However, the deviations for these trials are negligible (5-6 K), as Figure 66, Figure 67, Figure 68 and Figure 69 show.

Figure 70, Figure 71, Figure 72 and Figure 73 demonstrate the experimental and simulated weld geometries. For P = 2 and 3 kW laser powers, the calculated weld geometry is similar to the experimental profile. However, the simulations slightly under-predict the width and the depth of the welds. Focusing on trials using P = 4 kW laser power, the simulations over-predict the penetration and under-predict the weld width. Relative errors in the weld geometry predictions are presented in Table 13.

Process parameters	Penetration error [%]	Weld width error [%]
2kW, 0.5 m/min	11	14
3kW, 0.5 m/min	1	16
4kW, 0.5 m/min	16	11
4kW, 0.1 m/min	7	6

Table 13 - Relative errors in the prediction of the weld geometry

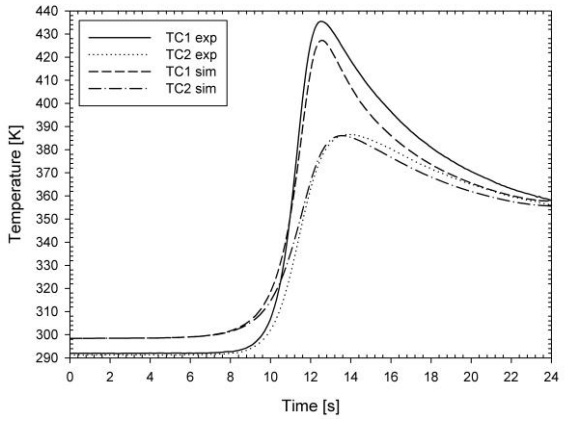

Figure 66 - Temperature history for P = 2 kW, d = 9 mm, v = 0.5 m/min

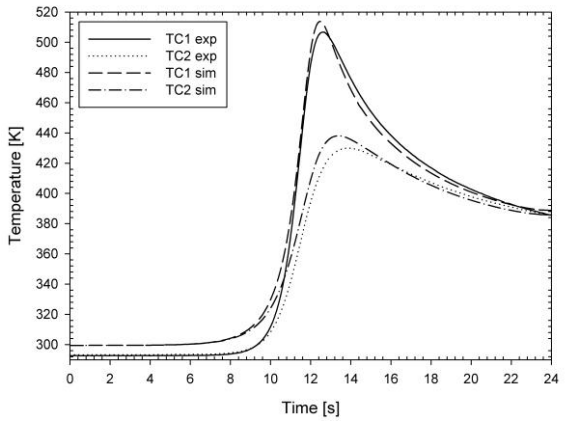

Figure 67 - Temperature history for P = 3 kW, d = 9 mm, v = 0.5 m/min

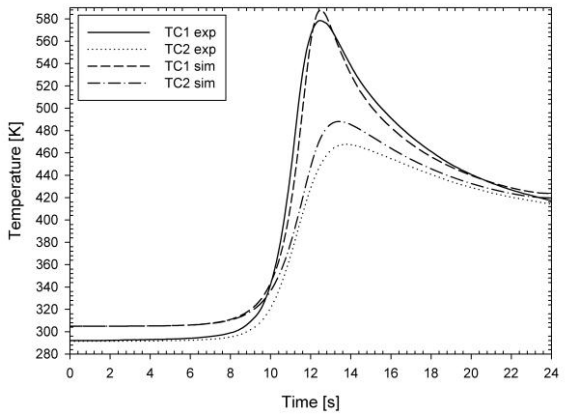

Figure 68 - Temperature history for P = 4 kW, d = 9 mm, v = 0.5 m/min

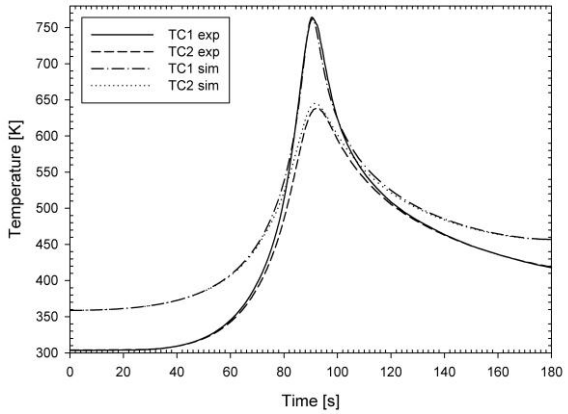

Figure 69 - Temperature history for P = 4 kW, d = 7.5 mm, v = 0.1 m/min

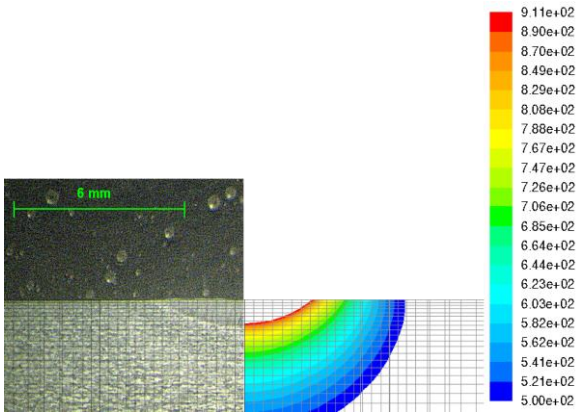

Figure 70 - Weld profile for P = 2 kW, d = 9 mm, v = 0.5 m/min

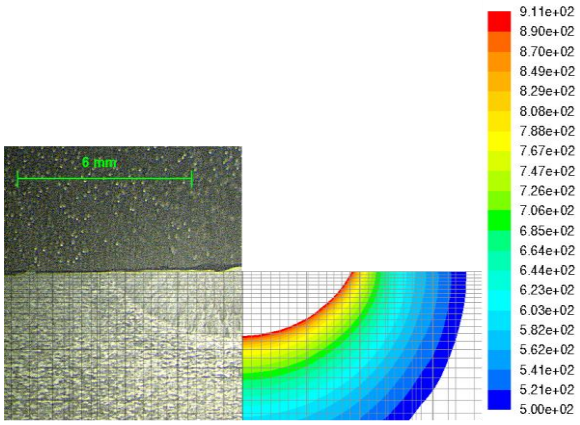

Figure 71- Weld profile for P = 3 kW, d = 9 mm, v = 0.5 m/min

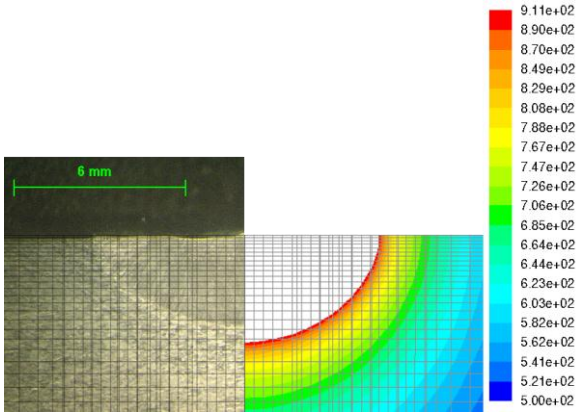

Figure 72- Weld profile for P = 4 kW, d = 9 mm, v = 0.5 m/min

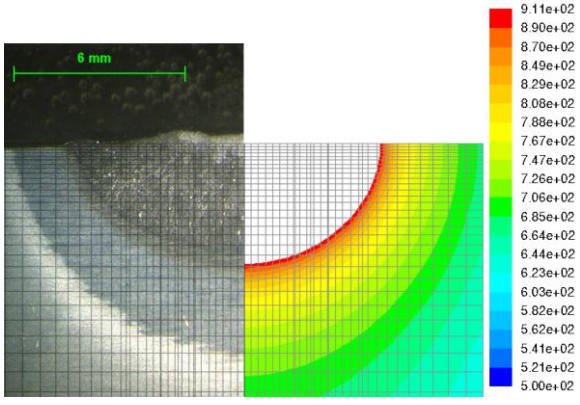

Figure 73 - Weld profile for P = 4 kW, d = 7.5 mm, v = 0.1 m/min

Figure 66, Figure 67 and Figure 68 demonstrate that the numerical model gives good description of the thermal cycle for the v = 0.5 m/min welding speed trials. The observed good agreement between the experimental and the calculated cooling rates suggests accurate prediction of the surface convection parameters.

Focusing on the trial with v = 0.1 m/min welding speed, accuracy of the model is limited. As noted on Figure 69, the calculated heating and cooling rates deviate from the measurement data. To explain the observed behaviour, the applied steady state heat transfer model was investigated.

Dimensional analysis was performed to assess the relative importance of convective and conductive heat transfer. Considering the relevant terms of the heat transfer equation, the heat transfer ratio is:

$$r_{HT} = v\,\Delta x\,\rho\,c_p / k. \qquad (18)$$

For the sake of the dimensional analysis, constant thermal properties were used. Considering Δx = 0.15 m half length of the sample, cp = 800 J/kgK and k = 120 W/mK, the heat transfer ratio for the v = 0.1 m/min travel speed trial is r_{HT} = 4.61.

As the dimensional analysis shows, convection is almost five times stronger than thermal diffusion. Although convection is dominant, diffusion has a considerable influence on the heat transfer in the v = 0.1 m/min travel speed trial. The artificial temperature increment observed in the first part of the heating cycle is presumably caused by thermal diffusion. This shortcoming inevitably affects the heating rate as well.

For the v = 0.5 m/min travel speed trials performed on the 200 mm long plates, the heat transfer ratio is r_{HT} = 15.36. For these runs, convection is one order of magnitude greater than thermal diffusion. As a result, artificial temperature increments are negligible in these cases. Thus, calculated heating and cooling rates match with the experimental values.

Reduction of the absorptivity as the welding speed changes from 0.5 m/min to 0.1 m/min can be explained based on thermal effects. The slower heat source

causes more efficient pre-heating of the material ahead of the beam. This likely destroys the graphite coating, thus reduces the absorptivity.

The weld profiles presented on Figure 70 to Figure 73 show good agreement with the measured real weld geometries. The simulation results match with the experiments for welds with various aspect ratios. This suggests that the developed conduction-based thermal model of the weld pool is accurate.

The most perceptible difference between the measured and calculated penetration occurs for the P = 4 kW trial, using v = 0.5 m/min welding speed. It is worth noticing that the same trial produced the highest over-prediction of the simulated peak temperatures. Therefore, such over-prediction of the penetration is not surprising.

7.3.3 Effect of welding parameters in conduction mode and comparison between the statistical model and the numerical model

In order to further investigate the effect of beam diameter on the penetration, relevant cuts of the 4 kW regression surface, Figure 61, have been considered at welding speeds 0.1, 0.5 and 2 m/min. To the same end, numerical simulations at these welding speeds have been performed. Simulations have been carried out for beam diameter ranging from 3 mm to 12 mm. Figure 74 demonstrates the penetration depths in the function of beam diameter for various welding speeds.

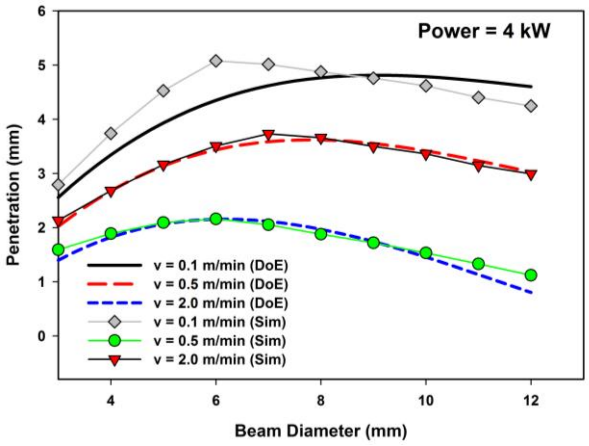

Figure 74 - Variation of the penetration with the beam diameter with different welding speeds

Figure 75 shows the variation of the penetration depth for different laser powers, as the beam diameter changes. Similarly to Figure 74, curves without symbols represent results from the regression analysis and curves plotted with symbols denote the simulation data.

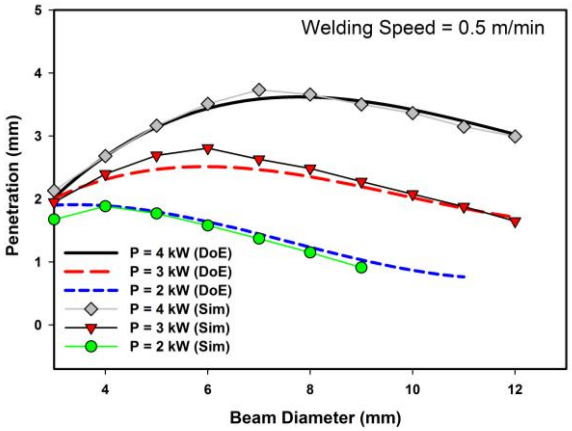

Figure 75 - Variation of the penetration with the beam diameter for different powers

The simulation results and the penetrations obtained in the regression analysis showed very similar values. The only noticeable deviation occurred for the 4 kW case with the welding speed of 0.1 m/min, shown on Figure 74. Here, the simulation results over-predicted the penetrations calculated from the regression analysis for smaller beam diameters.

Penetration curves shown in Figure 74 and Figure 75 have similar tendencies. For small beams, the penetration increases with increasing beam diameter until reaching the maximum value. This penetration maximum defines the optimal beam size. After the peak, the penetration decreases with increasing beam diameter.

The influence of process parameters – power and welding speed – on the optimum beam diameter has been studied based on Figure 74 and Figure 75. Increasing welding speed decreases the optimum beam diameter, for a constant power, see Figure 76. The optimum beam diameter increases with increasing power.

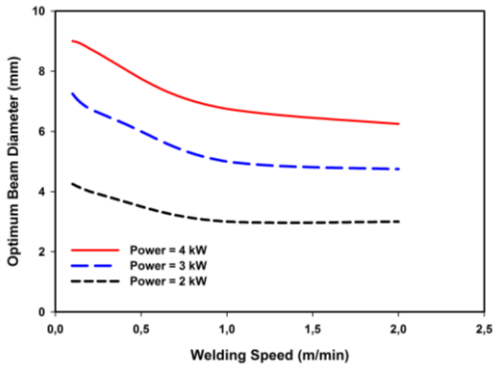

Figure 76 - Variation of the Optimum Beam Diameter with Welding Speed for different power levels

Width curves shown in Figure 77 have similar tendencies to the penetration curves, Figure 74 and Figure 75. For small beams, the width increases with increasing beam diameter until reaching the maximum value. After this peak, the width decreases with increasing beam diameter.

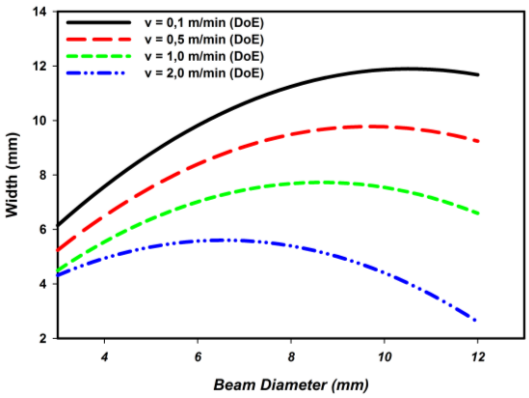

Figure 77 - Variation of the width with the beam diameter for different welding speeds and power of 3 kW

Investigating the regression analysis and simulation results for different powers and welding speeds shows that the beam diameter has significant effect on the penetration, Figure 74 and Figure 75.

The right portion of the curves, in Figure 74 and Figure 75, shows the variation of the penetration for larger beams. In this region, penetration decreases with increasing beam diameter. This trend can be easily explained on the basis of simple heat transfer phenomena. Increasing beam diameter practically results in decreasing power density. According to heat transfer theory, there is a direct relation between power density and penetration depth. As a consequence, decreasing power density decreases penetration.

The left portion of the curves, in Figure 74 and Figure 75, however shows opposite trend. In the region of small spot sizes, increasing beam diameter results in increasing penetration. This practically means that decreasing power density increases penetration in this region. This trend clearly contradicts simple heat transfer theory. The observed trend suggests that penetration behaviour in this regime is governed by a different mechanism, which is interaction time [249]. Interaction time is the heating time of the process on the centreline of the weld and it is the ratio between the beam diameter and the welding speed. Combining Figure 60 with Figure 78 allows a better understanding of the mechanisms involved. For a constant power and welding speed as we increase the beam diameter the power density is decreasing while the interaction time is

increasing, Figure 78. On the left portion of the curves, in Figure 74 and Figure 75, the surface temperature is at vaporisation temperature, based on Figure 60. This means that the decrease of the power density, by increasing the beam diameter, does not change the temperature at the surface. However, this increases the interaction time which results in an increase of the penetration until the optimum beam diameter is reached.

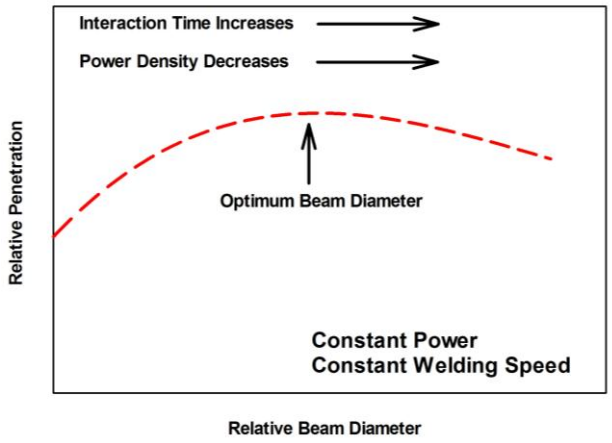

Figure 78 - Variation of the penetration, with beam radius for a constant power and welding speed

The increase of optimum beam diameter with the increase of power can be explained based on the definition of power density. Increasing power requires the increment of the beam diameter in order to maintain similar power density and so maintain the same thermal mechanisms. Optimum beam diameter is also affected by the welding speed. Increasing welding speed reduces the interaction time. Therefore, higher power density is required to cause the same thermal effect.

Investigating the regression analysis for different welding speeds shows that the beam diameter has an effect on the width, Figure 77.

The right portion of the curves, in Figure 77, shows the variation of the width for larger beams. In this region, width decreases with increasing beam diameter. This can be easily explained based on a simple heat transfer phenomena. The

increase in beam diameter results in decreasing the power density. As a consequence the power density is not sufficient to cause melting, especially at the edges of the laser beam.

7.4 Conclusions

In this paper a continuous wave Fibre Laser was used in the defocus position in order to investigate the importance of the beam diameter in laser conduction welding. The study led to the following conclusions:

- It is possible to evaluate that when increasing the beam diameter there is an increase in the penetration, while the surface temperature is maintained at the vaporisation temperature. However, when the surface temperature goes below the vaporisation temperature, a decrease of the penetration happens. The point of transition between the increase and the decrease of penetration is the optimum beam diameter, which results in the maximum penetration.
- The optimum beam diameter depends on the welding speed and the power. For higher levels of power the optimum beam diameter is larger. On the other hand, the optimum beam diameter increases with the decrease of the welding speeds.
- Based on the statistical model obtained, it would be possible, in the range of parameters used, to obtain penetrations of 4.9mm. However this value is only limited by the range of parameters used for these trials.
- The applied numerical model predicted the same effect of beam diameter on the penetration, as was observed from statistical model and from experimental data.
- The applied numerical model provides accurate description of the thermal field for 0.5 m/min travel speed.
- Accuracy of the numerical steady state model is limited for low travel speed.
- During the development of the model it was concluded that the absorptivity changes occur with travel speed due to the pre-heating of

the material and thus removal of the graphite coating in front of the laser beam.

- Both the statistical model and the numerical model provided good approximation with the experimental values

8 Characterisation of Residual Stress State in Laser Welded Low Carbon Mild Steel Plates Produced in Keyhole and Conduction Mode

This chapter presents a paper examining the residual stress state of welds done in conduction mode and in keyhole mode. Characterisation of residual stress state was performed in 4 mm low carbon steel plates laser welded in keyhole and conduction mode. Residual stress characterisation was carried at the ENGIN-X strain scanner at the ISIS, UK. It was shown that although the maximum magnitude of tensile residual stress is similar in welded specimens manufactured under different welding modes the distribution profile is quite different. The conduction welding mode resulted into a larger tensile stress domain as compared to the keyhole mode. This also resulted in a different magnitude of balancing compressive residual stress field. Understanding of such different stress profiles is important for application of such advanced welding processes in joining of design efficient structural material.

E. Assunção did the welding development, planning of the experiments, and analysis of the welds. As well as writing the proposal for beam time at ISIS.

S. Ganguly provided his expertise and knowledge in residual stress measurement and analysis.

A. Paradowska assisted in preparing and measuring the welded samples.

S. Williams and D. Yapp provided supervision and technical advice.

E. Assunção S. Ganguly, D. Yapp, S. Williams, A. Paradowska. "Characterisation of residual stress state in laser welded low carbon mild steel plates produced in keyhole and conduction mode". Journal of Science and Technology of Welding & Joining, 2011, Volume 16, Issue 3, pp 239-243.

8.1 Introduction

Laser welding has two different operational regimes, conduction and keyhole welding. The key difference between these two modes is the power density applied to the welding area. Conduction mode takes place when the power density is not sufficient to cause boiling. In keyhole mode the power density used is high enough to cause vaporisation and create a keyhole in the melt pool [98, 99]. Welding processes generate an integrated structure with a changed microstructure in the fusion and associated heat affected zone along with the creation of a variably distributed residual stress field across the weld. For material engineers it is vital to characterise the residual stress state in a welded structure as residual stresses can have a significant effect on the integrity of the structure while in service[272]. The other important aspect is the distortion of the welded structure, resulting from the generation of residual stress, which may render the structure unusable or add additional cost to repair before putting it into service[273] . In this work residual stress characterisation has been performed on welds produced by laser welding in keyhole and conduction modes. Residual strain measurement was carried out using a spallation neutron source and the stress was analysed.

The main cause of residual stress generation is the compressive plastic yielding that occurs ahead of the molten zone as the material heats and expands during welding. The compressive plastic flow is not balanced by tensile plastic flow during cooling resulting in formation of a tensile residual stress field in and around the weld zone with a balancing compressive stress field further out in the parent material. When the balancing compressive stress field exceeds the critical buckling load, distortion of the welded structure occurs. Therefore, in order to eliminate distortion it is necessary to reduce the tensile stress field across the weld which would reduce the compressive stress field generated in order to balance the tensile stress field [274]. Currently there are several techniques that allow the minimisation of the distortions caused by welding[275-279].

The beneficial characteristics of keyhole welding, especially large penetration depth and relatively small heat affected zone attracted more industrial applications. However, keyhole welding also has several problems that may lead to high levels of porosities and other weld defects [3, 75, 76]. This welding mode, because of its high penetrability, is used for a wide range of applications in different industrial sectors e.g. pipeline, aluminium alloys welding[39, 40] , magnesium alloys welding[61, 280] and stainless steel welding[49].

Conduction mode is the alternative to keyhole mode of welding. The main advantages of conduction welding is the high flexibility and control over its heat input which results in high quality welds free of porosity, undercut and humping. Also conduction welding results in spatter free welds as the weld pool is much less turbulent as compared to keyhole mode. This mode operates at a lower power density and does not involve any significant vaporisation [146]. Conduction mode welding is used mainly in welding aluminium alloys[100], however, more investigations are now being focussed and new applications for this laser welding mode are being introduced[223]. Normally laser welding is selected over other welding processes because of its characteristics of high power density with low heat input. This results in a reduction in generation of residual stresses and distortion. The application of conduction instead of key-hole mode would increase the heat input and thereby also result in an increase of the residual stresses and the distortion. Therefore, it is necessary to have a comparative quantification and characterisation of the residual stresses magnitude and distribution profile for the conduction and key-hole modes of laser welding. This would allow a better understanding on the application based suitability of using these two different welding modes.

8.2 Experimental technique

8.2.1 Preparation of welded samples:

An IPGYLR-8000 continuous wave fibre laser with a maximum power of 8000 W and a wavelength of 1070 nm was used in manufacturing the welded specimens. The laser beam is delivered by a fibre of 300 µm diameter. A 125 mm collimating lens and a 500 mm focal length lens was used which resulted into a beam diameter of 1.2 mm at the focal spot. The focal position, the beam diameter and the beam profile for the lens used was determined using a Primes GmbH Focus monitor system. The welds made with spot diameter larger than 1.2 mm (diameter of the laser spot in the focal position) were obtained by appropriate positioning of the sample in a de-focussed position of the laser beam to obtain the required beam diameter.

The welding parameters necessary to produce conduction and keyhole mode were determined by conducting several experiments and by observing the macrographs of the weld profiles. The parameters used for manufacturing the specimens using different welding modes are shown in Table 14. All the welds were made in bead on plate configuration.

Table 14 - Different welding parameters used

Welding mode	**Keyhole**	**Conduction**	**Conduction**
Beam Diameter (mm)	1.2	9	15
Power (kW)	8	3	3
Welding Speed (m min^{-1})	3.5	0.5	0.5
Heat Input (kJ mm-1)	0.137	0.36	0.36

The material used was 4 mm thick S355 mild steel. The plates were cleaned using a wire brush and then with acetone in order to avoid contamination of the welds. The chemical composition of the S355 grade is shown in Table 15. For the metallographic preparation all the samples were mounted, polished and etched using 2% Nital etchant.

Table 15 - Chemical composition (wt%) of S355 mild steel

C	Si	Mn	Cr	Ni	Cu
Max 0.15	0.25/ 0.55	1.00/ 1.65	Max 0.25	Max 0.45	Max 0.3

A schematic view of the specimen and the measurement locations were shown in Figure 79. The imaginary cross sectional plane ABCD was near the mid-length of the weld. It can be seen that two different through thickness lines across the weld were measured to understand the variation of stress generation through the thickness.

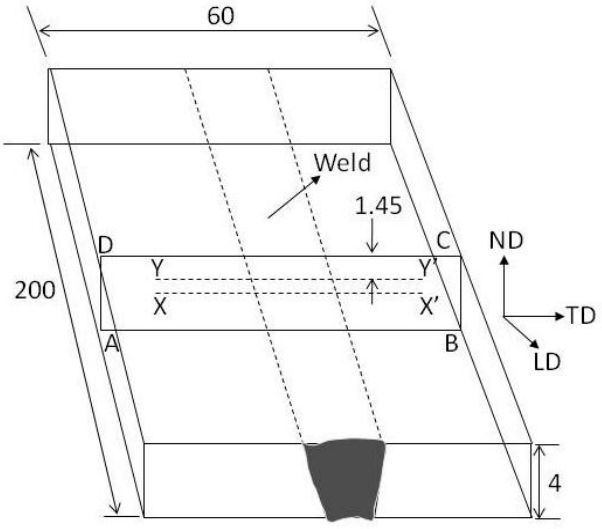

Figure 79 – Schematic view of the specimen and the measurement locations.

The welding direction is taken as the longitudinal direction and other two orthogonal directions across the weld and through the thickness was

considered as the transverse and normal directions. Stress analysis was carried out from the measured strain with the reasonable assumption that these are the principal strain directions.

8.2.2 Neutron strain scanning:

The neutron diffraction experiment was carried out at the ENGIN-X strain scanner at the spallation neutron source at ISIS, RAL, Oxford, UK. The ENGIN-X, strain scanner at ISIS operates on the time-of-flight principle where the detectors were kept at a fixed position of ±90° to the incident beam. The experimental sample is positioned in a way that two principal strain directions are measured in the two detectors separated by 180°. At ENGIN-X the experimental specimen is irradiated with pulses of white neutron beam with well defined energy spectrum. The time-of-flight of each neutron in a pulse would depend on the wavelength. Therefore, at a fixed diffraction angle of 90°, neutrons with a specific time-of-flight range would be diffracted by a specific set of crystallographic plane. The details of ENGIN-X could be found elsewhere[281] . The most advantageous thing of using a spallation neutron source like ENGIN-X is in its ability to simultaneously refine a range of crystallographic planes thereby minimising the anisotropy that may exist in between different crystallographic directions. In the present experiment a TOF range of 20-40 msec was used which resolved into an inter-planar spacing of 1.1 to 2.1 Å. The {110}, [282] and {211} families of crystallographic planes were analysed. An incoming beam dimension of 2 mm × 2 mm was used for the longitudinal strain measurement while 2 mm × 10 mm was used for transverse and normal strain directions. A 2 mm collimator was used for all the measurements. The diffraction geometry resulted in a cuboid gauge volume of 2×2×2 mm^3 in longitudinal strain direction and 2×10×2 mm^3 in transverse and normal strain directions. Refinement of the diffraction spectrum was performed using the General Structure Analysis System (GSAS) programme which gave a average lattice parameter (a) of the irradiated volume[283] .

Welding produces a change in composition along the fusion line which results in a change in the lattice parameter in and around the fusion zone, therefore, for interpretation of strain it is necessary to measure a stress free reference which would be relieved for any elastic macro-stress but would reflect the change in lattice parameter due to compositional variation. However, in the present case due to the low dimension (~ 4 mm) in the through thickness direction a plane stress condition was assumed i.e. the normal direction is of insufficient constraint to hold any significant internal stress field. The stress free reference (a_0) and then the stress was then analysed using the following equations[284] ;

$$a_0 = \frac{1-\nu}{1+\nu} a_N + \frac{\nu}{1+\nu}(a_L + a_T) - -(19)$$

Where a_0 is the stress free reference computed from the measured lattice parameters in longitudinal (a_L), transverse (a_T) and normal (a_N) strain directions and ν is the Poisson's ratio. The strain was then computed in accordance with equation 20.

$$\varepsilon_{L,T} = \frac{a_{L,T} - a_0}{a_0} - -(20)$$

The stress was then computed using equation 21.

$$\sigma_{L,T} = \frac{E}{(1-\nu^2)}(\varepsilon_L + \nu\varepsilon_{L,T}) - -(21)$$

8.3 Results

8.3.1 Weld Macrographs:

The cross-sectional macrographs of samples used for characterising the residual stresses are shown in Figure 80. It is evident that the macrograph shown in Figure 80 a) was welded in keyhole mode while Figure 80 b) and c) were produced in conduction mode. Residual stresses were analysed in these three welded samples and were compared in this study.

8.3.2 Residual stress measurements

Figure 81 shows the longitudinal stress variation along the mid-thickness and 1.45 mm from the surface for the specimens welded in conduction mode. It can be seen that there is no through thickness variation of the stress magnitude and distribution across the weld. This is due to the fact that the thermal cycle that causes the stress through the thickness was uniform. Although the actual penetration depth is less than half of the plate thickness, the residual stress magnitude did not show any significant variation as the through thickness dimension is relatively small.

Keyhole welding mode a)	**Conduction welding mode** b)	**Conduction welding mode** c)
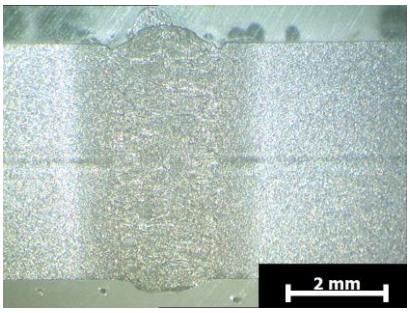	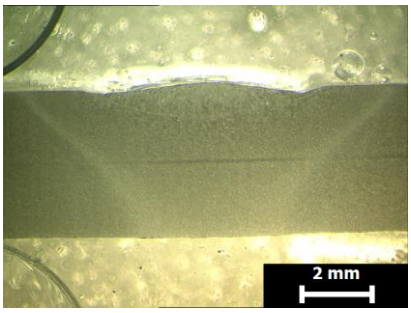	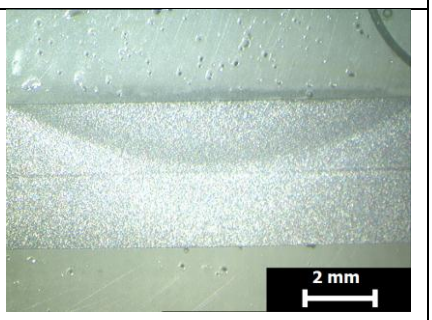
Beam Diameter = 1.2 mm **Welding Speed = 3.5 m min^{-1}** **Power = 8 kW** **Heat Input = 0.137 kJ mm^{-1}**	**Beam Diameter = 9 mm** **Welding Speed = 0.5 m min^{-1}** **Power = 3 kW** **Heat Input = 0.36 kJ mm^{-1}**	**Beam Diameter = 15 mm** **Welding Speed = 0.5 m min^{-1}** **Power = 3 kW** **Heat Input = 0.36 kJ mm^{-1}**

Figure 80 - Macrographs of the laser welds made in keyhole and conduction welding mode

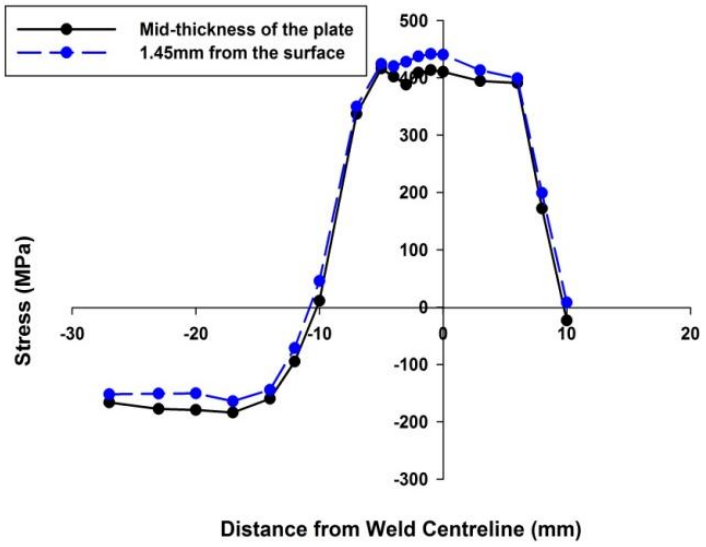

Figure 81 - Comparison of the longitudinal residual stress at 1.45 mm from the surface and at mid-thickness of the plate of the sample in conduction mode with a beam diameter of 9 mm

The mid-thickness of the plate longitudinal stress variation across the weld in the sample produced in keyhole mode and that of the two samples produced in conduction mode are shown in Figure 82 to Figure 84. Also shown on these figures is the width of the weld zone on the top surface as measured from the macrographs. It can be seen that the magnitude of the longitudinal residual stress reached up to 400 MPa in all the three specimens.

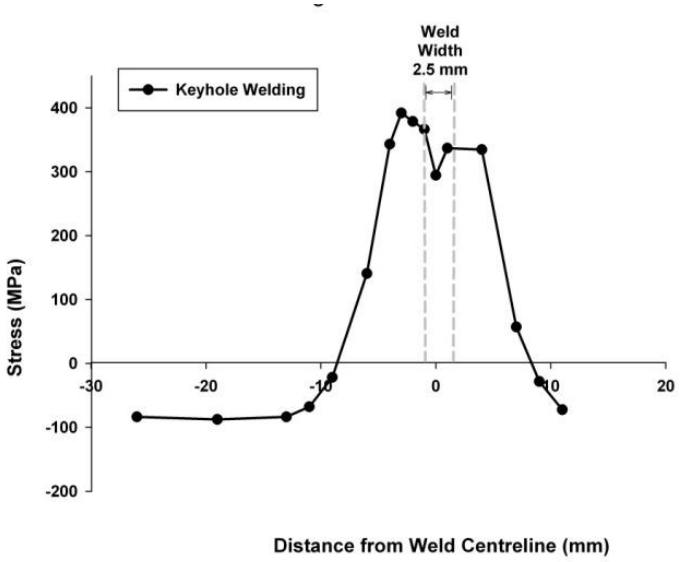

Figure 82 - Longitudinal residual stress of the keyhole welded sample

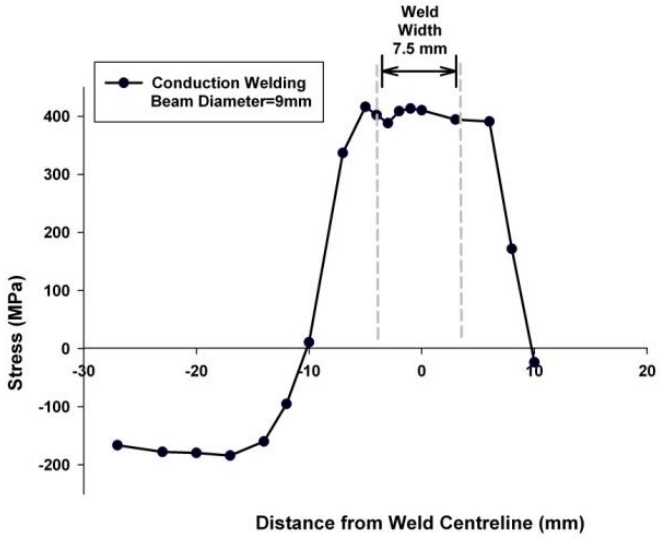

Figure 83 - Longitudinal residual stress of the conduction mode welded with a beam diameter of 9 mm

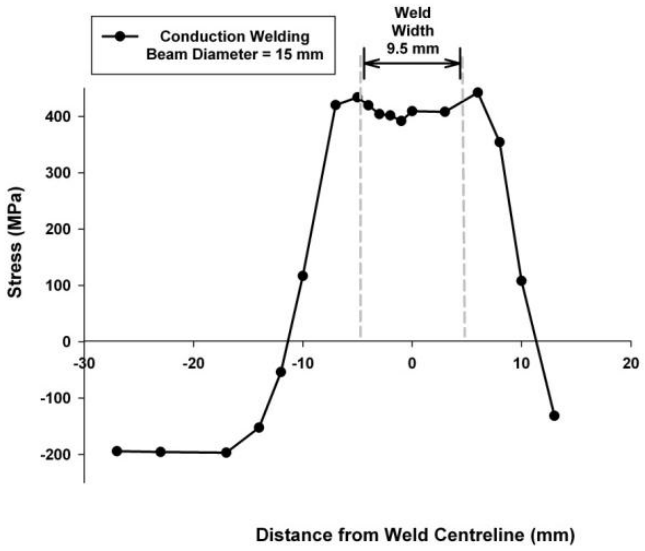

Figure 84 - Longitudinal residual stress of the conduction mode welded with a beam diameter of 15 mm

There is a proportional increase in the width of the peak residual stress plateau across the weld centre with increase in weld width. The weld width is dependent on the laser spot diameter, even if the heat input is identical. However, the dimension of the weld width is not identical to the beam diameter. This is because the power density near the edge of the beam diameter will be less and might not be sufficient to cause melting of the base material. Therefore, the width of the tensile stress plateau will depend on both the heat input and the beam diameter.

Figure 85 combines the longitudinal stress variation results showed in Figure 82 to Figure 84. The difference in width of the tensile peak for the three welds can be seen. It is also evident that the balancing compressive stress field has also been changed substantially with a much larger value for samples welded under conduction mode. This increased compressive stress field has significant implications in the generation of distortion. Also the stress engineering strategy [277, 278, 285, 286] for residual stress mitigation at the time of welding would be different for both welding modes. Keyhole mode has an irregular heat distribution pattern across the weld. This could be the reason for the asymmetry in the residual stress profile. On the other hand, conduction mode is a much

more stable process which means that the heat distribution is more regular and so the residual stress results present a more symmetric profile.

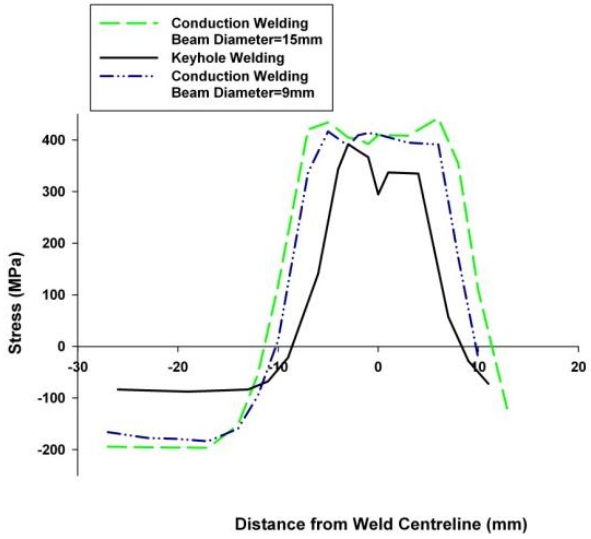

Figure 85 - Comparison of the longitudinal residual stress of the welds obtained in keyhole and conduction mode

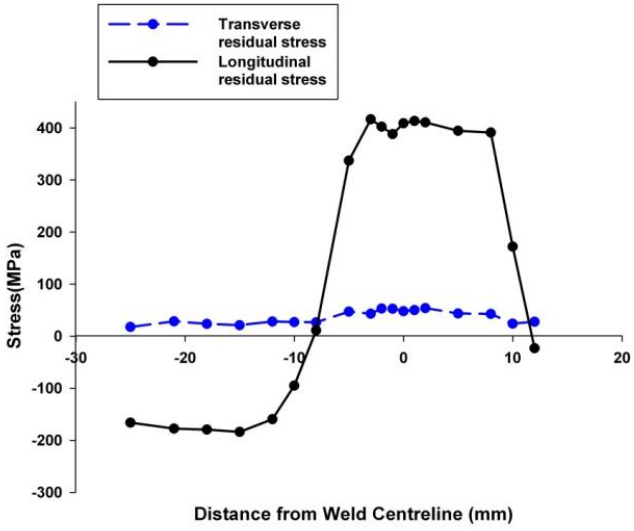

Figure 86 - Longitudinal and transverse residual stresses of the conduction mode welded with a beam diameter of 9 mm

Figure 86 shows the longitudinal and transverse stress distribution profiles for conduction welded specimen with beam diameter 9 mm. It can be clearly seen

that the transverse residual stress magnitude is insignificant as compared to the longitudinal stress.

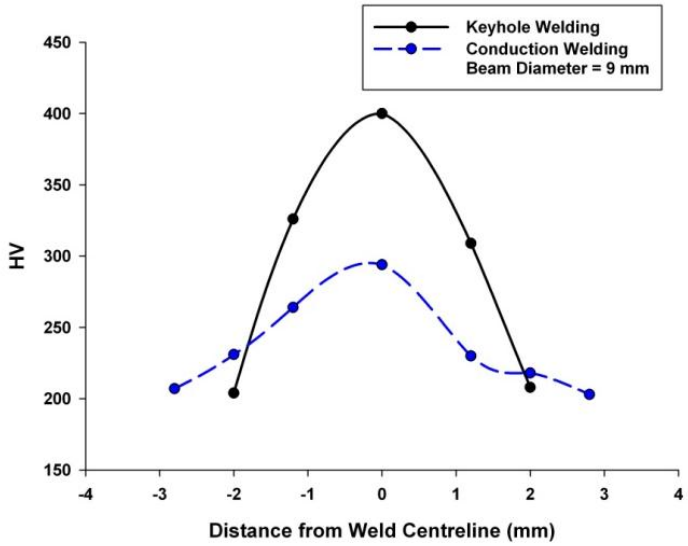

Figure 87 - Hardness profile of keyhole laser welding and conduction laser welding

The comparison of the hardness profiles in Figure 87, shows that the keyhole laser weld has a much higher hardness in the fusion zone compared to the conduction laser weld. This can be attributed to the fact that the cooling rate in keyhole welding is much faster with a lower heat input as compared to the conduction welding. In keyhole mode the energy density in the spot is much higher as compared to the conduction mode, the heat input is lower as the process can operate faster. Therefore, the cooling rate is much higher in keyhole mode as compared to the conduction mode. The accelerated cooling rate would result in hard intermediate phase formations which would influence the hardness profile of the welds. The residual stress generation, on the other hand, remains comparable as both processes are fusion based and causes plastic yielding in front of the weld pool.

The keyhole and conduction modes of laser welding are unique in their characteristics. The applicability of these two distinctive processes depend on several factors e.g. productivity requirement, welding set-up tolerance, qualitative requirements and other operative factors. Residual stress

characterisation is increasingly becoming important with introduction of more competitive and design efficient structures. Therefore, characterisation of residual stress profile is important to understand the implication of adopting such processes for safety critical structural welding and fabrications.

8.4 Conclusion

- The peak magnitude of residual stress was found to be similar for the keyhole and conduction modes of welding.
- The area under the tensile domain of the stress is much higher in conduction mode which means the balancing compressive stress generated is also much larger. This may have significant implications, for structural integrity, and distortion of welded components.
- The width of residual tensile stress plateau depends on the heat input and the beam diameter.
- There is a significant difference in distribution profile between the two modes of welding.
- In keyhole laser welding the combination of low heat input with high welding speeds results in a faster cooling rate. This results in significantly high fusion zone hardness as compared to welds made in conduction mode.

9 Summary and discussion

There are two distinct modes in laser welding, conduction and keyhole. Understanding the differences between these two laser welding modes, , is crucial when deciding which process to use. In this research the transition between these two modes has been studied in detail.

Keyhole mode laser welds features high penetration, high productivity and high aspect ratio leading researchers to focus deeply on this topic. In contrast conduction mode welding has not been studied extensively. However conduction mode has a definite role in laser welding, not only due to the stability of the process, but also because of the high quality welds obtained.

This research first focused on a detailed study of the transition between conduction and keyhole mode using a continuous wave (cw) laser. The effect of different process parameters, such as power density, interaction time and beam diameter, was investigated. A deviation from the usual definition of the transition between conduction and keyhole mode based on a single power density, completely independent of other process parameters was found. The actual power density at which transition between the two modes occurs is also dependent on interaction time and on beam diameter. An increase of interaction time results in a decrease of the power density at which the transition occurs. Similarly, an increase of beam diameter also results in a decrease of the power density at which the transition occurs. The study also revealed that there is a transition region of power density between conduction and keyhole mode. This is contrary to results published in the current literature and the claims that the transition between conduction and keyhole is sharp [98-100]. The transition mode shows characteristics of the two other welding modes. This includes a rougher top profile with some undercut, characteristic of keyhole mode, but with a low aspect ratio which is characteristic of conduction mode. However, while both conduction and keyhole welding modes show an increase of penetration depth with an increase of power density, assuming constant interaction time and beam diameter, in the transition mode the rate of increase of the

penetration with power density is reduced. The identification of this transition region is a significant finding considering that the definition that separated conduction mode from keyhole mode has its origins in the 1980's [1].

The next stage of the research focused on understanding how the thermal properties of different materials influence the transition from conduction to keyhole mode. By analysing how penetration depth varies with power density, for a constant interaction time and beam diameter, it was possible to evaluate that all three materials (aluminium, mild steel and stainless steel) showed a transition mode between conduction and keyhole mode and that, for all materials, the transition mode is characterised by having a very small increase of the penetration with an increase in power density. In this study all the materials were graphite coated in order to assure very similar coupling efficiencies and that the observed behaviour was due to the thermal properties of the materials. To the authors' knowledge no prior work has been published in comparing the behaviour of materials with different thermal properties in conduction and in keyhole mode. In this work it was determined that lower and upper limits of conduction mode are influenced by the thermal properties of the materials.

The next part of the research extended the study of the transition from conduction to keyhole mode to pulsed wave (pw) lasers. From the previous stage of the research for cw lasers the transition mode between conduction and keyhole mode can be effectively identified. However for pulsed wave lasers the transition mode is much less evident and harder to identify. During this research a comparison of the effects of power density, interaction time and beam diameter between cw and pw laser welds was made. This highlighted that pw laser welds have much higher penetration efficiency than cw laser welds. These differences in behaviour can be attributed to a combination of two effects. The first one relates to the fact that there is a surface tension gradient driven fluid flow which acts in opposition to the formation of a keyhole. Overcoming this surface tension is one of the origins of the transition mode. In cw welding there is additional fluid flow towards the keyhole due the translation of the weld pool

through the material. This delays the formation of the keyhole further and leads to the wide transition region observed in cw welding. This also leads to the differing penetration depths observed for cw and pw laser welds. The size of the difference depends on the interaction time. The other effects relates to the fact that the pulsed laser has a higher spatial peak power density. At shorter interaction times the gap in penetration depths for the pw laser welds compared to cw laser welds is higher than at higher interaction times.

A further part of this research was the study of conduction mode laser welding of aluminium and how the beam diameter affects the penetration depth. A comparison was made between an empirical statistical regression model and a finite volume model. This was done in order to identify the mechanisms governing the weld geometry. It was possible to identify with both models that there is an optimum beam diameter for a given laser power and travel speed, where the penetration is maximum. The effect of power and welding speed on the optimum beam diameter was also evaluated. For higher levels of power the optimum beam diameter is larger, while for lower values of welding speed the optimum beam diameter is lower. Both numerical and empirical modelling can be used to identify the optimum beam diameter in laser conduction welding.

In the final part of this research a characterisation of the residual stresses obtained in keyhole and in conduction mode welding was made. It was shown that the peak magnitude residual stress obtained in both modes was similar, however the profiles obtained had significant differences. By comparing these two modes it was possible to determine that the width of the residual tensile stress plateau across the weld zone depends not only on the heat input, as shown in previous work [274], but also on the beam diameter of the laser at constant heat input. Due to the much higher area under the tensile domain of the residual stress field, when in conduction mode, the balancing compressive residual stress generated is also much higher leading to higher distortions. This larger compressive residual stress means that buckling distortion is more likely

in conduction welds compared to keyhole welds. Conduction mode has higher residual stresses, however it has a softer fusion zone.

Using conduction mode increases the range of applications of laser welding. The high stability of conduction mode welding allows precise control of the process and in very high quality welds with no spatter, porosity or undercut. During the duration of this work some applications were developed using conduction mode laser welding. These applications highlight the characteristics of conduction mode laser welding and are shown in APPENDIX A.

This research has significantly improved the understanding of the conduction laser welding process. It has also investigated thoroughly the transition region between conduction and keyhole mode welding.

10 Conclusion and future work

10.1 Conclusion

During this study of the transition from conduction mode to keyhole mode lots of unknown effects were seen. The following conclusions derived from the objectives shown in Chapter 2 are presented as follows.

Transition behaviour between conduction and keyhole mode laser welding.

- The power density at transition between conduction and keyhole mode is not a unique value. The actual value is also dependent on the interaction time and on beam diameter.
- In continuous wave laser welding there is transition mode between conduction mode and keyhole mode, characterised by a reduced rate of increase of the penetration depth with power density.
- The welds obtained in the transition mode show characteristics of the other two welding modes.
- The aspect ratio can be used to distinguish between conduction mode and keyhole mode. However the aspect ratio value that separates conduction mode from keyhole mode is also dependent on the interaction time used and also on the beam diameter

Material property effects in laser conduction welding

- The power density values that limits conduction mode are dependent on the material thermal properties.
- Aluminium, due to its higher thermal conductivity, has a higher penetration efficiency in conduction mode, followed by mild steel and then by stainless steel.
- In keyhole mode the penetration depth of all the materials is very similar. So the material thermal properties in keyhole mode have less influence on the penetration depth than in conduction mode.

Comparison between pulsed wave and continuous wave laser welding

- In pulsed wave laser welding there is also a transition mode, however much less evident than in continuous wave laser welding
- In welds done under the same conditions of power density, interaction time and beam diameter the pulsed wave laser welds has higher penetration efficiency when compared to continuous wave laser welds

Parameter effects in laser conduction welding

- For a given laser power and travel speed there is an optimum beam diameter where the penetration depth is maximum
- Both numerical and empirical modelling can be used to identify the optimum beam diameter in laser conduction welding

Residual stress effects in laser conduction welding

- The peak magnitude of residual stress for keyhole and conduction modes of welds is very similar but the width of the tensile zone is much wider in conduction mode
- The balancing compressive stress generated by a conduction mode weld is much larger than the one generated by a keyhole mode weld due the wider tensile peak.
- The width of residual tensile stress plateau depends on the heat input and the beam diameter.

10.2 Future work

Deeper comparison between continuous wave laser welding and pulsed wave laser welding

To add to the knowledge of continuous wave laser welding and pulsed wave laser welding the comparison, using interaction time and power density as welding parameters, between these two laser types should be extended to other materials. This would allow an evaluation of the effects of the materials thermal properties in each laser type. Also, a comparison using a modulated laser system, a laser that can operate in continuous wave or pulsed wave, this would allow a comparison using the same beam profile.

Investigation of the optimum welding parameters in long pulsed conduction laser welding

The advantages of conduction laser welding mode could be transferred to “long” pulsed laser welding. The issue of using a pulsed laser welding system in conduction laser welding is that the penetrations is limited by the pulse duration, this could be overcome by using pulses with longer durations (higher than 1 second duration). An investigation into the effect of power, beam diameter and pulse duration (which is the interaction time) would add to the knowledge of conduction mode laser welding. This would also allow an extra comparison between the welds done with a moving laser beam and a stationary laser beam using interaction time, power and beam diameter as the common welding parameters.

Investigation into the effect of the laser beam shape using interaction time and beam diameter as the welding parameters

All the work shown in this thesis was made using a circular laser beam. The use of different shaped laser beams (for example elliptical) would allow a better understanding of the effect of interaction time for different beam shapes in laser welding, both continuous and pulsed wave laser welding. The investigation of the effect of a different shape laser beam should be done not only to look into

the transition between conduction and keyhole mode, but also in the comparison between continuous wave and pulsed wave laser welding and in the identification of the optimum beam diameter in conduction mode.

Evaluation of the effect of different shielding gases on the transition between conduction and keyhole mode

Following the work shown in this thesis the next step would be the investigation of the effect of different shielding gases at different concentrations on the transition between conduction mode and keyhole mode and on the optimum beam diameter. This investigation would allow a deeper understanding of the effect of surface tension, which is influenced by the shielding gases, on the transition between conduction and keyhole mode. Also on the effect that surface tension will have on the shape of the weld when operating in conduction mode.

Deeper characterisation and understanding of the transition between conduction mode and keyhole mode

A better characterisation, which will lead to a better understanding, of the transition between conduction mode and keyhole mode should be made. Evaluation of the laser beam absorption, also known as coupling efficiency, as the power density increases, starting from where no melting takes place and going through conduction mode, transition mode and finishing in deep keyhole mode would add considerable knowledge to all these modes. Adding to this the capture of high speed video and thermal data would also provide important information that would add to the knowledge of the transition between the different modes, but also to a better understanding of each mode (conduction, transition and keyhole mode) individually.

Investigation of the effect of wavelength on the transition between conduction mode and keyhole mode

Study the effect of using different lasers with different wavelengths. Using different wavelengths in the three different modes and in the transition between

the welding modes will allow a better understanding into the real effect of wavelength in each welding mode. A comparison between the coupling efficiency and the wavelength of the laser, for the different welding modes, will allow a better choice of the laser to use depending on which welding mode will be applied.

Investigation of the effect of different alloy elements in aluminium on the transition between conduction mode and keyhole mode

The study of the material properties effect on the transition between conduction mode and keyhole mode could be extended to different aluminium alloys. A comparison between different alloys would allow a better understanding on how different alloys elements influence the keyhole formation.

REFERENCES

1. Bass, M., Laser materials processing. 1983, New York: Elsevier Science Pub.

2. Quintino, L., et al., Welding with high power fiber lasers - A preliminary study. Materials and Design, 2007. 28(4): p. 1231-1237.

3. Ready, J.F. and D.F. Farson, LIA handbook of laser materials processing. 2001, Orlando, Fla.: Laser Institute of America. xxv, 715 p.

4. Schwartz, J., Fibre lasers steal the show. Photonics Spectra, 2009. 43(8).

5. Kratky, A., D. SchuÃ¶cker, and G. Liedl. Processing with kW fibre lasers - Advantages and limits. in Proceedings of SPIE - The International Society for Optical Engineering. 2009. Lisboa.

6. Timmermann, A., et al. Next generation high-brightness diode lasers offer new industrial applications. in Proceedings of SPIE - The International Society for Optical Engineering. 2008. San Jose, CA.

7. Kimberley, G., Fiber lasers make their mark. Welding Design & Fabrication, 2006. 79(9): p. 24.

8. Foster, H., High power CO2 lasers--a review. Optics & Laser Technology, 1972. 4(3): p. 121-128.

9. Emmelmann, C. and S. Lunding, High Power Disk Laser Technology – Design and potential for laser macro applications, in ICALEO 2002. 2002.

10. Strohmaier, S., et al., High-power, high-brightness direct-diode lasers. Optics and Photonics News. 21(10): p. 24-29.

11. Chen, G.L., Study the application of laser welding in the automotive transmission parts, in Advanced Materials Research. Guilin. p. 3682-3686.

12. Black, A. and S. Copley, Laser technology for materials processing. Advanced Materials and Processes. 168(1): p. 31-32.

13. Carter, A. and E. Li. Recent progress in high-power fiber lasers for high-power and high-quality material processing applications. in Proceedings of SPIE - The International Society for Optical Engineering. 2006. Tianjin.

14. Ream, S.L., Disc and fiber gain ground. Industrial Laser Solutions, 2005.

15. Behringer, M. and H. Konig, Diode Lasers for Industrial applications, in ICALEO 2005. 2005.

16. Parker, D. and D.N. Payne, Fibre Lasers:The new wave in material processing, in ICALEO 2005. 2005.

17. Schubert, E., et al., Light-weight structures produced by laser beam joining for future applications in automobile and aerospace industry. Journal of Materials Processing Technology, 2001. 115(1): p. 2-8.

18. Sepold, G., E. Schubert, and I. Zerner. Laser Beam Joining of dissimilar materials. in IIW. 1999. Lisbon.

19. Staufer, H., Laser hybrid welding and laser brazing at AUDI and VW. Welding in the World, 2006. 50(7-8): p. 44-50.

20. Roetzer, I., Laser-Beam welding makes aircraft lighter, in Fraunhofer Magazine. 2005. p. 36-37.

21. Loffler, K., The future of lasers in the automotive industry. Photonics Spectra, 2006. 40(1): p. 68-70.

22. Ramasamy, S. and C.E. Albright, CO2 and Nd-YAG laser beam welding of 5754-O aluminium alloy for automotive applications. Science and Technology of Welding and Joining, 2001. 6(3): p. 182-190.

23. Wu, Q., et al., Research on laser welding of vehicle body. Optics & Laser Technology, 2008. 40: p. 420-426.

24. Behler, K., et al., Laser beam welding of low weight materials and structures. Materials and Design, 1997. 18(4-6): p. 261-267.

25. Ribolla, A., G.L. Damoulis, and G.F. Batalha, The use of Nd:YAG laser weld for large scale volume assembly of automotive body in white. Journal of Materials Processing Technology, 2005. 164-165: p. 1120-1127.

26. Schumacher, J., et al., Laser Beam Welding of Aircraft Fuselage Panels in ICALEO 2002. 2002.

27. Salminen, A., et al. A study about suitability of different welding processes for the production of aluminum stiffeners for ship structure. in ICALEO 2009 - 28th International Congress on Applications of Lasers and Electro-Optics, Congress Proceedings. 2009. Orlando, FL.

28. Olschok, S., U. Reisgen, and U. Dilthey. Robot application for laser-GMA hybrid welding in shipbuilding. in 26th International Congress on Applications of Lasers and Electro-Optics, ICALEO 2007 - Congress Proceedings. 2007. Orlando, FL.

29. Lee, M.Y. Weldability of austenitic and dual phase stainless steel on fiber laser welding for pipe industry. in ICALEO 2009 - 28th International Congress on Applications of Lasers and Electro-Optics, Congress Proceedings. 2009. Orlando, FL.

30. Gook, S., A. Gumenyuk, and M. Rethmeier. Weld seam formation and mechanical properties of girth welds performed with laser-GMA-hybrid process on pipes of grade X65. in 29th International Congress on Applications of Lasers and Electro-Optics, ICALEO 2010 - Congress Proceedings. Anaheim, CA.

31. Yang, S., R. Sarrafi, and R. Kovacevic. Hybrid 4KW fiber laser-GMAW welding of half-inch mild steel. in 29th International Congress on Applications of Lasers and Electro-Optics, ICALEO 2010 - Congress Proceedings. Anaheim, CA.

32. Liu, J., et al., Joint strength of laser-welded titanium. Dental Materials, 2002. 18: p. 143-148.

33. Reclaru, L., C. Susz, and L. Ardelean, Laser beam welding. Timisoara Medical Journal. 60(1): p. 86-89.

34. Fornaini, C., et al. Laser welding by dental Nd:YAG device. in AIP Conference Proceedings. 2009. Firenze.

35. Bertrand, C. and A. Poulon-Quintin, Proposals for optimization of laser welding in prosthetic dentistry. Journal of Prosthodontics. 19(1): p. 69-76.

36. Safarevich, S., et al. Fiber laser welding of high integrity implantable medical devices. in 26th International Congress on Applications of Lasers and Electro-Optics, ICALEO 2007 - Congress Proceedings. 2007. Orlando, FL.

37. Miller, D., et al., Welding of platinum jewellery alloys. Platinum Metals Review, 2007. 51(1): p. 23-26.

38. Arias, R., et al. Laser welding of tube to tube-sheet joint in steam generators for nuclear power plants. in 29th International Congress on Applications of Lasers and Electro-Optics, ICALEO 2010 - Congress Proceedings. Anaheim, CA.

39. Katayama, S., et al., Fibre laser welding of aluminium alloy. Welding International, 2009. 23(10): p. 744-752.

40. Lima, M.S.F., et al. Laser beam welding aerospace aluminum using fiber lasers. in Proceedings of SPIE - The International Society for Optical Engineering. 2009. Lisboa.

41. Kuo, T.Y. and H.C. Lin, Effects of pulse level of Nd-YAG laser on tensile properties and formability of laser weldments in automotive aluminum alloys. Materials Science and Engineering A, 2006. 416(1-2): p. 281-289.

42. El-Batahgy, A. and M. Kutsuna, Laser beam welding of AA5052, AA5083, and AA6061 aluminum alloys. Advances in Materials Science and Engineering, 2009. 2009.

43. Dausinger, F. Laser welding of aluminum alloys: From fundamental investigation to industrial application. in Proceedings of SPIE - The International Society for Optical Engineering. 2000. Osaka, Jpn: Society of Photo-Optical Instrumentation Engineers.

44. Cicala, E., et al. Optimisation of T-joint properties in Al-Mg-Si alloy laser welding. in 24th International Congress on Applications of Lasers and Electro-Optics, ICALEO 2005 - Congress Proceedings. 2005. Miami, FL.

45. Choi, K.D., Y.N. Ahn, and C. Kim. Weld strength improvement for al alloy by using laser weaving method. in ICALEO 2009 - 28th International Congress on Applications of Lasers and Electro-Optics, Congress Proceedings. 2009. Orlando, FL.

46. Lee, K.D., K.Y. Park, and I.C. Ha. Three dimensional robot laser welding of aluminum 6063-T6 pipes with filler wire. in ICALEO 2004 - 23rd International Congress on Applications of Laser and Electro-Optics, Congress Proceedings. 2004. San Francisco, CA.

47. Zhang, X., et al. Welding of thick stainless steel plates up to 50mm with high brightness lasers. in ICALEO 2009 - 28th International Congress on Applications of Lasers and Electro-Optics, Congress Proceedings. 2009. Orlando, FL.

48. Zhang, X., E. Ashida, and S. Tarasawa. Properties of welded joint for narrow gap laser welding of austenitic stainless steels. in 29th International Congress on Applications of Lasers and Electro-Optics, ICALEO 2010 - Congress Proceedings. Anaheim, CA.

49. Kawahito, Y., M. Mizutani, and S. Katayama, High quality welding of stainless steel with 10 kW high power fibre laser. Science and Technology of Welding and Joining, 2009. 14(4): p. 288-294.

50. Hafez, K.M. and K. Seiji, Fiber laser welding of AISI 304 stainless steel plates. Yosetsu Gakkai Ronbunshu/Quarterly Journal of the Japan Welding Society, 2009. 27(2).

51. Klimpel, A., et al. Study of titanium sheets HPDL welding phenomenon. in ICALEO 2004 - 23rd International Congress on Applications of Laser and Electro-Optics, Congress Proceedings. 2004. San Francisco, CA.

52. Curcio, F., et al. A basic study on the high power diode laser welding of a titanium alloy. in ICALEO 2004 - 23rd International Congress on Applications of Laser and Electro-Optics, Congress Proceedings. 2004. San Francisco, CA.

53. Wu, B., et al. Influences of gap size on the fatigue strength of welded titanium alloy overlap joints. in ICALEO 2009 - 28th International Congress on Applications of Lasers and Electro-Optics, Congress Proceedings. 2009. Orlando, FL.

54. Block, B., et al. High-strength titanium laser welding with a subsequent combination of mechanical and laser heat treatment. in ICALEO 2004 - 23rd International Congress on Applications of Laser and Electro-Optics, Congress Proceedings. 2004. San Francisco, CA.

55. Wang, S.H., M.D. Wei, and L.W. Tsay, Tensile properties of LBW welds in Ti-6Al-4V alloy at evaluated temperatures below 450 C. Materials Letters, 2003. 57: p. 1815-1823.

56. Caiazzo, F., et al., Ti6Al4V sheets lap and butt joints carried out by CO2 laser: mechanical and morphological characterization. Journal of Materials Processing Technology, 2004. 149: p. 546-552.

57. Costa, A., et al., Analysis of Beam Material Interaction in Welding of Titanium with Fiber Lasers. Materials and Manufacturing Processes, 2007. 22: p. 798-803.

58. Moalem, A., et al. Enhancing process stability in infrared laser micro welding of copper using frequency converted short prepulses. in 29th International Congress on Applications of Lasers and Electro-Optics, ICALEO 2010 - Congress Proceedings. Anaheim, CA.

59. Petring, D. and V. Nazery Goneghany. Learning more about laser beam welding by applying it to copper and copper alloys. in 29th International Congress on Applications of Lasers and Electro-Optics, ICALEO 2010 - Congress Proceedings. Anaheim, CA.

60. Hess, A., et al. Benefits from combining laser beams with different wavelengths (green and IR) for copper welding. in 29th International Congress on Applications of Lasers and Electro-Optics, ICALEO 2010 - Congress Proceedings. Anaheim, CA.

61. Cao, X., et al., A review of laser welding techniques for magnesium alloys. Journal of Materials Processing Technology, 2006. 171(2): p. 188-204.

62. Lee, M.Y., W.S. Chang, and B.H. Yoon. Nd:YAG laser welding of AZ31 sheet for car industry. in ICALEO 2006 - 25th International Congress on Applications of Laser and Electro-Optics, Congress Proceedings. 2006. Scottsdale, AZ.

63. Lee, M.Y. Development of MG tube using laser welding for bike frame. in 29th International Congress on Applications of Lasers and Electro-Optics, ICALEO 2010 - Congress Proceedings. Anaheim, CA.

64. Wahba, M., et al. High-brightness disk laser welding of magnesium alloys. in 29th International Congress on Applications of Lasers and Electro-Optics, ICALEO 2010 - Congress Proceedings. Anaheim, CA.

65. Zhu, J., L. Li, and Z. Liu, CO2 and diode laser welding of AZ31 magnesium alloy. Applied Surface Science, 2005. 247: p. 300-306.

66. Kutsuna, M. and T. Kurokawa. Study of porosity formation in CO2 laser welding of magnesium alloys. in ICALEO 2004 - 23rd International Congress on Applications of Laser and Electro-Optics, Congress Proceedings. 2004. San Francisco, CA.

67. Pandremenos, J., K. Salonitis, and G. Chryssolouris. CO2 laser welding of AHSS. in ICALEO 2009 - 28th International Congress on Applications of Lasers and Electro-Optics, Congress Proceedings. 2009. Orlando, FL.

68. Yang, S., B. Carlson, and R. Kovacevic. Laser keyhole welding of galvanized high-strength steel in a gap-free lap joint configuration. in 29th International Congress on Applications of Lasers and Electro-Optics, ICALEO 2010 - Congress Proceedings. Anaheim, CA.

69. Arias, R., et al. Laser welding applied to advanced high strength steels for automotive applications. in 29th International Congress on Applications of Lasers and Electro-Optics, ICALEO 2010 - Congress Proceedings. Anaheim, CA.

70. Pieters, R.R.G.M., M.Y. Krasnoperov, and I.M. Richardson. Laser welding of high strength steels. in ICALEO 2003 - 22nd International Congress on Applications of Laser and Electro-Optics, Congress Proceedings. 2003. Jacksonville, FL.

71. Liu, Z., M. Kutsuna, and G. Xu. Fiber laser welding of 780MPA high strength steel. in ICALEO 2006 - 25th International Congress on Applications of Laser and Electro-Optics, Congress Proceedings. 2006. Scottsdale, AZ.

72. Ahmad, A. and V. KujanpÃ¤Ã¤. Laser absorption in CO2 laser welding of medium, high and ultra high strength steels. in ICALEO 2009 - 28th International Congress on Applications of Lasers and Electro-Optics, Congress Proceedings. 2009. Orlando, FL.

73. Vollertsen, F. and C. Thomy. Welding with fiber lasers from 200 to 17000 W. in 24th International Congress on Applications of Lasers and Electro-Optics, ICALEO 2005 - Congress Proceedings. 2005. Miami, FL.

74. Havrilla, D. and M. Holzer. High power disk lasers - Advances & applications. in Proceedings of SPIE - The International Society for Optical Engineering. San Francisco, CA.

75. Duley, W.W., Laser welding. 1999, New York ; Chichester: Wiley. ix, 251p.

76. Duley, W.W., Laser processing and analysis of materials. 1983, New York ; London: Plenum. xiii,463p.

77. Zhou, J., et al. Melt flow and porosity formation in pulsed laser keyhole welding. in Proceedings of the ASME Heat Transfer/Fluids Engineering Summer Conference 2004, HT/FED 2004. 2004. Charlotte, NC.

78. Yoshioka, S., et al. Monitoring of Nd:YAG laser spot welding -detection of porosity defect by weld sound. in 24th International Congress on Applications of Lasers and Electro-Optics, ICALEO 2005 - Congress Proceedings. 2005. Miami, FL.

79. Mizutani, M., S. Katayama, and A. Matsunawa. X-Ray observation of keyhole instability in zinc molten pool and estimation of recoil pressure in laser welding. in PICALO 2004 - 1st Pacific International Conference on Applications of Laser and Optics, Conference Proceedings. 2004. Melbourne, VIC.

80. Kumar, N., et al., Keyhole depth instability in case of CW CO2 laser beam welding of mild steel. Sadhana - Academy Proceedings in Engineering Sciences. 35(5): p. 609-618.

81. Paleocrassas, A.G. and J.F. Tu, Inherent instability investigation for low speed laser welding of aluminum using a single-mode fiber laser. Journal of Materials Processing Technology. 210(10): p. 1411-1418.

82. Eriksson, I. and A.F.H. Kaplan. Evaluation of laser weld monitoring - A case study. in ICALEO 2009 - 28th International Congress on Applications of Lasers and Electro-Optics, Congress Proceedings. 2009. Orlando, FL.

83. Weberpals, J. and F. Dausinger. Fundamental understanding of spatter behavior at laser welding of steel. in ICALEO 2008 - 27th International Congress on Applications of Lasers and Electro-Optics, Congress Proceedings. 2008. Temecula, CA.

84. Cao, X., et al., Research and progress in laser welding of wrought aluminum alloys. I. Laser welding processes. Materials and Manufacturing Processes, 2003. 18(1): p. 1-22.

85. Cao, X., et al., Research and progress in laser welding of wrought aluminum alloys. II. Metallurgical microstructures, defects, and mechanical properties. Materials and Manufacturing Processes, 2003. 18(1): p. 23-49.

86. Cam, G. and M. Kocak, Progress in joining of advanced materials. International Materials Reviews, 1998. 43(1): p. 1-44.

87. Cam, G. and M. Kocak, Progress in joining of advanced materials. Part 2: Joining of metal matrix composites and joining of other advanced materials. Science and Technology of Welding and Joining, 1998. 3(4): p. 159-175.

88. Hu, B. and I.M. Richardson, Autogenous laser keyhole welding of aluminum alloy 2024. Journal of Laser Applications, 2005. 17(2): p. 70-80.

89. Weston, J., Surface related features of laser welding of aluminium alloys. ISIJ International, 2000. 40(SUPPL.): p. S6-S9.

90. Weston, J., Laser welding of aluminium alloys using different laser sources. 2003, Department of Materials Science and Metallurgy, University of Cambridge: Cambridge.

91. Ion, J.C., Laser beam welding of wrought aluminium alloys. Science and Technology of Welding and Joining, 2000. 5(5): p. 265-276.

92. Morgan, S. and S. Williams, Hybrid laser conduction welding, in 55th Annual Assembly of International Institute of Welding. 2002: Copenhagen, Denmark.

93. Tam, S.C., et al., A review of the laser processing of aircraft components. Journal of Materials Processing Tech., 1990. 23(2): p. 177-194.

94. Nath, A.K., et al., Laser power coupling efficiency in conduction and keyhole welding of austenitic stainless steel. Sadhana - Academy Proceedings in Engineering Sciences, 2002. 27(PART 3): p. 383-392.

95. Weston, J.W., E.R., Coupling for laser welds in aluminium alloys. Department of Materials Science and Metallurgy, University of Cambridge.

96. Fuerschbach, P., Melting efficiency in fusion welding, in The Metal Science of Joining. 1992.

97. Mallory, L.C., R.F. Orr, and W. Wells, Effect of anodizing on laser welding of aluminium, in Laser Materials Processing III. 1989.

98. Steen, W.M., Laser material processing. 3rd ed. ed. 2003, New York ; London: Springer. 448 p.

99. Ion, J.C., Laser processing of engineering materials : principles, procedure and industrial application. 2005, Amsterdam ; Oxford: Elsevier/Butterworth-Heinemann. xviii, 556 p.: ill.; 26 cm.

100. Sanchez-Amaya, J.M., et al., Laser welding of AA 5083 samples by high power diode laser. Science and Technology of Welding and Joining, 2009. 14(1): p. 78-86.

101. Nakamura, S., et al., Detection technique for transition between deep penetration mode and shallow penetration mode in CO2 laser welding of metals. Journal of Physics D: Applied Physics, 2000. 33(22): p. 2941-2948.

102. Basu, S. and T. DebRoy, Liquid metal expulsion during laser irradiation. Journal of Applied Physics, 1992. 72(8): p. 3317-3322.

103. He, X., J.W. Elmer, and T. Debroy, Heat transfer and fluid flow in laser microwelding. Journal of Applied Physics, 2005. 97(8): p. 1-9.

104. Zhou, J., H.L. Tsai, and P.C. Wang, Transport phenomena and keyhole dynamics during pulsed laser welding. Journal of Heat Transfer, 2006. 128(7): p. 680-690.

105. Jouvard, J.M., K. Girard, and O. Perret, Keyhole formation and power deposition in Nd:YAG laser spot welding. Journal of Physics D: Applied Physics, 2001. 34(18): p. 2894-2901.

106. Semak, V.V., et al., Effect of surface tension on melt pool dynamics during laser pulse interaction. Journal of Physics D: Applied Physics, 2006. 39(3): p. 590-595.

107. Cho, J.H., et al., Weld pool flows during initial stages of keyhole formation in laser welding. Journal of Physics D: Applied Physics, 2009. 42(17).

108. Fabbro, R., et al., Study of keyhole behaviour for full penetration Nd-Yag CW laser welding. Journal of Physics D: Applied Physics, 2005. 38(12): p. 1881-1887.

109. Semak, V. and A. Matsunawa, The role of recoil pressure in energy balance during laser materials processing. Journal of Physics D: Applied Physics, 1997. 30(18): p. 2541-2552.

110. Semak, V.V., B. Damkroger, and S. Kempka, Temporal evolution of the temperature field in the beam interaction zone during laser material processing. Journal of Physics D: Applied Physics, 1999. 32(15): p. 1819-1825.

111. Semak, V.V., et al. A concept for hydrodynamic model of keyhole formation

and support during laser welding. in ICALEO 1994. 1994.

112. GÃ¤rtner, P. and R. Weber. Spatter formation and keyhole observation with high speed cameras - Better understanding of the keyhole formation. in ICALEO 2009 - 28th International Congress on Applications of Lasers and Electro-Optics, Congress Proceedings. 2009. Orlando, FL.

113. Kar, A. and J. Mazumder, Mathematical modeling of key-hole laser welding. Journal of Applied Physics, 1995. 78(11): p. 6353-6360.

114. Lee, J.Y., et al., Mechanism of keyhole formation and stability in stationary laser welding. Journal of Physics D: Applied Physics, 2002. 35(13): p. 1570-1576.

115. Metzbower, E.A., Keyhole formation. Metallurgical Transactions B, 1993. 24(5): p. 875-880.

116. Ki, H., P.S. Mohanty, and J. Mazumder, Modeling of laser keyhole welding: Part II. Simulation of keyhole evolution, velocity, temperature profile, and experimental verification. Metallurgical and Materials Transactions A: Physical Metallurgy and Materials Science, 2002. 33(6): p. 1831-1842.

117. Ki, H., P.S. Mohanty, and J. Mazumder, Modeling of laser keyhole welding: Part I. Mathematical modeling, numerical methodology, role of recoil pressure, multiple reflections, and free surface evolution. Metallurgical and Materials Transactions A: Physical Metallurgy and Materials Science, 2002. 33(6): p. 1817-1830.

118. Wang, R., Y. Lei, and Y. Shi, Keyhole modeling during laser deep penetration welding, in Applied Mechanics and Materials. Changsha. p. 252-257.

119. Fabbro, R. and K. Chouf, Dynamical description of the keyhole in deep penetration laser welding. Journal of Laser Applications, 2000. 12(4): p. 142-148.

120. Pang, S., et al. Three dimensional simulation transient keyhole evolution during laser keyhole welding. in Proceedings of SPIE - The International Society for Optical Engineering. 2009. Wuhan.

121. Jin, X.Z. and L.J. Li, A conduction model for deep penetration laser welding based on an actual keyhole. Optics & Laser Technology, 2003. 35(1): p. 5-12.

122. Solana, P. and J.L. OcaÃ±a, A mathematical model for penetration laser welding as a free-boundary problem. Journal of Physics D: Applied Physics, 1997. 30(9): p. 1300-1313.

123. Klein, T., et al., Oscillations of the keyhole in penetration laser beam welding. Journal of Physics D: Applied Physics, 1994. 27(10): p. 2023-2030.

124. Beyer, E., et al. DEVELOPMENT AND OPTICAL ABSORPTION PROPERTIES OF A LASER INDUCED PLASMA DURING CO//2-LASER PROCESSING. in Proceedings of SPIE - The International Society for Optical Engineering. 1984. Linz, Austria: SPIE.

125. Carlsaw, H.S. and J.C. Jaeger, Conduction of Heat in Solids. 2nd ed. 1959: University Press.

126. Liu, J.T., D.C. Weckman, and H.W. Kerr, The effects of process variables on pulsed Nd:YAG laser spot welds: Part I. AISI 409 stainless steel. Metallurgical Transactions B, 1993. 24(6): p. 1065-1076.

127. Weckman, D.C., H.W. Kerr, and J.T. Liu, The effects of process variables on pulsed Nd:YAG laser spot welds: Part II. AA 1100 aluminum and comparison to AISI 409 stainless steel. Metallurgical and Materials Transactions B: Process Metallurgy and Materials Processing Science, 1997. 28(4): p. 687-700.

128. Zhang, X., et al. Laser welding mode transition and influence of thermal focusing on mode transition. in Proceedings of SPIE - The International Society for Optical Engineering. 1996. Beijing, China.

129. Buvanashekaran, G., et al., A study of laser welding modes with varying beam energy levels. Proceedings of the Institution of Mechanical Engineers, Part C: Journal of Mechanical Engineering Science, 2009. 223(5): p. 1141-1156.

130. Sibillano, T., et al., Optical detection of conduction/keyhole mode transition in laser welding. Journal of Materials Processing Technology, 2007. 191(1-3): p. 364-367.

131. Chen, W., X. Zhang, and J. Ren, Study of welding mode transition and stability of welding process in high laser welding. Chinese Journal of Lasers, 1996. 23(7).

132. Zhang, X., W. Chen, and J. Ren, Effects of processing parameters on mode and stability of laser welding, in Photonics West'96. 1996.

133. Von Allmen, M., Laser drilling velocity in metals. Journal of Applied Physics, 1976. 47: p. 3.

134. Semak, V.V., G.A. Knorovsky, and D.O. MacCallum, On the possibility of microwelding with laser beams. Journal of Physics D: Applied Physics, 2003. 36(17): p. 2170-2174.

135. Anisimov, S.I., Sov. Phys., 1968. JETP 27(168).

136. Colegrove, P., et al. Evaluation of a drilling model approach to represent laser spot microwelding. in ASM Proceedings of the International Conference: Trends in Welding Research. 2009. Pine Mountain, GA.

137. Ahmed, N., New Developments in Advanced Welding. 2005: CRC Press.

138. Zhao, C.X., et al., The effect of oxygen on transitional Marangoni flow in laser spot welding. Acta Materialia.

139. Limmaneevichitr, C. and S. Kou, Visualization of Marangoni convection in simulated weld pools. Welding Journal (Miami, Fla), 2000. 79(5): p. 126-s.

140. Limmaneevichitr, C. and S. Kou, Experiments to simulate effect of Marangoni convection on weld pool shape. Welding Journal (Miami, Fla), 2000. 79(8).

141. Limmaneevichitr, C. and S. Kou, Visualization of marangoni convection in simulated weld pools containing a surface-active agent. Welding Journal (Miami, Fla), 2000. 79(11): p. 324-s.

142. Chan, C.L., J. Mazumder, and M.M. Chen, THREE-DIMENSIONAL AXISYMMETRIC MODEL FOR CONVECTION IN LASER-MELTED POOLS. Materials Science and Technology, 1987. 3(4): p. 306-311.

143. Chan, C., J. Mazumder, and M.M. Chen. THREE-DIMENSIONAL MODEL FOR CONVECTION IN LASER MELTED POOL. in LIA (Laser Institute of America). 1985. Boston, MA, USA: Laser Inst of America.

144. Cary, H.B., Modern welding technology. 2nd ed. ed. 1989, Englewood Cliffs, N.J.: Prentice Hall. 787p.

145. Okon, P., et al. Laser welding of aluminium alloy 5083. in ICALEO 2002 - 21st International Congress on Applications of Laser and Electro-Optics, Congress Proceedings. 2002. Scottsdale, AZ.

146. Bardin, F., et al., Process control of laser conduction welding by thermal imaging measurement with a color camera. Applied Optics, 2005. 44(32): p. 6841-6848.

147. Bardin, F., et al. Real-time temperature measurement for process monitoring of laser conduction welding. in ICALEO 2004 - 23rd International Congress on Applications of Laser and Electro-Optics, Congress Proceedings. 2004. San Francisco, CA.

148. Esposito, C., Duarelio, G., Cingolani, A., On the Conduction Welding Process of Steels with CO2 Lasers. Optics and Lasers in Engineering 3, 1982: p. 139-151.

149. Paul, A. and T. Debroy, Free surface flow and heat transfer in conduction mode laser welding. Metallurgical Transactions B, 1988. 19(6): p. 851-858.

150. Zhao, H. and T. Debroy, Weld metal composition change during conduction mode laser welding of aluminum alloy 5182. Metallurgical and Materials Transactions B: Process Metallurgy and Materials Processing Science, 2001. 32(1): p. 163-172.

151. Kell, J., et al. HOLOGRAPHIC DIFFRACTIVE OPTICAL ELEMENTS ALLOW IMPROVEMENTS IN CONDUCTION LASER WELDING OF STEELS. in ICALEO 2006. 2006.

152. Breck, H., J.J. Ewing, and J. Hecht, Introduction to Laser Technology. Third Edition ed.: IEEE Press.

153. Du, J., et al., Weld geometry and tensile strength in laser welded thin sheet metals. Science and Technology of Welding and Joining, 2000. 5(5): p. 304-309.

154. Benyounis, K.Y., A.G. Olabi, and M.S.J. Hashmi, Effect of laser welding parameters on the heat input and weld-bead profile. Journal of Materials Processing Technology, 2005. 164-165: p. 978-985.

155. Olsen, F.O. and L. Alting, Pulsed Laser Materials Processing, ND-YAG versus CO2 Lasers. CIRP Annals - Manufacturing Technology, 1995. 44(1): p. 141-145.

156. Upadhyaya, B.N., et al., A highly efficient 5 kW peak power Nd:YAG laser with time-shared fiber optic beam delivery. Optics & Laser Technology, 2008. 40: p. 337-342.

157. Kleine, K.F., W.J. Fox, and K.G. Watkins. Micro welding with pulsed single mode fiber lasers. in ICALEO 2004 - 23rd International Congress on Applications of Laser and Electro-Optics, Congress Proceedings. 2004. San Francisco, CA.

158. Tzeng, Y.F., Process characterization of pulsed Nd:YAG laser seam welding. International Journal of Advanced Manufacturing Technology, 2000. 16(1): p. 10-18.

159. Yang, Y.P., et al., Integrated computational model to predict mechanical behaviour of spot weld. Science and Technology of Welding and Joining, 2008. 13(3): p. 232-239.

160. Tzeng, Y.F., Process Characterisation of Pulsed Nd:YAG Laser Seam Welding. The International Journal of Advanced Manufacturing Technology, 2000. 16(1): p. 10-18.

161. Sufizadeh, A.R. and S.A.A. Akbari Mousavi, Investigations on the effects of process parameters for Nd: YAG pulsed laser welding of 630 and 321 stainless steels. International Journal of Microstructure and Materials Properties. 5(2-3): p. 221-233.

162. Sabbaghzadeh, J., et al., Effect of process parameters on the melting ratio in overlap pulsed laser welding. Metallurgical and Materials Transactions B: Process Metallurgy and Materials Processing Science, 2008. 39(2): p. 340-347.

163. Mohanty, P.S., A. Kar, and J. Mazumder, A modeling study on the influence of pulse shaping on keyhole laser welding. Journal of Laser Applications, 1996. 8(6): p. 291-297.

164. Malek Ghaini, F., et al., Weld metal microstructural characteristics in pulsed Nd: YAG laser welding. Scripta Materialia, 2007. 56(11): p. 955-958.

165. Kaplan, A.F.H., et al., Keyhole Laser Spot Welding in ICALEO 2002. 2002.

166. De, A., et al., Finite element simulation of laser spot welding. Science and Technology of Welding and Joining, 2003. 8(5): p. 377-384.

167. Fujinaga, S., et al., Direct observation of keyhole behaviour during pulse modulated high-power Nd:YAG laser irradiation. Journal of Physics D: Applied Physics, 2000. 33(5): p. 492-497.

168. Grabas, B. The use of conduction model in laser weld profile computation. in Proceedings of SPIE - The International Society for Optical Engineering. 2007. Szczecin-Swinoujscie.

169. Mannik, L. and S.K. Brown, A relationship between laser power, penetration depth and welding speed in the laser welding of steels. Journal of Laser Applications, 1990. 2(3 & 4): p. 4.

170. Fabbro, R., Melt pool and keyhole behaviour analysis for deep penetration laser welding. Journal of Physics D: Applied Physics. 43(44).

171. Postma, S., et al., Penetration control in laser welding of sheet metal. Journal of Laser Applications, 2002. 14(4).

172. Kuo, T.Y., Effects of pulsed and continuous Nd-YAG laser beam waves on welding of Inconel alloy. Science and Technology of Welding and Joining, 2005. 10(5): p. 557-565.

173. Fuerschbach, P.W. and G.R. Eisler, Effect of laser spot weld energy and duration on melting and absorption. Science and Technology of Welding and Joining, 2002. 7(4): p. 241-246.

174. Ludovico, A.D., et al. Laser welding of the AA 2024-T3 aluminium alloy by using two different laser sources (Nd:YAG or CO2). in Proceedings of SPIE - The International Society for Optical Engineering. 2005. Prague.

175. Moorhead, A.J. and P.W. Turner, Welding a thermocouple gauge to Apollo lunar sample return containers. Welding Journal, 1970. 49: p. 15-21.

176. Emerson, W.F., Laser-beam welding seals electronic packages. Welding Design and Fabrication, 1996. 69(4): p. 43-44.

177. Bertrand, C., The laser welding technique applied to the non precious dental alloys procedure and results. British Dental Journal, 2001. 190(5): p. 255-257.

178. Fuerschbach, P.W. and D.A. Hinkley, Pulsed Nd:YAG laser welding of cardiac pacemaker batteries with reduced heat input. Welding Journal (Miami, Fla), 1997. 76(3): p. 103-109.

179. Sanchez-Amaya, J.M., et al., Laser welding of aluminium alloys 5083 and 6082 under conduction regime. Applied Surface Science, 2009. 255(23): p. 9512-9521.

180. Xiao, R., P. Dong, and K. Chen. Laser beam welding of dissimilar materials. in ICALEO 2009 - 28th International Congress on Applications of Lasers and Electro-Optics, Congress Proceedings. 2009. Orlando, FL.

181. Theron, M., C. Van Rooyen, and L.H. Ivanchev. CW Nd:YAG laser welding of dissimilar sheet metals. in 26th International Congress on Applications of Lasers and Electro-Optics, ICALEO 2007 - Congress Proceedings. 2007. Orlando, FL.

182. Yasuyama, M., K. Ogawa, and T. Taka, Spot welding of aluminium and steel sheet with an insert of aluminium clad steel sheet: dissimilar metal joining of aluminium an steel sheet (1st report). Welding International, 1996: p. 965-970.

183. Sun, X., et al., Resistance spot-welding of aluminium alloy to steel with transition material - from process to performance - part I: experimental study. Welding Journal, 2004. 83: p. 188-95.

184. Andrews, D., Joining aluminium to mild steel by argon arc welding. Welding Journal, 1962: p. 650-8.

185. Bel'chuk, G., Investigation of certain features of the argon-arc welding of aluminium and its alloys to steel. Weld Prod, 1961. 5: p. 14-20.

186. Roulin, M., et al., Strength and structure of furnace-brazed joints between aluminium and stainless steel. Welding Journal, 1999. 78: p. 151-5.

187. Fukumoto, S., et al., Friction welding process of 5052 aluminium alloy to 304 stainless steel. Materials science Technol, 1999. 15: p. 1080-6.

188. Kawai, G., et al., Friction weldability of aluminium alloys to carbon steel. Welding International, 2000: p. 101-7.

189. Sierra, G., et al., Steel to aluminium key-hole laser welding. Materials Science and Engineering A, 2007. 447(1-2): p. 197-208.

190. Laukant, H., E. Guimaraens, and U. Glatzel. Laser beam aluminium-steel joints - Mechanical and dynamical properties and detailed microstructural analysis of intermetallic FeAl-phases. in 26th International Congress on Applications of Lasers and Electro-Optics, ICALEO 2007 - Congress Proceedings. 2007. Orlando, FL.

191. Sierra, G., et al. Which laser process for steel to aluminium joining? in ICALEO 2006 - 25th International Congress on Applications of Laser and Electro-Optics, Congress Proceedings. 2006. Scottsdale, AZ.

192. Sierra, G., et al., Galvanised steel to aluminium joining by laser and GTAW processes. Materials Characterization, 2008. 59(12): p. 1705-1715.

193. Kreimeyer, M., F. Wagner, and G. Sepold. Development of a combined joining-forming process for aluminum-steel joints. in ICALEO 2004 - 23rd International Congress on Applications of Laser and Electro-Optics, Congress Proceedings. 2004. San Francisco, CA.

194. Kreimeyer, M. and G. Sepold. Processing of Laser Joined Aluminum-Steel Tailored Blanks in Overlap and Butt Joint Configuration. in ICALEO 2002 - 21st International Congress on Applications of Laser and Electro-Optics. 2002. Scottsdale, Arizona.

195. Min, D., et al., Effects of heat input on the low power Nd:YAG pulse laser conduction weldability of magnesium alloy AZ61. Optics and Lasers in Engineering. 49(1): p. 89-96.

196. Williams, S., G. Scott, and N. Calder, Direct diode laser welding of aerospace alloys. Laser Opto, 2001. 33: p. 50-54.

197. Bachmann, F., Industrial applications of high power diode lasers in materials processing. Applied Surface Science, 2003. 208-209: p. 125-136.

198. Abe, N., et al., Applicability of a High Power Diode Laser to Aluminum Alloy Welding in ICALEO 2002. 2002.

199. Abe, N., et al., Aluminum alloy welding by using a high power direct diode laser. Journal of Laser Applications, 2006. 18(4): p. 289-293.

200. Abe, N., et al., The effect of direct diode laser beam size in heat conduction lap welding of a thin film on a thick substrate, in Ceramic Transactions. 2007: Kurashiki. p. 381-388.

201. Funada, Y. and N. Abe. Micro Welding of Thin Stainless Steel Foils with a Direct Diode Laser. in 22nd International Congress on Applications of Lasers & Electro-Optics. 2003. Jacksonville, USA.

202. Funada, Y. and N. Abe. Lap Welding with Direct Diode Laser of Thin Foils on Thick Substrate. in 23rd International Congress on Applications of Lasers & Electro-Optics. 2004. San Francisco, USA.

203. Bassani, P., et al., Effect of process parameters on bead properties of A359/SiC MMCs welded by laser. Composites Part A: Applied Science and Manufacturing, 2007. 38(4): p. 1089-1098.

204. Abbas, G., L. Li, and Z. Liu, Effect of high power diode laser surface melting on wear resistance of magnesium alloys, in 15th International Conference on Wear of Materials. 2005: San Diego, USA.

205. Abbas, G., et al. Diode laser surface treatment of magnesium alloy AZ61. in ICALEO 2004 - 23rd International Congress on Applications of Laser and Electro-Optics, Congress Proceedings. 2004. San Francisco, CA.

206. Abbas, G., L. Li, and Z. Liu, Effect of high power diode laser surface melting on corrosion resistance of magnesium alloys, in 34th International MATADOR Conference. 2004: Manchester, UK.

207. Grueninger, A., et al., Surface texturing by laser cladding. Journal of Laser Applications, 2011. 23(2).

208. Schubert, E., et al., Laser beam cladding: A flexible tool for local surface treatment and repair. Journal of Thermal Spray Technology, 1999. 8(4): p. 590-596.

209. Partes, K. and G. Sepold, Modulation of power density distribution in time and space for high speed laser cladding. Journal of Materials Processing Technology, 2008. 195(1-3): p. 27-33.

210. Del Val, J., et al., Laser micro-cladding: A novel laser additive technique to produce hard micro-coatings, in ICALEO 2010. 2010.

211. Kathuria, Y.P., Role of beam interaction time in laser cladding process. Materials Science and Technology, 2001. 17(11): p. 1451-1454.

212. Partes, K., et al. Increased efficiency in laser cladding by optimization of beam intensity and travel speed. in Proceedings of SPIE - The International Society for Optical Engineering. 2006. Dresden.

213. Santhanakrishnan, S., F. Kong, and R. Kovacevic. Process parameters analysis of high power direct diode laser cladding. in 29th International Congress on Applications of Lasers and Electro-Optics, ICALEO 2010 - Congress Proceedings. Anaheim, CA.

214. Emamian, A., S.F. Corbin, and A. Khajepour. Study on laser parameters effect on morphology of in-situ Fe-TiC particles deposition on mild steel using

laser cladding process. in 29th International Congress on Applications of Lasers and Electro-Optics, ICALEO 2010 - Congress Proceedings. Anaheim, CA.

215. Sears, J.W. Laser additive manufacturing WC and WC forming alloys and powder blends. in ICALEO 2009 - 28th International Congress on Applications of Lasers and Electro-Optics, Congress Proceedings. 2009. Orlando, FL.

216. Aubry, P., et al. Parameter study and process control on laser cladding for direct manufacturing of 3D metallic structures. in 26th International Congress on Applications of Lasers and Electro-Optics, ICALEO 2007 - Congress Proceedings. 2007. Orlando, FL.

217. Aubry, P., et al. Direct fabrication of a TI-47AL-2CR-2NB alloy by direct metal deposition. in 29th International Congress on Applications of Lasers and Electro-Optics, ICALEO 2010 - Congress Proceedings. Anaheim, CA.

218. SankarÃ©, S., et al. Additive laser manufacturing of small metallic components by laser micro-cladding. in ICALEO 2009 - 28th International Congress on Applications of Lasers and Electro-Optics, Congress Proceedings. 2009. Orlando, FL.

219. Binetruy, C., et al. Analysis of laser welding of long fiber reinforced composites. in 29th International Congress on Applications of Lasers and Electro-Optics, ICALEO 2010 - Congress Proceedings. Anaheim, CA.

220. Franz, C., S. Mann, and S. Kaierle. Comparison of process monitoring strategies for laser transmission welding of plastics. in 26th International Congress on Applications of Lasers and Electro-Optics, ICALEO 2007 - Congress Proceedings. 2007. Orlando, FL.

221. Bucurel, R. and G. Hlifka, Laser Beam Welding Process Automates Underwater Repairs. Welding Journal, 2010.

222. Assuncao, E., L. Quintino, and R. Miranda, Comparative study of laser welding in tailor blanks for the automotive industry. International Journal of Advanced Manufacturing Technology. 49(1-4): p. 123-131.

223. Assuncao, E., et al., Conduction mode - Broadening the range of applications for laser welding, in 63rd Annual Assembly & International Conference of the International Institute of Welding. 2010: Istanbul, Turkey.

224. Reitemeyer, D., T. Seefeld, and F. Vollertsen. Online focus shift measurement in high power fiber laser welding. in 29th International Congress on Applications of Lasers and Electro-Optics, ICALEO 2010 - Congress Proceedings. Anaheim, CA.

225. Seefeld, T. Chances and challenges in processing with high brightness lasers. in 29th International Congress on Applications of Lasers and Electro-Optics, ICALEO 2010 - Congress Proceedings. Anaheim, CA.

226. Dasgupta, A.K. and J. Mazumder, Laser welding of zinc coated steel: An alternative to resistance spot welding. Science and Technology of Welding and Joining, 2008. 13(3): p. 289-293.

227. Resch, M. and A.F.H. Kaplan, Heat conduction modelling of laser welding. Lasers in Engineering, 1998. 7(3-4): p. 229-240.

228. Yilbas, B.S., A.F.M. Arif, and B.J. Abdul Aleem, Laser welding of low carbon steel and thermal stress analysis. Optics and Laser Technology.

229. Widaatalla, A., D. Shetty, and T. Eppes. Optimization of parameters for effective welding of aerospace components. in ICALEO 2006 - 25th International Congress on Applications of Laser and Electro-Optics, Congress Proceedings. 2006. Scottsdale, AZ.

230. De, A. and T. DebRoy, A smart model to estimate effective thermal conductivity and viscosity in the weld pool. Journal of Applied Physics, 2004. 95(9): p. 5230-5240.

231. Zacharia, T., S.A. David, and J.M. Vitek, Effect of evaporation and temperature-dependent material properties on weld pool development. Metallurgical Transactions B, 1991. 22(2): p. 233-241.

232. Zacharia, T., et al., Modeling of fundamental phenomena in welds. Modelling and Simulation in Materials Science and Engineering, 1995. 3(2): p. 265-288.

233. Wang, R., Y. Lei, and Y. Shi, Numerical simulation of transient temperature field during laser keyhole welding of 304 stainless steel sheet. Optics and Laser Technology. 43(4): p. 870-873.

234. Zhou, J., H.L. Tsai, and P.C. Wang. Effects of electromagnetic force on melt flow and weld shape in laser keyhole welding. in ICALEO 2004 - 23rd International Congress on Applications of Laser and Electro-Optics, Congress Proceedings. 2004. San Francisco, CA.

235. Tanriver, U., et al., Effects of absorptivity, shielding gas speed, and contact media on sheet metal laser welding. Science and Technology of Welding and Joining, 2000. 5(5): p. 310-316.

236. Mackwood, A.P. and R.C. Crafer, Thermal modelling of laser welding and related processes: a literature review. Optics & Laser Technology, 2005. 37(2): p. 99-115.

237. Assuncao, E., S. Williams, and D. Yapp, Interaction time and beam diameter effects on the conduction mode limit. Optics and Lasers in Engineering, (0).

238. Mills, K.C., Recommended values of thermophysical properties for selected commercial alloys, ed. N.P. Laboratory and A. International. 2002: Woodhead Publishing Limited.

239. He, X., T. DebRoy, and P.W. Fuerschbach, Composition change of stainless steel during mlcrojoinlng with short laser pulse. Journal of Applied Physics, 2004. 96(8): p. 4547-4555.

240. Bag, S., A. Trivedi, and A. De, Development of a finite element based heat transfer model for conduction mode laser spot welding process using an adaptive volumetric heat source. International Journal of Thermal Sciences, 2009. 48(10): p. 1923-1931.

241. Michaleris, P. and A. Debiccari, Prediction of welding distortion. Welding Journal (Miami, Fla), 1997. 76(12): p. 172-s.

242. Bolt, P.J., N.A.P.M. Lamboo, and P.J.C.M. Rozier, Light-weight structures produced by laser beam joining for future applications in automobile and aerospace industry. Journal of Materials Processing Technology, 2001. 115(1): p. 2-8.

243. Mackwood, A.P. and R.C. Crafer, Thermal modelling of laser welding and related processes: A literature review. Optics and Laser Technology, 2005. 37(2): p. 99-115.

244. Krasnoperov, M.Y., R.R.G.M. Pieters, and I.M. Richardson, Weld pool geometry during keyhole laser welding of thin steel sheets. Science and Technology of Welding and Joining, 2004. 9(6): p. 501-506.

245. Karkhin, V.A., V.V. Plochikhine, and H.W. Bergmann, Solution of inverse heat conduction problem for determining heat input, weld shape, and grain structure during laser welding. Science and Technology of Welding and Joining, 2002. 7(4): p. 224-231.

246. Fuerschbach, P.W., Measurement and prediction of energy transfer efficiency in laser beam welding. Welding Journal (Miami, Fla), 1996. 75(1): p. 24-s.

247. Salminen, A. and H. Piili, The effect of parameters on process behavior and efficency in fiber laser welding. Welding in the World, 2009. 53(SPECIAL ISSUE): p. 307-312.

248. Kawahito, Y., M. Kito, and S. Katayama, In-process monitoring and adaptive control for gap in micro butt welding with pulsed YAG laser. Journal of Physics D: Applied Physics, 2007. 40(9): p. 2972-2978.

249. Assuncao, E., S. Williams, and D. Yapp, Interaction time and beam diameter effects on the conduction mode limit. Optics and Lasers in Engineering, 2012. 50(6): p. 823-828.

250. Lu, S., H. Fujii, and K. Nogi, Marangoni convection and gas tungsten arc weld shape variations on pure iron plates. ISIJ International, 2006. 46(2): p. 276-280.

251. Amara, E.H. and R. Fabbro, Modelling of gas jet effect on the melt pool movements during deep penetration laser welding. Journal of Physics D: Applied Physics, 2008. 41(5).

252. Brown, K.R., M.S. Venie, and R.A. Woods, Increasing use of aluminum in automotive applications. JOM, 1995. 47(7): p. 20-23.

253. Han, L., et al., Advanced joining technologies for aluminium assembly for the automotive industry. Key Engineering Materials, 2009. 410-411: p. 105-116.

254. SÃ¡nchez-Amaya, J.M., et al., Laser welding of AA 5083 samples by high power diode laser. Science and Technology of Welding and Joining, 2009. 14(1): p. 78-86.

255. Haboudou, A., et al., Reduction of porosity content generated during Nd: YAG laser welding of A356 and AA5083 aluminium alloys. Materials Science and Engineering A, 2003. 363(1-2): p. 40-52.

256. Tobar, M.J., et al., Experimental and simulation studies on laser conduction welding of AA5083 aluminium alloys. Physics Procedia. 5(Part 2): p. 299-308.

257. Assuncao, E., S. Williams, and D. Yapp. Interaction time effects on the transition between conduction and keyhole laser welding. in 29th International

Congress on Applications of Lasers and Electro-Optics, ICALEO 2010 - Congress Proceedings. Anaheim, CA.

258. Trivedi, A., S. Bag, and A. De, Three-dimensional transient heat conduction and thermomechanical analysis for laser spot welding using adaptive heat source. Science and Technology of Welding and Joining, 2007. 12(1): p. 24-31.

259. Bos, J.A., Chen, M.A., On the prediction of weld pool size and heat affected zone in Shallow-Pool Welding. Transport Phenomena in Materials Processing and Manufacturing ASME, 1996. 336.

260. Russo, A.J.e.a., Two-Dimensional Modelling of Conduction-Mode Laser Welding. L.I.A., 1984. 44 (ICALEO): p. 8-15.

261. Montgomery, D., Design and Analysis of Experiments. 5th ed. 1997: John Wiley & Son, Inc.

262. Chakraborty, N., Thermal transport regimes and effects of Prandtl number in the molten pool transport in laser surface melting processes', Numerical Heat Transfer. Numerical Heat Transfer, 2008. 53(3): p. 273-294.

263. Kim, W.H., H.G. Fan, and S.J. Na, Effect of various driving forces on heat and mass transfer in arc welding. Numerical Heat Transfer, 1997. 32(6): p. 633-652.

264. Mundra, K., T. DebRoy, and K.M. kelkar, Numerical prediction of fluid flow and heat transfer in welding with a moving heat source. Numerical Heat Transfer, 1996. 29: p. 115-129.

265. Oreper, G.M. and J. Szekely, A comprehensive representation of transient weldpool development in spot welding operations. Mettallurgical Transaction A, 1986. 18: p. 1325-1332.

266. Goldak, J.A., A. Chakravarti, and M. Bibby, A new finite element model for welding heat sources. Mettallurgical Transaction A, 1986. 18: p. 1325-1332.

267. De, A. and T. DebRoy, A smart model to estimate thermal conductivity and viscosity in the weld pool. Journal of Applied Physics, 2004. 95(9): p. 5230-5240.

268. Lienhard IV, J.H., A heat transfer textbook. 2008: Phlogiston Press, Cambridge Massachusetts.

269. Richards, D.G., PhD. 2009, University of Manchester.

270. Tsai, M.C. and S. Kou, Marangoni convection in weld pools with a free surface. International Journal for Numerical Methods in Fluids, 1989. 9(12): p. 1503-1516.

271. Farzadi, A., A.H. Serajzadeh, and A.H. Kokabi, Investigation of weld pool in aluminium alloys: geometry and solidification microstructure. International Journal of Thermal Sciences, 2010. 49: p. 809-819.

272. Withers, P.J. and H.K.D.H. Bhadeshia, Residual stress part 1 - Measurement techniques. Materials Science and Technology, 2001. 17(4): p. 355-365.

273. Williams, S. and A. Steuwer, Residual Stress in friction stir welding, in Fricton stir welding.From basics to applications, D. Lohwasser and Z. Cehn, Editors. 2010, Woodhead Publishing Limited: Cambridge UK. p. 215-244.

274. Colegrove, P., et al., Welding process impact on residual stress and distortion. Science and Technology of Welding and Joining, 2009. 14(8): p. 717-725.

275. Xu, D., et al., New technique to control welding buckling distortion and residual stress with noncontact electromagnetic impact. Science and Technology of Welding and Joining, 2009. 14(8): p. 753-759.

276. Wen, S.W., et al., Rolling to control residual stress and distortion in friction stir welds. Science and Technology of Welding and Joining. 15(6): p. 440-447.

277. Altenkirch, J., et al., Residual stress engineering in friction stir welds by roller tensioning. Science and Technology of Welding and Joining, 2009. 14(2): p. 185-192.

278. Altenkirch, J., et al., Mechanical tensioning of high-strength aluminum alloy friction stir welds. Metallurgical and Materials Transactions A: Physical Metallurgy and Materials Science, 2008. 39(13): p. 3246-3259.

279. Price, D.A., et al., Distortion control in welding by mechanical tensioning. Science and Technology of Welding and Joining, 2007. 12(7): p. 620-633.

280. Zhu, J., L. Li, and Z. Liu, CO₂ and diode laser welding of AZ31 magnesium alloy. Applied Surface Science, 2005. 247(1-4): p. 300-306.

281. Santisteban, J.R., et al., ENGIN-X: A third-generation neutron strain scanner. Journal of Applied Crystallography, 2006. 39(6): p. 812-825.

282. 2003, E.P.a.o.t.c.o.J., Directive 2002/96/EC, in on waste Electrical and Electronic Equipment.

283. Larson, A.C. and R.B. VonDreele, General Structure Analysis System (GSAS). 1994, Los Alamos National Laboratory: Los Alamos, NM, USA.

284. Albertini, G., et al., Comparative neutron and X-ray residual stress measurements on Al-2219 welded plate. Materials Science and Engineering A, 1997. 224(1-2): p. 157-165.

285. Nagy, T., et al., Distortion Mitigation in Welded Ship Panels, in International Workshop on Thermal Forming and Welding Distortion. 2008: Bremen.

286. Richards, D.G., et al., Global mechanical tensioning for the management of residual stresses in welds. Materials Science and Engineering A, 2008. 489(1-2): p. 351-362.

APPENDIX A

Conduction mode - Broadening the range of applications for laser welding

This section presents a paper that was shown at the 63rd Annual Assembly & International Conference of the International Institute of Welding. Conduction laser welding opens up a range of innovative applications for laser welding. This relatively novel mode of laser processing expands the application potential significantly beyond what is normally achieved today. The main reason for this could be attributed to the different characteristics of conduction process when compared to keyhole laser welding. An example is the higher stability of conduction which results in welds of higher quality and better control of the welding process. Despite the advantages of conduction laser welding, it is yet to be exploited significantly for industrial applications and there are very few applications for which this mode of operation is used. This paper is aimed at presenting different varieties of applications for conduction laser welding using a fibre laser. This ranges from high quality aluminium welds to laser brazing of stainless steel to metal foams. The objective of this paper is to highlight the main features of conduction laser welding process and exemplify some conduction laser welding applications.

E. Assuncao did the welding development, planning of the experiments, and analysis of the welds.

S. Williams provided supervision and technical advice. As well as some of the application shown in this paper were ideas originally suggested by S. Williams.

S. Ganguly provided his expertise and knowledge in interpretation of the results obtained.
D. Yapp provided supervision and technical advice.

Introduction

Laser welding depending on the processing conditions has broadly two different operational regimes conduction and keyhole welding. The beneficial characteristics of keyhole welding, especially large penetration depth and relatively small heat affected zone attracted more industrial applications. However, keyhole welding also presents several problems that may lead to high levels of porosities and other weld defects [3, 75, 76]. In keyhole mode welding most of the beam is absorbed which may be disadvantageous when welding high reflectivity materials (e.g. aluminium). This is due to the fact that much power is needed to start the keyhole but as soon as it starts the absorptivity jumps from 3% to 98% which may cause damage to the welded structure [98].

On the other hand, conduction laser welding has been slightly neglected by industry despite several advantages. Conduction welding can be a viable alternative to keyhole welding mainly due to the fact that it is a very stable process and easier to obtain high quality welds free of pores and spatter [145]. Conduction mode of welding occurs when the vaporisation of the material is insignificant, in other words, when the thermal intensity is not high enough to cause boiling [146]. Conduction laser welding can also be achieved with significantly low laser cost, because it does not require a high beam quality or a very high power [99]. The following text will present examples of some of the applications of conduction mode laser welding.

One of the main applications of conduction laser welding is welding aluminium alloys. The high strength to weight ratio of aluminium made it a preferred choice for structural applications in the transportation and aerospace sector[242]. The welds obtained using keyhole laser welding in aluminium have tendency to form porosity and weld metal cracking. Normally the porosity presented is associated to gas entrapment during solidification and vaporisation of elements with low boiling point[179]. Another issue of keyhole welding is formation of solidification cracking, mainly at high welding speeds[42]. In order to overcome these issues in laser welding some studies on welding of aluminium were carried out using conduction mode. Using this mode it was possible to obtain welds with no

porosity or cracking [100, 145, 179]. Conduction laser welding also presents better mechanical properties when compared to keyhole laser welding due to the loss of elements and due to the fast cooling rates obtained in keyhole [145].

Another application of conduction laser welding is in joining of dissimilar materials [18]. The use of dissimilar materials in the automotive and aircraft industry has initiated several researches in trying to join different materials like aluminium to steel. Due to the difficulty of this type of welding several studies using resistance spot welding [182, 183],arc welding [184, 185], brazing [186] and Friction Stir Welding [187, 188] have been made. However, in recent years laser welding has been introduced as an alternative for welding steel to aluminium. Studies using keyhole welding in order to join aluminium to steel were made [189] but with limited success. Nevertheless, studies using conduction laser welding have shown very good results [192-194]. The advantage of using conduction laser welding in this application is related to the stability of the process that allows a better control of the temperature in the interaction area between the aluminium and the steel [193].

Conduction laser mode is also used in laser cladding for surface treatment and repair. The use of this laser mode allows a more accurate and precise way of repairing components. Due to a better control of the heat cycle it is possible to produce functionally gradient materials and graded coatings [208, 212].

The present works aims at presenting several applications of conduction laser welding and how this process can be adopted with other fusion welding process e.g. TIG or MIG originating hybrid conduction weld. In this paper some examples of conduction laser welds carried out at the Welding Engineering Research Centre (WERC), Cranfield University were presented and analyzed in terms of its suitability for different critical applications.

Experimental Procedure

The welds presented in this paper were made using an IPGYLR-8000 Fibre laser with a maximum power of 8000 W and a wavelength of 1070 nm. The system consists of a feeding fibre of 200 µm and a process fibre of 300 µm. During these experiments the optical setup used was a 125 mm collimating lens and a 500 mm focusing lens. Parameters like power used, beam diameter and welding speed were adjusted according to the application studied. In order to obtain different beam diameters a defocused laser beam was used. Each application has a specific experimental setup which will be explained in the relevant sections chapter.

Applications

In the following chapters some applications of conduction laser welding are presented.

Aluminium laser welding in conduction mode

The material used was 12 mm thick aluminium alloy 2024. The chemical composition of this alloy is presented in Table A 1. The surface of the aluminium was wire brushed and then coated with graphite in order to help the coupling of the laser beam to the material. In order to obtain the 5.25 mm beam diameter the laser beam was defocused. The welds obtained in this experiments were evaluated in terms of weld zone profile, porosity and cracking which are the most common defects when laser welding aluminium.

Table A 1 - Chemical composition of Aluminium alloy 2024

Element (wt%) 2024 – T3									
Al	Cr	Cu	Fe	Mg	Mn	Si	Ti	Zn	Others
90.7-94.7	Max 0.1	3.8 – 4.9	Max 0.5	1.2 – 1.8	0.3 – 0.9	Max 0.5	Max 0.15	Max 0.25	0.15

Figure A 1 show one of the welds obtained using conduction laser welding of aluminium. The parameters used in this experiment were a power of 4.5 kW, a welding speed of 0.6 m/min and a beam diameter of 5.25 mm.

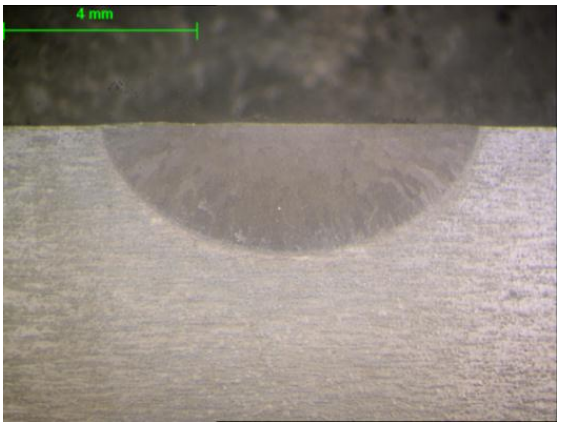

Figure A 1 - Metallographic image of the weld bead

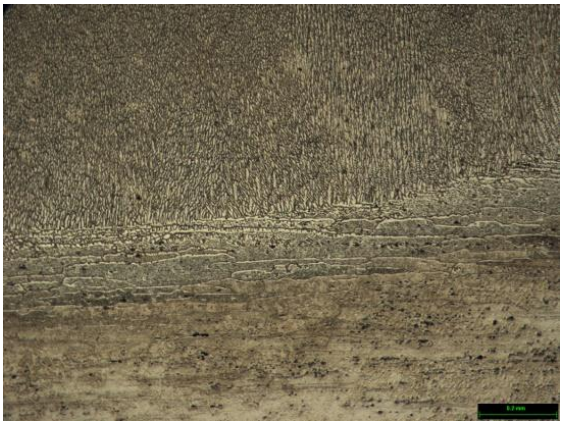

Figure A 2 - Micrograph of the melted area and heat affected zone of the weld

Evaluating Figure A 1 and Figure A 2 it is possible to see that the common defects associated to laser welding of aluminium, like porosity and cracking, are not present. The weld bead profile also presents a very flat top surface. The main advantage of this mode during welding of aluminium alloys is no vaporization which is one of the main causes of porosity. Other advantage is the slow cooling that improves the weld bead geometry.

High quality low carbon steel welds

Tests were made in 12 mm plates of S275 mild steel in order to evaluate the welds obtained when using conduction mode. Table A 2 presents the chemical composition of the S275 mild steel. The surface of the plate was wire brushed and then cleaned with acetone. In order to obtain the 5 mm beam diameter the laser beam was defocused. PureShield Argon was used as shielding gas with a flow rate of 10 l/min.

Table A 2 - Chemical composition of S275 mild steel

Element (wt%) S275 mild steel				
C	Mn	Si	P	Fe
0.25	1.60	0.50	0.05	Balance

During welding no spatter was observed. The absence of spatter is also related to the fact that in conduction mode there is no vaporization, which causes spatter.

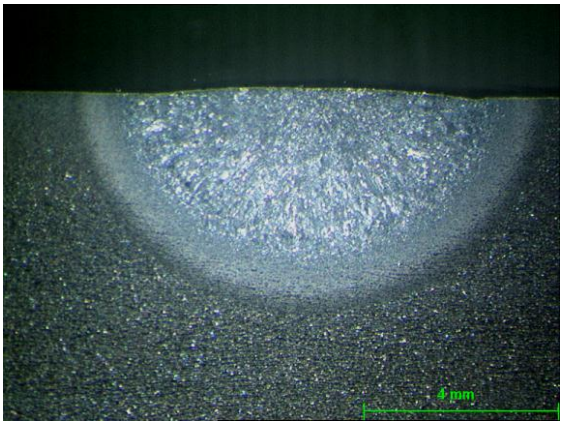

Figure A 3 - Macro-profile of a conduction weld in S275 mild steel

The weld in Figure A 3 was obtained using 7kW of power, a beam diameter of 5 mm and a welding speed of 0.3 m/min. The results emphasise one of the main characteristics of conduction welding, which is the stability of the process, noticeable. This also results into good surface appearance. The fact that during welding no spatter occurs explains why using this process it is possible to obtain a weld profile with no undercut and porosity.

Joining Aluminium to steel

In this experiment the materials used were AA2024 (composition shown in Table A 1) and a low ferritic carbon steel, the composition is shown in Table A 3.

Table A 3 - Chemical composition of Low carbon Steel

Element (wt%) Low Carbon Steel								
C	Si	Mn	P	S	Cr	Ni	Cu	Fe
0.15	0.17	0.52	0.019	0.021	0.1	0.1	0.1	Balance

Complete overlap welds were made using steel on top and the aluminium on the bottom. This configuration gives better weld quality mainly due to the thermal characteristics of both materials. The thermal conductivity of aluminium being higher than that of steel, when aluminium is used on top it results into a much larger interfacial area. This is because the heat tends to flow along the interface in the aluminium part rather than heating the steel. When steel was used on top the thermal conductivity of the two materials allow a better conduction of heat from the steel to the aluminium.

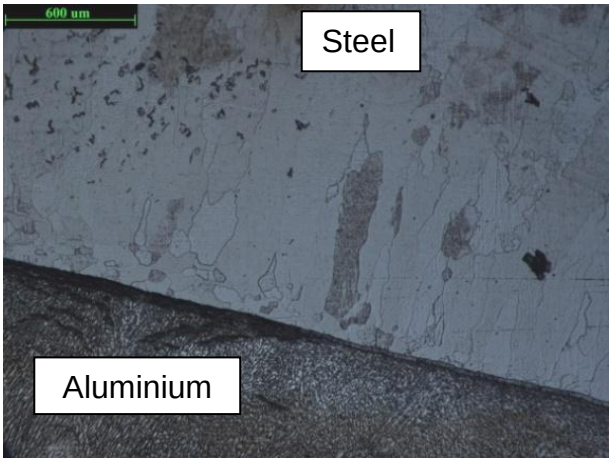

Figure A 4 - Micrograph of the interface between aluminium and steel

Figure A 5 - Micrograph with higher magnification of the interfacial area

The parameters used in the weld presented in Figure A 4 and Figure A 5 were a Laser power of 4 kW, a beam diameter of 13 mm and a welding speed of 0.5

m/min. There was no defect on the joint area between steel and aluminium including the interfacial area. It is possible to see that there is a thin layer of intermetallics formed due to interfacial reaction between the two materials. The mechanical properties of the joint were found not to be affected by this thin intermetallic layer.

Welding aluminium to steel is very difficult to implement. The use of conduction laser welding allows a better control of the heat delivered to the work piece. In order words by using this laser welding mode it is possible to control the melting of both materials, which for this specific application is of great importance. The main idea is to conduct the heat generated by the laser beam through the steel without melting the steel or by just having very small amount of melted material and melt the aluminium underneath.

Laser brazing of stainless steel to metal foams

In this experiment two different varieties of metallic materials were used. The first one was 304L Stainless steel, the composition of this material is presented in Table A 4. The other material was nickel-chromium metal foam in two different grades. The grades used were the 1116 grade with maximum of 16 pores per sq- inch and the 3743 grade with a maximum of 43 pores per sq-inch. Both the foams used were 5 mm thick.

Table A 4 - Chemical composition of 304L Stainless Steel

Element (wt%) 304L Stainless Steel								
C	Mn	Si	Ph	Ag	Cr	Ni	N	Fe
0.03	2.0	0.75	0.045	0.03	14.0	12.0	0.1	Balance

The welding operation was carried out in lap configuration with the stainless steel on top of the metal foam. In order to have a proper coupling with the laser the stainless steel was coated with graphite. In the junction of the two materials Silver braze foil was used. The composition of the brazing foil is presented in Table A 5

Table A 5 - Chemical composition of the brazing foil

Element (wt%) Brazing Foil			
Ag	Cu	Zn	Cd
40.0	19.0	20.0	20.0

The principle of this application was the use of conduction mode in order to conduct the heat using the stainless steel allowing the foil to be melted which will then wet both the surfaces to form the joint The final results, shown in Figure A 6 and Figure A 7, where obtained using a 15 mm beam diameter, 0.3 m/min welding speed and a power of 1.4 kW.

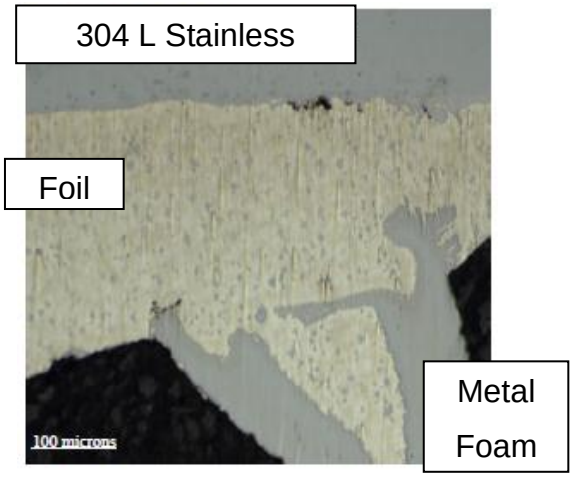

Figure A 6 - Micrograph of laser braze joint of stainless steel to 1116 Grade foam

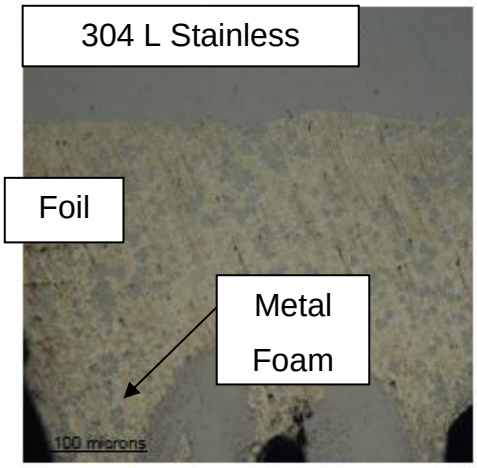

Figure A 7 - Micrograph of laser braze joint of stainless steel to 3743 Grade foam

The use of conduction mode in laser brazing showed significant advantages. When compared to other processes fusion welding processes e.g.TIG, MIG and torch brazing conduction mode laser brazing has the advantage of higher productivity. In terms of the overall quality of the joint, laser brazing showed very good results. Vacuum brazing is the only other technique that can produce equivalent or superior joints as compared to laser conduction brazing. However, this process can be applied to samples of any size while in vacuum brazing the size is limited by the size of the vacuum furnace. This application highlights another property of conduction mode which is the stability of the process that allows a better control of the heat along the work piece. To summarize laser brazing in conduction mode presented not only very good results but also as process with high productivity, flexibility and stability.

Laser-Arc hybrid conduction welding

The material used in this part of the paper was 1.6 mm thick plates of aluminium alloy 2024; the composition of this material is presented in Table A 1. All the welds were made in butt joint configuration. The surface of the aluminium was

wire brushed and cleaned with acetone. The 5 mm beam diameter was obtained by defocusing the laser beam. The TIG power supply used was a Migatronic BDH 440 Commander with an electrode of 3.2 mm diameter. In this experiment AC TIG mode was used with 70% cleaning during the positive half cycle in order to pre clean the surface and reduce the top surface oxidation. PureShield Argon was used as the protective shielding gas and also as trailing and back shielding. The filler wire used was 1.2 mm diameter 2139 which has a composition of aluminium and 6% of copper. The wire was fed perpendicular to the welding direction. In order to control distortion a vacuum fixture was used.

The idea of using TIG in order to assist conduction mode welding of aluminium is to prevent reflection of the laser beam by aluminium workpiece. The TIG process will pre-melt the surface of the aluminium allowing a better coupling by the laser beam avoiding the use of graphite on the surface of the aluminium. In order to achieve this, trials were taken with the TIG torch leading and the laser beam trailing.

Figure A 8 present an example of a weld obtained using hybrid laser in conduction mode plus TIG welding process. In this sample the parameters used were the following, 2 kW of laser Power, a Beam Diameter of 5 mm, TIG current of 80 A, wire feed speed of 2.3 m/min and a welding speed of 1 m/min.

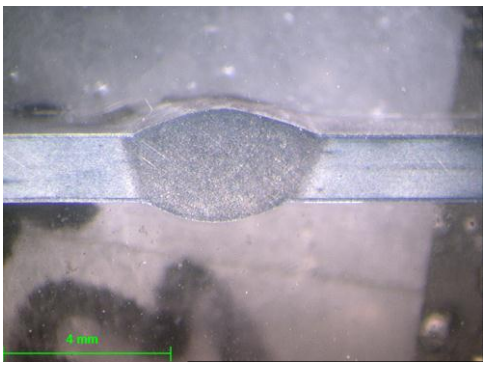

Figure A 8 - Macrograph of the TIG plus laser in conduction mode weld

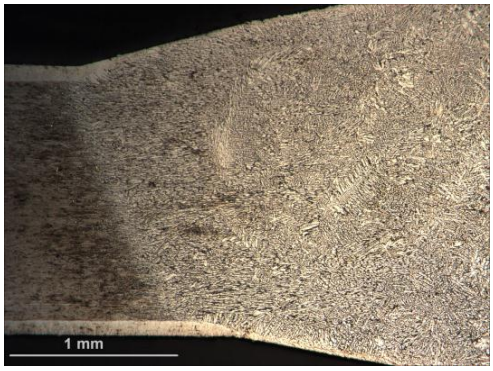

Figure A 9 - Micrograph of the TIG plus laser in conduction mode weld

Based on Figure A 8 and Figure A 9 it is possible to see that by using the welding process it is possible to obtain extremely high quality welds, with no porosity, cracks, undercut or spatter. Also the use of a hybrid process solves the problem of reflection of the laser beam when welding aluminium alloys in conduction mode without the use of surface treatment to help absorption.

Conclusion

The use of conduction laser welding described in this paper show a whole range of possibilities for advanced and critical joining applications. Laser conduction mode of welding was shown to be extremely applicable where high quality and stable welds are required. The fact that in conduction mode there is hardly any vaporisation of elements, defects like porosity, excessive spatter, undercut etc. are eliminated improving the overall aspect and properties of the weld bead. Larger beam diameter used in conduction mode allows a bigger fit up tolerance. Normally conduction laser welding is associated to the welding of aluminium; although the whole range of applications is yet to be fully explored.